Université de Sherbrooke

Study of the NHE6/RACK1 interaction : design of a peptidic inhibitor directed towards prevention of hypoxia-induced chemoresistance

Par
Pierre-Paul Pelletier
Programme d'immunologie

Mémoire présenté à la Faculté de médecine et des sciences de la santé
en vue de l'obtention du grade de maître ès sciences (M. Sc.)
en immunologie

Sherbrooke, Québec, Canada
Juillet, 2017

Membres du jury d'évaluation
Pre Claire Dubois, Service d'immunologie, Département de pédiatrie
Pr Subburaj Ilangumaran, Service d'immunologie, Département de pédiatrie
Pr Jean-Luc Parent, Service de rhumatologie, Département de médecine

RÉSUMÉ

Étude de l'interaction NHE6/RACK1 : développement d'un inhibiteur peptidique visant à prévenir la chimiorésistance induite par l'hypoxie

Par
Pierre-Paul Pelletier
Programme d'immunologie, Département de pédiatrie

Mémoire présenté à la Faculté de médecine et des sciences de la santé en vue de l'obtention du diplôme de maitre ès sciences (M.Sc.) en immunologie, Faculté de médecine et des sciences de la santé, Université de Sherbrooke, Sherbrooke, Québec, Canada, J1H 5N4

Les cellules tumorales exposées à l'hypoxie sont connues pour développer une résistance accrue aux traitements de chimiothérapie. Ce phénomène est attribué à plusieurs facteurs. Tout d'abord, peu de drogue en circulation atteignent les régions hypoxiques tumorales mal perfusées. Le métabolisme des cellules tumorales en hypoxie est altéré de façon à créer un milieu extracellulaire sur-acidifié qui nuit à la perméabilité membranaire de certaines drogues. Des mécanismes cellulaires tels que l'arrêt du cycle cellulaire, l'inhibition de l'apoptose et l'expression de pompes à efflux s'additionnent aux facteurs tissulaires de résistance. En 1996, il fut observé que des cellules MCF7 résistantes à la doxorubicine possédaient des compartiments intra-vésiculaires plus acides que leurs homologues sensibles à la doxorubicine. Selon le modèle de protonation, séquestration et sécrétion (PSS), proposé pour expliquer cette découverte, les drogues qui agissent à titre de bases faibles peuvent être séquestrées dans des compartiments acides suite à leur protonation et être sécrétées par la suite. Nos résultats ont démontré que la culture en hypoxie mène à une acidification des compartiments intra-vésiculaires accompagnée d'une augmentation de la résistance aux traitements d'agents chimiothérapeutiques de type anthracycline dans des lignées cellulaires de divers types de cancer. L'imagerie confocale nous a permis d'observer une localisation extranucléaire de la doxorubicine qui co-localise de façon partielle avec un marqueur endosomal, la transferrine. Cette étude cherchait d'abord à évaluer l'implication de l'échangeur endosomal NHE6 dans l'acidification intravésiculaire produite par l'hypoxie. De plus, le projet visait à concevoir une stratégie pour contrer cette acidification et améliorer la réponse aux anthracyclines. Les résultats obtenus démontrent que l'hypoxie affecte la localisation de NHE6 ce qui contribue à l'acidification intravésiculaire des endosomes. Le changement de localisation de NHE6 s'effectue suite à une interaction directe et transitoire avec la protéine d'échafaudage RACK1. L'expression d'un peptide de compétition dérivé d'une séquence de 62 aa de NHE6, nous permet de contrer la délocalisation de l'échangeur, de réduire l'ampleur de l'acidification intravésiculaire et d'atténuer la résistance aux anthracyclines causés par l'hypoxie. Une analyse *in-silico* reposant sur la conservation de résidus fonctionnels, les propriétés biochimiques des interfaces d'interaction protéine-protéine transitoires, ainsi qu'un protocole de raffinement d'arrimage moléculaire, a permis de mettre en lumière une courte portion de la région d'interaction susceptible de permettre l'ancrage de NHE6 à travers une cavité à la surface de RACK1.

Mots clés : Chimiorésistance, hypoxie, pH intracellulaire, NHE6, RACK1, tumeur

SUMMARY

Study of the NHE6/RACK1 interaction : design of a peptidic inhibitor for the prevention of hypoxia-induced chemoresistance

By
Pierre-Paul Pelletier
Immunology Program

Thesis presented to the Faculty of Medicine and Health Sciences for the obtention of a Master's Degree in Sciences (M.Sc.) in Immunology, Faculty of Medicine and Health Sciences, Université de Sherbrooke, Sherbrooke, Québec, Canada, J1H 5N4

Tumor cells exposed to hypoxia are known to develop resistance to chemotherapy. Several components have been shown to contribute to such resistance. Previous studies indicate that only a small amount of the drug in circulation is able to penetrate poorly perfused hypoxic areas of tumors. Hypoxia alters the metabolism of tumor cells and leads to acidosis of the extracellular fluid thus altering the ability of various drugs to cross lipid bilayers. Compounded with resistance factors observed in living tissues are cellular mechanisms such as cell cycle arrest, inhibition of apoptosis and the expression of drug efflux pumps. In 1996, it was observed that doxorubicin resistant MCF7 cells have more acidic intra-vesicular compartments than their doxorubicin sensitive counterparts. According to the protonation, sequestration and secretion (PSS) model, which was proposed as an explanation for the aforementioned discovery, drugs that act as weak bases can be sequestered in acidic compartments following protonation and eventually be secreted. Our results obtained in several cancer cell lines have shown that the incubation of the cells under hypoxic conditions leads to an acidification of intra-vesicular compartments and an increased resistance to anthracycline. Using confocal imaging we were able to visualize extranuclear doxorubicin spots that partially co-localized with the transferrin endosomal marker. The initial goal of this study was to evaluate the implication of the endosomal Na^+/H^+ exchanger, NHE6, in intra-vesicular acidification induced by hypoxia. Additionally, the project aimed to elaborate a strategy to counter this acidification and to improve the response to anthracycline drugs. Our results demonstrate that hypoxia affects NHE6 localization which contributes to intra-vesicular acidification. NHE6 change of localization takes place through a direct transient interaction with the scaffold protein RACK1. Expression of a competition peptide derived from a 62 aa sequence of NHE6, was used to block NHE6 delocalization, to reduce the magnitude of intra-vesicular acidification and to attenuate the effect of anthracycline resistance caused by hypoxia. An *in-silico* analysis based on the conservation scores of functional residues, biochemical properties of transient protein-protein interfaces, as well as a molecular docking refinement protocol, has allowed us to detect a short segment of the region of interaction that may be necessary for NHE6 anchorage on a surface cavity of RACK1.

Keywords: Chemoresistance, hypoxia, intracellular pH, NHE6, RACK1, tumor

TABLE OF CONTENTS

LIST OF FIGURES

LIST OF TABLES

LIST OF ABBREVIATIONS

ABC	ATP-binding cassette
ALDH	Aldehyde dehydrogenase
ALL	Acute lymphoblastic lymphoma
AMAS	Analysis of Multiply Aligned Sequences
BCRP	Breast cancer resistance protein
BSA	Bovine serum albumin
CA	Carbonic anhydrase
CDKN2A	Cyclin-dependent kinase inhibitor 2A
CFTR	Cystic fibrosis transmembrane regulator
ChK	Checkpoint kinase
ClC	Chloride channel
CML	Chronic myelogenous leukemia
CSC	Cancer stem cells
c-SNARF	Carboxy seminaphtharhodafluor
DAPI	4',6'-diamidino-2-phenylindole
DMSO	Dimethyl sulfoxide
ECF	Extracellular fluid
ECM	Extracellular matrix
EGFR	Epidermal growth factor receptor
EMDR	Environment mediated drug resistance
EMEM	Eagle's minimum essential medium
EMT	Epithelial-mesenchymal transition
FAK	Focal adhesion kinase
FBS	Fetal bovine serum
GF	GF109203X
GNB2L1	Guanine nucleotide-binding protein subunit beta-2-like-1
GPCR	G-protein coupled receptor

GSH	Glutathione
GTPase	Guanosine triphosphate cyclohydrolase
HA	Hemagglutinin
HCC	Hepatocellular carcinoma
HER2	Human epidermal growth factor-2
HIF	Hypoxia inducible factor
HPTS	8-Hydroxypyrene-1,3,6-Trisulfonic Acid (or pyranine)
HRE	Hypoxia responsive element
HRP	Horseradish peroxidase
IFP	Interstitial fluid pressure
IGF1R	Insulin-like growth factor 1 receptor
ID	Intrinsically disordered
IF	Immunofluorescence
IP	Immunoprecipitation
IRS	Insulin receptor substrate
I_sc	Interface energy score
LDH	Lactate dehydrogenase
LOX	Lysyl oxidase
MBP	Maltose binding protein
MCT	Monocarboxylate transporter
MDR	Multidrug resistance
MD_raw	Meta-Disorder predictor
MMP	Matrix metalloproteinase
MORFs	Molecular recognition features
MSA	Multiple sequence alignment
NADPH	Nicotinamide adenine dinucleotide phosphate
NHE	Sodium-hydrogen exchanger
PAGE	Polyacrylamide gel electrophoresis
PBS	Phosphate-buffered saline
PDB	Protein Data Bank
PDBU	Phorbol 12,13-dibutyrate

PDGFR	Platelet-derived growth factor receptor
PFK-1	Phosphofructokinase-1
P-gp	P-glycoprotein
PHDs	HIF-specific prolyl-hydroxylases
pHe	Extracellular pH
pHi	Intracellular pH
PI3K	Phosphatidylinositol 3-kinase
PFA	Paraformaldehyde
PKC	Protein kinase C
PKM2	Pyruvate kinase M2
PRMs	Proline-rich motifs
PSS	Protonation, sequestration and secretion
PTEN	Phosphatase and tensin homolog
PVDF	Polyvinylidene fluoride membrane
pVHL	Von Hippel-Lindau tumor suppressor protein
RACK1	Receptor for activated C kinase 1
RCSB	Research Collaboratory for Structural Bioinformatics
ROS	Reactive oxygen species
SDS	Sodium dodecyl sulfate
Stat3	Activator of transcription factor 3
TAF	Tumor-associated stromal fibroblasts
TBS	Tris-buffered saline
TFEB	Transcription factor EB
TGN	Trans-Golgi network
TIGAR	TP53-inducible glycolysis and apoptosis regulator
TNBC	Triple negative breast cancer
V-ATPase	Vacuolar ATPase

1. INTRODUCTION

1.1 Clinical Consequences of the Chemoresistance Problematic Faced in Oncology

Several projects from which rose precursors to modern chemotherapy took place during World War II, including the nitrogen mustards, alkylating agents that were the first chemotherapeutic agents used to treat cancer (DeVita and Chu, 2008). The early compounds used for chemotherapy were typically biological compounds isolated from living organisms that would later be chemically modified to give rise to chemotherapeutic classes with a large number of synthetic analogs. Examples of such include: analogs of folic acid, the first antifolates developed and tested during the 1940's (DeVita and Chu, 2008), 5-flurouracyl, a modified uracil nucleobase (DeVita and Chu, 2008), both vincristine and vinblastine, plant alkaloids isolated from *Catharanthus roseus* (Moudi *et al*, 2013) and both daunorubicin and doxorubicin, anthracyclines that were isolated from the gram-positive soil bacteria *Streptomyces peucetius* (Di Marco *et al,* 1981). These projects would eventually lead to the development of compounds that became regularly used in the 1960's for cancer treatment in the clinic alongside surgery, hormone therapy and radiotherapy (DeVita and Rosenberg, 2012). The latest forms of cancer treatment to have made their appearance in clinical practice are immunotherapy and targeted therapy in the late 1990's (DeVita and Rosenberg, 2012).

Following early success in the late 1990's and early 2000's of the Bcr-Abl tyrosine kinase inhibitor Imatinib (Gleevec) used to treat chronic myelogenous leukemia (CML), targeted therapies used in personalized medicine have been widely acclaimed as the future of cancer therapy because of high success rates and few side effects (DeVita and Chu, 2008). However targeted therapies present their own set of challenges: they rely heavily on biomarkers for diagnostic purposes, each therapy can only be used for a limited subset of patients presenting the specific molecular target and they have limited potential for treatment of cancers with intratumor heterogeneity (Curigliano and Criscitiello, 2014). Steady progress has been made in the development and usage of targeted therapies over the last two decades, however research to identify practical biomarkers and to fully understand the consequences of tumor heterogeneity is still in its early stages. Therefore, it remains to be seen to which extent

targeted therapy can rise to the future challenges of oncology (Fisher et al, 2013). First-line treatments for solid tumors such as surgery and radiotherapy have limited benefits when used alone for tumors in advanced stages with poorly defined borders and in which metastases have occurred (Kirkwood *et al*, 2013). Likewise, these techniques can rarely be used effectively to treat cancers such as leukemia and lymphoma that do not depend on the formation of solid tumors (Greaves, 2016). For all of these reasons, despite high toxicity, chemotherapy remains one of the most commonly used forms of treatment in oncology. For many types of cancers primary chemotherapy offers the best option to improve progression free survival although it is not used for curative purposes (Table 1) (DeVita and Chu, 2008). Combination chemotherapy is used effectively for the treatment of several types of leukemia and lymphoma, it is also used as neoadjuvant therapy to reduce tumor size before surgical resection and as adjuvant therapy to reduce the likelihood of local or metastatic recurrence post-surgery (DeVita and Chu, 2008). Adjuvant chemotherapy used in a post-surgical setting generally yields greater benefit than equivalent primary therapy used in cases of unresectable tumors (Kirkwood *et al*, 2013). Cancer staging and use of prognosis factors is becoming increasingly precise and intricate to help guide the choice of therapy regimen that yields the best risk/benefit ratio for each individual patient.

Table 1: Types of cancer in which clinical practice indicates primary chemotherapy for advanced cases and in which adjuvant therapy is indicated following surgery.

Type of cancer	Primary chemotherapy	Adjuvant chemotherapy
Anaplastic astrocytoma		√
Bladder	√	
Breast	√	√
Cervical	√	√
Colorectal	√	√
Esophageal	√	
Gastric	√	√

Head and Neck	√	√
Melanoma		√
Nasopharyngeal	√	
Non-small cell lung	√	√
Osteogenic sarcoma		√
Ovarian	√	√
Pancreatic	√	
Prostate	√	

(Adapted with permission from DeVita and Chu, 2008, American Association for Cancer Research License n° 4107690780581)

Cancer treatments that fall under the umbrella term of chemotherapy are drugs that inhibit cancer growth by impairing mitosis in fast dividing cells. They are thus cytotoxic compounds that differ from targeted therapies, hormone therapy and immune therapy because of their lack of specificity and of their significant toxicity. Although cytotoxic drugs are the preferred treatment in many cases as described above and have shown better effects than alternatives for prolonging remission, it remains that response rates are low and that development of resistance as manifested by relapse is nearly universal. Treatment regimens that include anthracycline such as doxorubicin have represented one of the most viable options for decades for the treatment of aggressive tumors. As for all the classes of chemotherapeutic agents, resistance regularly arises and deeply compromises the response to such an adjuvant therapy regimen.

Chemoresistance has been observed to occur across all types of cancers irrespectively of the tissue of origin. It has been categorized under two large categories based upon the response to the initial therapy; cancer that does not respond to initial therapy is deemed intrinsic resistance whereas cancer that returns after an initially successful therapy is called acquired resistance (Lippert *et al*, 2011). Examples of cancers that display intrinsic resistance, which is also called primary resistance, include acute lymphoblastic lymphoma (ALL) where approximately 20% of adult patients exhibit resistance when they first undergo treatment (Thomas *et al,* 1999). Patients with adenocarcinoma that undergo the prescribed treatment of

chemotherapy with surgery are 50 to 70% likely to relapse within a year and in most of those cases a phenotype of chemoresistance is acquired (Castells et al., 2012). Breast cancer is by far the most common form of cancer in women worldwide, affecting approximately 1 of 8 women at one point during their lifetime and accounting for about 14% of new cancer cases (Ferlay *et al*, 2015; Verwey *et al*, 2016). Aside from being highly prevalent, breast cancer is a type of cancer that is known to have frequent recurrences in the form of treatment resistant tumors during the years that follow surgery with neoadjuvant or adjuvant therapy (Arnason and Harkness, 2015). It has been estimated that 40% of breast cancer patients undergoing conventional treatment will eventually relapse and in the majority of those cases the returning tumors will be from metastasis; this is at least partially due to development of resistance to either chemotherapy or radiation therapy (Smalley, 2013). Although conventional therapy is usually effective for the treatment of a primary tumor it is much less so for treatment of resistant secondary tumors at the sites of metastasis (Verwey *et al*, 2016). Treatment outcome thus depends largely on tumor aggressiveness and metastatic potential. Breast cancer classification based on the presence or absence of the estrogen, progesterone and human epidermal growth factor-2 (HER2) receptors gives insight into the treatment approach to be used and into the aggressiveness of the tumor (Verwey *et al*, 2016). Triple negative breast cancer (TNBC) tumors are the most challenging to treat because they are insensitive to hormone therapy, are the most aggressive and are the most likely to recur in the form of resistant tumors from metastatic sites (O'Reilly *et al*, 2015). Effective treatments for TNBCs are currently lacking and urgently needed; predictive factors to guide treatment for this type of cancer also need to be developed and refined (Rakha & Chan, 2011).

Two alternate models have been postulated to explain the origin of chemotherapy resistant cells (Zharedine and Borden, 2013). In the first model, a small number of quiescent cancer stem cells (CSC) are thought to have properties that enable them to initiate tumor formation and to provoke resistance (Nguyen *et al*, 2012). According to the second model, called environment mediated drug resistance (EMDR), the tumor microenvironment plays a large role in modulating the entrance of tumor cells into a dormant state (Meads *et al*, 2009). This dormant state allows them to survive long enough under selective pressure to undergo genetic alterations that confer drug resistance even when exiting the dormant state (Meads *et al*,

2009). Proponents for either model have put together strong supporting arguments in both cases and although most investigators in the field of chemoresistance prefer to explain their findings according to one model, there is no reason why they could not be complementary. For the remainder of this dissertation, we have chosen to rationalize our findings under the lens of the EMDR model although we recognize that resistance arising as described in the CSC model may also have occurred.

Extrinsic microenvironment factors leading to chemoresistance that fall under the scope of the EMDR model can be either physical factors, soluble factors or can be linked to cell-adhesion mediators. Known physical factors include hypoxia and acidosis whereas known soluble factors include cytokines, chemokines and growth factors; cell-adhesion mediators include changes to integrins and other cell-adhesion molecules that often take place during epithelial-mesenchymal transition (EMT) (Meads *et al*, 2009).

Because the development of human cancer usually involves genomic instability that leads to an accumulation of point mutations and epigenetic modifications, a majority of tumors are comprised of highly heterogeneous populations of cells (Caulin and Maley, 2011. Epithelial breast carcinomas are a particularly striking example in which it has been reported that high intra-tumor diversity was found in 97% of tumors examined (Wild *et al,* 2000). Mutations acquired in cancer sub-populations can provide survival advantages for certain contexts, such as under therapeutic pressure. In such contexts, heterogeneous tumors obey the Darwinian law of evolution by natural selection; tumor clones that have undergone favourable adaptations are able survive therapy whereas all or most other clones are eliminated (Greaves, 2007). Although therapy might initially appear to have been successful because of tumor shrinkage, a niche of highly resistant cells in a dormant state (Meads *et al*, 2009) may remain and can eventually repopulate the tumor to cause relapse.

The problematic behind chemoresistance acquired under therapeutic selective pressure is compounded by the fact that favourable adaptations to one therapy will also negatively affect the efficacy of ensuing therapies. This phenomenon is associated with poor treatment outcome and prognosis, and it is recognized as multidrug resistance (MDR) (Ullah, 2008).

Specific mechanisms of MDR and examples will be described in a later section; for the scope of this thesis, we will discuss MDR in the context of chemotherapy resistance although it also occurs in response to other distinct compounds such as for antibiotics.

Cancer resistance to therapy is not singly limited to chemotherapy; resistance to targeted therapies and to immunotherapy have been observed and described. Unlike for chemotherapy, mechanisms of resistance to these therapies tend to involve specific molecular targets and pathways and do not typically give rise to MDR. The targeting of oncogenes around which cancer cells develop oncogene addiction has become a popular strategy for the design of therapies (Weinstein and Joe, 2008). That is because in many cases cancer cells become over reliant on these oncogenes and cannot survive if they become inactivated. In the case of tyrosine kinase oncogenes, mutations to gatekeeper residues of the kinase domain has been shown to lead to constitutive activation of the enzyme which renders targeted therapies ineffective; such examples have notably been demonstrated for BCR-ABL fusion protein, for epidermal growth factor receptor (EGFR), and for platelet-derived growth factor receptor (PDGFR) isoforms α and β (Azam *et al,* 2008). In other cases, targeted pathways that were initially believed to be essential for tumor survival can effectively be substituted for by a parallel pathway. One such example is the emergence of the insulin-like growth factor 1 receptor (IGF1R) pathway following treatment with phosphatidylinositol 3-kinase (PI3K) inhibitors that gives rise to PI3K inhibitor resistant cell lines (Isoyama *et al,* 2012).

Novel cancer therapy regimens are now being engineered to attempt to overcome the ever-present problematic of chemoresistance. Improved understanding of molecular events leading to resistance has been imperative for the recent advances in this field. As proposed by Hall *et al* (2009), an effective strategy to overcome MDR could rely on identifying the new "Achilles' heel" of resistant tumors; a concept the authors refer to as collateral sensitivity (CS). According to this principle, adaptations that have made tumor cells resistant to one type of therapy may also hypersensitize them to other types of therapies. CS has certainly been observed and exploited for targeted therapies where PI3K inhibitor resistant cell lines have been treated in conjugation with selective IGF1R inhibitors for much more convincing outcomes (Isoyama *et al,* 2012). The concept of CS builds on the mathematical model of

tumor resistance to chemotherapy proposed by Coldman and Goldie (1983), in which being able to pinpoint alternating non-cross-resistant chemotherapy would be the optimal route for treatment. Therapies with specific cellular targets can now be used along with chemotherapy to exploit CS, a strategy that appears to be the most promising avenue for the development of future combination therapies.

1.1.1 Chemoresistance in Solid Tumors

Up to now, most of the research on resistance to chemotherapy has been focused on molecular adaptations of cancer cells leading up to cellular mechanisms of chemoresistance (Yu & Tannock, 2012). Many of the proposed therapeutic strategies that have emerged from these studies have however neglected to consider the effects that tumor microenvironment characteristics can have on hindering therapeutic efficacy (Wojtkowiak et at, 2012). Indeed, physiological factors can exacerbate resistance to chemotherapy by limiting the amount of drug in the circulation that reaches and penetrates tumor cells (Yu & Tannock, 2012). Physical microenvironment factors also act as stressors that, as per the EMDR model, select for molecular adaptations that favour survival under these harsh physical conditions and that coincidentally also confer increased resistance to chemotherapy (Doktorova *et al*, 2015). Although increased interstitial fluid pressure (IFP), nutrient deprivation, hypoxia and acidosis, might at first glance appear to act separately on resistance to chemotherapy, there is increasing evidence of the interplay that exists between these common physical factors of the tumor microenvironment. This section summarizes the current state of research regarding how extrinsic tumor microenvironment factors affect chemoresistance and highlights known interactions between these factors.

1.1.1.1 Increased Interstitial Fluid Pressure and Tumor Hypoxia

A fundamental difference between solid tumors and normal tissues is the increased rate of cancer cell proliferation. Because the rate of proliferation exceeds the capacity of existing and newly formed vasculature to provide a proper supply of nutrients and oxygen, it is a common feature of solid tumors to contain areas impoverished in nutrients and oxygen (Chan & Giaccia, 2007). In fact, O_2 has a diffusion limit of about 100-200 μm around tumor blood

capillaries which means that hypoxic regions usually start forming in tumors that reach 1-2 mm in diameter (Egeblad *et al*, 2010). It has been estimated that nearly 40% of all breast tumors contain important hypoxic areas associated with increased resistance to chemotherapy and radiotherapy (Ward *et al*, 2013). Oxygen concentration in these areas can drop below 0.3% whereas the oxygen concentration of normal breast tissues is typically around 9% (Chun *et al*, 2006). A correlation between hypoxia, chemoresistance and resistance to radiotherapy has also been observed in several other types of solid tumors (Jia & Nan, 2011). Resistance to radiotherapy is due, at least in part, directly to low oxygen concentrations; the mechanism of action of radiotherapy requires the formation of cytotoxic free radicals in a reaction with oxygen to damage the integrity of DNA and halter proliferation (Pajonk *et al*, 2010). Along with other factors, this phenomenon can increase resistance to radiation doses by 2-3-fold. Hypoxia is also recognized to enhance the invasive potential of tumors. In this regard, hypoxia was shown to contribute to local invasion and to increase incurrence of metastasis at distant sites (Jia & Nan, 2011). Studies examining transcription of miR-210, GLUT1 and carbonic anhydrase IX (CAIX) as well as protein expression of GLUT1 and CAIX in TNBC associated with a poor prognosis reveal that the hypoxic response is likely stronger than for other types of breast cancers (Ward *et al*, 2013). It is thus no surprise that tumor hypoxia has become a strong indicator of poor clinical prognoses for many types of cancers (Doktorova *et al*, 2015).

As a tumor expands within its host tissue, it exerts pressure onto the surrounding stroma that resists the increase in volume (Stylianopoulos, 2016). This phenomenon results in a stiffening of the tumor due to densification of the extra-cellular matrix (mostly hyaluronan and collagen) and stroma (Yu & Tannock, 2012). The mechanical stress that is generated by tumor expansion also compresses intratumoral and surrounding blood and lymphatic vessels (Stylianopoulos, 2016). As perfusion from blood vessels and lymphatic vessel fluid drainage are hindered, IFP is invariably elevated. This increased IFP poses a major barrier to chemotherapy by reducing the ability of drugs to penetrate tumor tissue (Yu & Tannock, 2012). Tumor capillaries can eventually collapse if their internal pressure is exceeded by IFP; tumor vasculature collapse further limits delivery of chemotherapy, of oxygen and of nutrients. As a whole, solid tumor vasculature has been shown to be more disorganized than

for normal tissues and the distance between functional capillaries of tumors is wider than for normal tissues. Since the tumor vasculature is constantly changing, the tumor microenvironment becomes a continuously fluctuating landscape of oxygen and nutrient gradients. Therapeutic strategies targeting the extracellular matrix (ECM) and stromal cells are being explored to help normalize the IFP and to improve chemotherapy delivery as well as restore normal vasculature architecture in tumors (Yu & Tannock, 2012). These strategies include disruption of Hedgehog signaling to deplete tumor-associated stromal fibroblasts (TAF) (Olive *et* al, 2009) or treatment with PEGPH20, an enzyme that degrades hyaluronan (Yu & Tannock, 2012).

The most studied mediators of the hypoxic response have undoubtedly been the Hypoxia inducible factor (HIF) transcription factors; dimeric complexes formed of a HIF1α, HIF2α or HIF3α labile subunit and a stable HIF1β (also called ARNT) which as a complex can bind hypoxia responsive elements (HRE) and act as important transcriptional regulators (Keith et al, 2012). HIF alpha subunits are labile under normal oxygen tension where they are modified by HIF-specific prolyl-hydroxylases (PHDs) and targeted for proteasomal degradation via E3ubiquitin ligase von Hippel-Lindau tumor suppressor protein (pVHL). Levels of HIF1α and HIF2α expression and ensuing activity of the mature dimeric complex are primarily controlled through this post-translational mechanism where PHDs require oxygen as a substrate to allow specific recognition of HIFα subunits by pVHL. Low oxygen tension thus leads to stabilization of HIFα subunit and modulation of HRE containing genes. Up to now, more than 100 genes controlled by HIF-1 have been identified and new targets are constantly being added to the list (Yu *et al*, 2017); it is thus understandable that most of the research on the hypoxic response has been focused on HIF1α which also happens to be ubiquitously expressed across human tissues unlike its HIFα counterparts. The remainder of the discussion on HIF transcription factors will thus focus on HIF1α; the dimeric protein containing HIF1α will be henceforth referred to as HIF-1.

Genes modulated by HIF-1 fall under a broad range of normal and abnormal cellular processes such as proliferation, cell cycle control, glycolysis, angiogenesis, erythropoiesis, invasion, migration and chemoresistance. Many of the genes identified thus far have been

associated with either cancer progression or maintenance (Ward *et al*, 2013). HIF-1α has been found to be commonly overexpressed across a wide range of malignant tumor types (Barar & Omidid, 2013). The list of genes modulated by HIF-1 is too extensive to be properly represented in this section but a few examples will be briefly presented to illustrate how HIF-1 can be linked to cancer progression and maintenance.

Several oncogenic driver mutations have been shown to increase HIF-1 irrespective of oxygen tension (Ward *et al*, 2013). Those include mutations leading to constitutive activation of Ras GTPases regulating MAPK/ERK pathway of growth and differentiation, of Src tyrosine kinase or of kinases from the PI3K/AKT/mTor pathway of cell cycle regulation. Likewise, activation of growth factor receptors such as IGF1R, EGF, HER2 and c-Met has also been shown to elevate levels of HIF-1 (Jia & Nan, 2011). A strong positive correlation with activity of these oncogenes as well as association with loss of function of phosphatase and tensin homolog (PTEN) and cyclin-dependent kinase inhibitor 2A (CDKN2A) tumor suppressor genes indicate a role for HIF-1 as a regulator of cancer growth and progression (Barar & Omidi, 2013).

Many of the cellular functions affected by the expression of HIF-1 favour cancer maintenance by contributing to a pro-survival phenotype. Among these, angiogenesis has repeatedly been shown to be associated with stabilization of HIF-1α (Bos *et al*, 2005). Cell cycle deregulation and activation of growth pathways alone would not allow a tumor to grow beyond a few millimetres in diameter due to poor vascularization and appearance of necrotic zones in the de-oxygenated core of the tumor (Yu & Tannock, 2012). By promoting angiogenesis under low, but not yet lethal oxygen tensions, HIF-1 allows renewal of blood vessels and continued growth of the tumor. These new vessels do little to re-establish proper drug perfusion in the tumor core as they are of poor integrity and form and abnormal architecture (Maugeri-Saccà *et al*, 2011).

Glucose metabolism is another function that is significantly altered by HIF-1 expression. HIF-1 is indeed one of the key factors that lead to increased reliance on glycolysis by cancer cells, a metabolic shift widely known as the “Warburg effect”. It should be noted that

although we focus here on the role of HIF-1 in promoting glycolysis, the Warburg effect denotes a wide-ranging observation of glycolysis reliance by cancer cells that go beyond the effect of hypoxia and HIF-1. HIF-1 acts as a regulator of glycolysis by promoting the expression of pyruvate kinase M2 (PKM2) (Porporato *et al*, 2011), which acts as a rate-limiting enzyme of this metabolic pathway as well as by promoting the expression of glucose transporters GLUT1 and GLUT4 (Marin-Hernandez *et al,* 2009). Since glycolysis does not strictly require oxygen for generation of adenosine triphosphate (ATP), this metabolic shift allows extended survival in regions impoverished in oxygen. The pro-survival effects of HIF1α however extend far beyond cancer cells exposed to hypoxia; in reality, HIF-1 also affects the metabolism of neighbouring cells under normoxia. That is because HIF-1 also controls the expression of lactate dehydrogenase (LDH) which is responsible for converting pyruvate, the end-product of glycolysis, into lactate (Semenza, 2009) as well as the ratio between plasma membrane monocarboxylate transporters 1 (MCT1) and 4 (MCT4) that respectively regulate its import and export (Ullah *et al,* 2006). The effect is a symbiotic relationship in which lactate is exported from tumor cells in hypoxia to be imported by tumor cells in normoxia and reutilized for oxidative phosphorylation; this mechanism allows for efficient glucose metabolism and optimized energy production.

Although cancer progression and maintenance are often discussed separately due to the different cellular processes involved, these sometimes involve common signaling pathways. Such is the case for the PI3K/AKT/HIF1α that has been shown to be involved with EMT and chemoresistance for breast cancer (Semenza, 2003), hepatocellular carcinoma (HCC) (Jiao & Nan, 2012) and other types of carcinomas. The important role of HIF1α stabilization in cancer maintenance is illustrated through the concomitant expression of several markers of EMT and MDR strongly correlated with poor treatment outcome. In the first case, lysyl oxidase (LOX) (Rebucci & Michiels, 2013) , SNAIL, vimentin and N-cadherin come to mind (Imai *et al*, 2003), whereas BCRP, MDR-1 and c-MYC are some of the key markers identified to be associated with both hypoxia sustained expression and resistance to chemotherapy (Davies *et al*, 2014).

Specifically, LOX is a family of enzymes that catalyzes a reaction forming aldehydes from the lysine residues side chain amines of ECM proteins (Mayorca-Guiliani & Erler, 2013). Follows from this reaction spontaneous formation of cross-linkages between elastin and collagen fibers as part of the maturation process of ECM; through this mechanism, LOX has been shown to promote the formation of metastatic niches in several cancer types (Bennewith & Dedhar, 2011). LOX enzymes have additionally been shown to act in invasion and migration in early stages of the metastatic cascade (Erler *et al*, 2006). These effects of the LOX enzymes are due, at least in part, to LOX-induced stabilization of the SNAIL protein, which is a critical regulator of EMT (Sahlgren *et al*, 2008). SNAIL protein contributes to the loss of the epithelial phenotype in carcinomas undergoing EMT as it acts as a transcriptional repressor of the epithelial marker E-cadherin. Amongst the other important HIF-1-dependent genes that facilitate invasion and metastasis are the type IV collagen degrading metalloproteinases MMP2 and MMP9 that act by weakening the integrity of basement membranes (Gilkes & Wirtz, 2014).

Many of the pro-survival characteristics observed in cells exposed to hypoxia have been associated to HIF1-induced genes that reprogram tumor cells to acquire stem cell-like characteristics (Crowder *et al*, 2014). Reprogramming of CSC genes through HIF proteins contributes to chemoresistance in several ways including by increasing genomic instability, by modifying the cell cycle, by favouring glycolysis (Crowder *et al*, 2014) or by controlling expression of multidrug efflux pumps (Jiao & Nan, 2012). Although HIF-1 is the most studied response to hypoxia and was most often reported as a mediator of chemoresistance and resistance to radiotherapy, it would be misleading to equate the pro-survival phenotype induced by hypoxia with HIF effects. A prominent example of a complementary mediator of chemoresistance prevalent in the hypoxic microenvironment would be the loss or inactivation of the P53 cell cycle regulator. The functional form of P53 indeed acts as a negative regulator of the hypoxic response by promoting proteasomal degradation of HIF proteins (Ward *et al*, 2013). HIF-independent stress response pathways as well as dysregulated reactive oxygen species (ROS) and redox mechanisms are also becoming increasingly associated with the hypoxia response and MDR (Crowder *et al*, 2014). The relative contribution of the different elements of the hypoxic response towards chemoresitance remains largely elusive and will

undoubtedly continue to be clarified in the coming years. Current evidence suggests that oxidative stress is more severe in areas of intermittent hypoxia and that this type of hypoxia, as opposed to chronic or acute hypoxia, is mainly responsible for resistance in solid tumors (Kwee, 2014). Further investigation into cancer redox mechanisms and MDR is thus warranted. The molecular mechanisms associated with the chemoresistance mediators mentioned herein will be described further along in this introduction.

1.1.1.2 Tumor Acidosis and Metabolism

As briefly mentioned earlier, lactate, as a by-product of glycolytic tumor cells, is exported through MCT4 to the extracellular fluid (ECF) (Draoui & Feron, 2011). Lactate will then be progressively shuttled into non-glycolytic cells including endothelial tumor cells to be used in oxidative phosphorylation (Ullah *et al,* 2006). As recognized by A. Weinberg and accepted by most of cancer researchers, metabolic reprogramming, distinguished by an increased rate of glucose metabolism through glycolysis, is now among the list of the hallmarks of cancer (Hanahan & Weinberg, 2011). Since increased glycolysis generates protons as by-products at a fast rate (Alfarouk *et al*, 2014); they tend to accumulate in cancer cells particularly under anaerobic conditions where protons cannot react with molecular oxygen to form water (Chiche *et al*, 2010). One of the ways by which tumor cells prevent acidification of intracellular pH is through MCT (primarily MCT4) symporter secretion of H^+ ions with lactate (Draoui & Feron, 2011). Proton extrusion from cancer cells however far exceeds what is needed to maintain intercellular pH equilibrium; in fact, proton export from cancer cells through both primary and secondary active transport machinery leads to proton gradient reversal across the plasma membrane (Alfarouk *et al*, 2014). Examples of other important transporters that mediate proton export from tumors include: V-ATPase proton pump, CAIX and sodium-hydrogen exchange 1 (NHE1). Whereas normal tissues have extracellular pH (pHe) around 7.4 and intracellular pH (pHi) around 7.2, pHe of tumors in acidosis is typically in the range of 6.6-6.8 and pHi in the range of 7.3-7.5 (Barar & Omidi., 2013). As distance from blood vessel increases and oxygen tensions drop, pHe also progressively diminishes and can go as low as pH 6.0 (Gatenby *et al*, 2017). **Figure 1** depicts some of the physical characteristics of the tumor microenvironment.

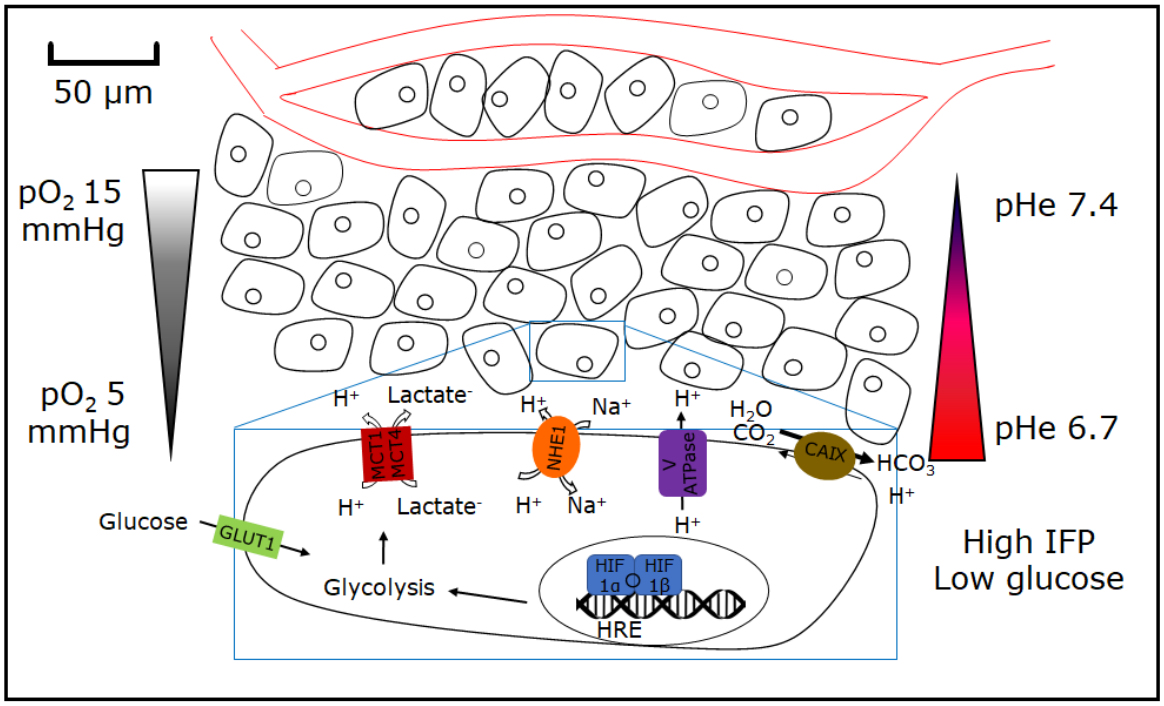

Figure 1. Physical characteristics of the tumor microenvironment

Depiction of oxygen concentration and pH gradients typical of the tumor microenvironment and of the main transporters involved in creating and maintaining tumor acidosis.

It has been argued that exposition to the harsh tumor microenvironment, that includes physical factors such as hypoxia and acidosis, selects specifically for tumor cells that display extensive proton export machinery (Wojtkowiak et at, 2012). The early stage at which pH reversal occurs during carcinogenesis indeed supports the idea that this adaptation plays a major role in cancer progression (Reshkin *et al*, 2014). In fact, cancer cells that cannot regulate their pHi have been shown to be less proliferative and to be less likely to form tumors (Ward *et al*, 2013).

The cancer cell's response to acidosis remains poorly understood; that is in part because findings from past studies have often been confounding. Four major cellular alteration features have however stood out in the literature: these are metabolic reprogramming, defense against ROS, triggering of autophagy and alterations in endo-lysosomal functions (Lamonte *et al*, 2013; Wojtkowiak et at, 2011 and Zhitomirsky & Assaraf, 2015).

Reversal of pH gradient in cancer cells has at times been reported to contribute to a switch from oxidative phosphorylation to glycolysis just has it has been reported to inhibit glycolysis. The foremost claim that the activity of glycolytic enzymes such as lactate dehydrogenase and phosphofructokinase-1 (PFK-1) is increased due lo lower intracellular pH (Calderon-Montano *et al,* 2011) whereas the later claim that these genes are down-regulated as a result of lactic acidosis (Chen *et al*, 2008). The divergence in these findings suggests that distinct cellular machinery must be important in determining the exact metabolic response to acidosis; the reason behind these seemingly conflicting results may lie with the P53 status of cells being studied. In fact, the P53 protein has been shown to be activated by tumor acidosis when functional and to reduce glycolysis through TP53-inducible glycolysis and apoptosis regulator (TIGAR) (Lamonte *et al*, 2013). Additionally, the same study showed that P53 activated through acidosis contributes to the activity of two other important metabolic pathways: the oxidative branch of the pentose phosphate pathway (PPP) necessary for novel ribose synthesis and glutaminolysis which is parallel pathway to glycolysis for ATP generation by cancer cells for their elevated energy requirements. These two pathways have in common the fact that they both increase the reductive potential of the cells, which leads us to the next feature of the acidosis response: defense against ROS. Consequently, the overall level of the reducing equivalent nicotinamide adenine dinucleotide phosphate (NADPH) is raised and serves to counteract the similar increase in ROS due to the stress generated by acidosis (Lamonte *et al*, 2013). Neutralization of oxidative stress under such harsh microenvironmental conditions is necessary to ensure prolonged tumor cell survival. Because the P53 dependent changes outlined above also coincide with decreased proliferation; it is unclear if the sum of these adaptations plays a role that is tumor suppressive or if they contribute to cancer maintenance. Increased pentose phosphate activity as induced by acidosis, has previously been associated with brain metastasis (Chen *et al*, 2007) and chemoresistance (Tamada *et al*, 2012). Importantly, an enhanced reductive potential, manifested through increased NADPH replenishment, is a recurring theme with other environmental stresses such as hypoxia, glucose deprivation and matrix detachment; it thus seems to be a key necessary feature for cancer cell extended survival in the tumor microenvironment.

Also consistent with the cellular responses to acidosis mentioned above, is the triggering of autophagy in response to starvation (Wojtkowiak *et al*, 2012). It appears that autophagy in this context is required as an adaptation to obtain biomolecules from recycled organelles to offset metabolic pathways skewed towards catabolism. Alteration of the endo-lysosomal compartments is the final feature of the response to acidosis and is closely related to the process of autophagy, which entails fusion of lysosomes and phagosomes to form phagolysosomes (Hosogi *et al*, 2014). Different studies in fact suggest tumor acidosis has the effect of increasing the number of lysosomes (Avnet *et al*, 2016), lowering their pH value (Zhitomirsky & Assaraf, 2015) and triggering the secretion of lysosomal components into the cytoplasm (Steffan *et al,* 2009). Low lysosomal pH in cancer as well as concomitant occurrence of autophagy, and transcription factor EB (TFEB) associated lysosomal biogenesis have been linked to prolonged survival under tumor microenvironment stress (Salerno *et al,* 2014) (Zhitomirsky & Assaraf, 2015). Aside from the induction of phagocytosis which was already discussed; release of lysosomal components and acidification of lysosomal compartments have both been shown to contribute to increased survival of tumor cells. Not only does low pHe acts on lysosomal trafficking to increase lysosomal exocytosis (Steffan *et al,* 2009) but it also increases the expression of lysosomal proteases such as MMP2, MMP9 and Cathepsin B (Wojtkowiak et at, 2011). In an acidic environment, these enzymes promote invasion of the ECM which ultimately also contributes to migration and survival. Early reports showed that low pHe can inhibit gap junction (Ruch *et al*, 1990), this finding taken with others that show low pHe favors mesenchymal type-like morphology (Amith *et al,* 2016) suggest that tumor acidosis may play a role in deconstruction of cell junctions to further contribute to cancer progression through EMT (Lamouille *et al,* 2014).

A steep gradient between the intracellular, extracellular and endo-lysosomal pH has been shown to contribute to decreased tumor responsiveness to chemotherapy (Wojtkowiak *et al, 2011)* and radiotherapy treatments (Ohtsubo *et al,* 2001). Although it appears that the characteristic of resistance to radiotherapy is mostly linked to the selection of tumor cells with defective P53 necessary for adaptation to chronic acidosis (Williams *et al,* 1999), chemoresistance is in turn largely due to the impact that altered pH has on the tissue and cell

distribution of the therapeutics themselves. Although the phenomena of impaired tissular and cellular distribution of chemotherapy has been observed on several occasions over the last few decades, it is only recently that it has become well understood and integrated under one overarching framework. The work of Robert J. Gillies and Yehuda J. Assaraf, among others, clearly explains how drug distribution is affected through inter-compartment pH gradients. Both authors have described a phenomenon coined as "ion trapping" (Wojtkowiak *et al,* 2011) that explains how the pH gradient acts as a physiological barrier for drugs or other molecules. This phenomenon is of relevance because for many drugs there exists a large difference in permeability between the nonionized species of a drug, that are more permeant, and the ionized species that can be much more impermeant. In the case of tumor acidosis, this phenomenon negatively impacts the capacity of weak base chemotherapeutics to effectively permeate through the cell membrane and ultimately reach their intended therapeutic target which generally is the cell nucleus. Even the small proportion of weak base therapeutics that does penetrate the plasma membrane is not guaranteed to reach the nucleus as it is also likely to passively diffuse and become trapped in acidic organelles such as lysosomes (Zhitomirsky & Assaraf, 2015). Similarly, molecules that enter cells through endocytosis can become entrapped in late endosomes or lysosomes as they are sorted to acidic lysosomes through the endo-lysosomal system. This phenomenon however cannot be generalized to all chemotherapeutic drugs as some drugs do not have ionizable species, and thus pH would not alter their membrane permeability, and others are weak acids which means the pH gradient found in tumor acidosis would positively affect their ability to cross the plasma membrane (Wojtkowiak *et al,* 2011).

In fact, based on the chemical structure of each drug and the pH value of cellular compartments, it is possible to calculate a partitioning coefficient on a logarithmic scale called Log P to describe the distribution of the equilibrium between two phases, one being the lysosomes and the other being the cytoplasm. Such calculated Log P values (Zhitomirsky & Assaraf, 2015) for common chemotherapeutic drugs are shown in table 2. Drugs with Log P values close to 1, such as is the case for doxorubicin and Mitoxantrone, would thus be partitioned at a ratio of 10 to 1 in favor of acidic compartments such as lysosomes as opposed to the cytoplasm.

Table 2: Calculated Log P values for lysosome and cytoplasm partitioning of common drugs used for cancer treatment

Drug	Log P	Lysosome trapping
Lapatinib	4.64	[+]
Gefitinib	3.75	[+]
Vincristine	3.13	[+]
Sunitinib	2.93	[+]
Pyrimethamine	2.75	[+]
Daunorubicin	1.73	[+]
Mitoxantrone	1.19	[+]
Doxorubicin	0.92	[+]
Pemetrexed	0.73	[-]
5-Fluorouracil	-0.66	[-]

Adapted with permission from Zhitomirsky & Assaraf, 2015.

Both extracellular space and intracellular compartments have been shown to entrap large amounts of chemotherapeutic drugs and to limit their effectiveness (Gerweck, 2006) (Zhitomirsky & Assaraf, 2015); the importance of both parallel occurrences should be taken into consideration while studying drug resistance since the extracellular space represents a much larger volume but lysosomes can reach much lower pH values neighboring pH 5 or lower. The phenomenon of "ion trapping" should certainly be taken into consideration in selecting the best therapeutic approaches for cancer treatment and for future design of cancer therapeutics (Wojtkowiak *et al,* 2011).

1.1.2 Cellular and Molecular Mechanisms of Chemoresistance

As recognized previously, the tumor microenvironment has a crucial role to play in the development of chemotherapy and is clearly an important driver in selecting molecular determinants for resistance to chemotherapy. This section provides an overview of specific cellular and molecular determinants of chemoresistance as currently recognized in the literature.

1.1.2.1 Drug Detoxification

Mechanisms of drug detoxification constitute a rather disparate group of processes that all share the characteristic of limiting chemotherapeutic drug activity; these processes can take an active form where drugs are inactivated by being metabolized or via chemical modifications, or they can take a passive form where the necessary activation mechanisms are repressed. A prime example of detoxification through a metabolic enzyme would be the ability of aldehyde dehydrogenases (ALDH), important biomarkers of CSC to remove various toxic aldehydes generated as intermediary metabolites of several chemotherapeutic drugs such as cyclophosphamides (Tomita *et al,* 2016). High expression of ALDH enzymes in breast CSCs has been strongly associated with increased resistance to chemotherapy and radiotherapy; effects that can be prevented through inhibition of ALDH activity (Croker & Allan, 2012). ALDH plays an analogous role in normal stem cells for protection against cellular stress and improvement of survival outcomes. Another common mechanism contributing to chemoresistance is the conjugation of an anionic group such as glutathione (GSH), glucuronate or sulfanate, to chemotherapeutic drugs (Homolya *et al,* 2003). Such chemical modifications transform many drugs in such a way that they become substrates to ATP-binding cassette (ABC) transporters that can then export such drugs outside cancer cells. These multidrug resistance efflux pumps will be discussed in more details in an incoming section. Finally, some chemotherapeutic drugs need to first be activated to become cytotoxic; cytarabine needs to undergo a series of phosphorylation to cytarabine triphosphate in order to be fully active (Sampath *et al*, 2006). Cancer cells have been known to adapt to cytarabine treatment by downregulating kinases responsible for phosphorylating the drug (Bardenheuer *et al*, 2005).

1.1.2.2 Multidrug Resistance Efflux Pumps

Transporters responsible for drug efflux and development of MDR mostly belong to the ATP-binding cassette (ABC) protein superfamily that can be subdivided into three subfamilies that each have different drug substrate specificities (Glavinas *et al*, 2004). ATP hydrolysis is the general mechanism used by ABC transporters to pump a variety of drugs outside of cells or inside vesicular compartments to lower intracellular drug concentrations (Nakanishi and Ross, 2012). Fueling ABC transporters represents a large burden for cancer cell metabolic needs, as approximately two ATP molecules are consumed to export each molecule of the substrate and ATP hydrolysis continues to a certain extent even in the absence of any substrate. There is yet no agreed upon naming convention for ABC transporters and each protein transporter tends to be referred to under several different names. The P-glycoprotein (P-gp), also called MDR-1, is expressed through the ABCB1 gene, whereas the Breast cancer resistance protein (BCRP) is expressed through the ABCG2 or MXR gene. These first two protein subfamilies mainly recognize and export large positively charged amphiphilic compounds whereas the final subfamily of ABC transporters the multidrug resistance proteins (MRPs), expressed through the ABCC gene, recognize neutral hydrophobic molecules or certain soluble anionic compounds (Glavinas *et al*, 2004). P-gp is known to transport and to lead to resistance against drugs such as vinca alkaloids, anthracyclines and paclitaxel (Gottesman et al.,2002). MCRP also transports anthracyclines and also recognizes topoisomerase inhibitors and mitoxantrone. Finally, MRP1 can transport many classes of chemotherapeutic compounds including vinca alkaloids and anthracyclines, although these compounds often need to have first been conjugated with glutathione (GSH), glucuronide or sulfate (Yin and Zang, 2011). There is evidence that certain selective pressures, such as cancer drug exposition, lead to differential P-gp localization (Petriz *et al*, 2004), which when targeted to the lysosomal membrane can lead to lysosomal drug sequestration (Chapuy *et al*, 2008).

1.1.2.3 Defects and Imbalances in Cell Death and Survival Pathways

There exist a multitude of adaptations that cancer cells may undergo involving modifications to cell death and survival pathways that ultimately result in increased resistance to chemotherapy. As these have been extensively described in the literature, to summarize these

adaptations could represent an entire review on its own; as such the current section merely seeks to acknowledge their vast role in EMDR and to provide a few examples. Of course, it isn't possible to discuss alterations to apoptotic pathways without mentioning selection of inactivating mutations to P53, s staple of apoptotic proteins that has wide ranging impacts on cellular function and that is correlated with de-novo resistance to doxorubicin in breast cancer (Arnason and Harkness, 2015). Alternatively, selective pressures may by contrast select for activating mutations to anti-apoptotic proteins such a B cell lymphoma 2 (Bcl-2) protein (Teicher, 2006). In many cases the effects of environmental pressures such as hypoxia and high pHi can prevent activation of G1/S checkpoint and activate checkpoint kinases 1 & 2 (ChK1 & ChK2) that coordinate the DNA damage responses with the cell cycle to facilitate progression through the G2 phase (Maugeri-Saccà *et al*, 2011). Hypoxia can also negatively affect several DNA damage response pathways including homologous recombination, non-homologous end joining and mismatch repair (Bristow and Hill, 2008); hypoxia may also result in telomere shortening and chromosomal instability (Verdun and Karlseder, 2007). Modifications to cell death and survival pathways may result from selection by exposition to a particular drug; however once acquired these adaptations are likely to cause resistance to a wide-ranging spectrum of drugs.

1.1.2.4 Compartmentalization and the PSS Model

The rationale behind the cellular mechanism of weak base therapeutics compartmentalization has previously been covered through the explanation of the lysosomal ion-trapping phenomenon. It must be noted that ion-trapping is in no way exclusive to lysosomes as it has also been observed to occur in other acidic cellular compartments such as endosomes (Lee & Tannock, 2006). Description of ion-trapping as a contributing factor to chemoresistance was first described in 1996 where following the initial observation that doxorubicin resistant MCF7 breast cancer cells have more acidic intra-vesicular compartments than their doxorubicin sensitive counterparts, the protonation, sequestration and secretion (PSS) model was proposed by Sanford Simon (Schindler *et al,* 1996) to rationalize increased resistance to doxorubicin. The first two step of the process are consistent with ion-trapping as previously described and the third step refers to secretion through efflux pumps or through simple exocytosis.

Cellular or molecular mechanisms leading up to compartmentalization of weak base therapeutics by cancer cells remain to be described. Doxorubicin is often used as model drug in experimental design involving microscopy as it has the advantageous property of emitting natural fluorescence (Lucien *et al,* 2014). This property allowed our laboratory to observe doxorubicin extranuclear spots reminiscent of the ion-trapping phenomenon (**Figure 2**) in HT1080 cells (Lucien *et al*, 2017). Similar findings had previously been obtained by other researchers (Lee & Tannock, 2006), but our results were the first indication that the tumor microenvironment, in this case hypoxia, could consistently increase drug sequestration. The current study will explore ramifications of this key finding and how improved understanding of this apparent mechanism of chemoresistance can be exploited in a novel therapeutic approach.

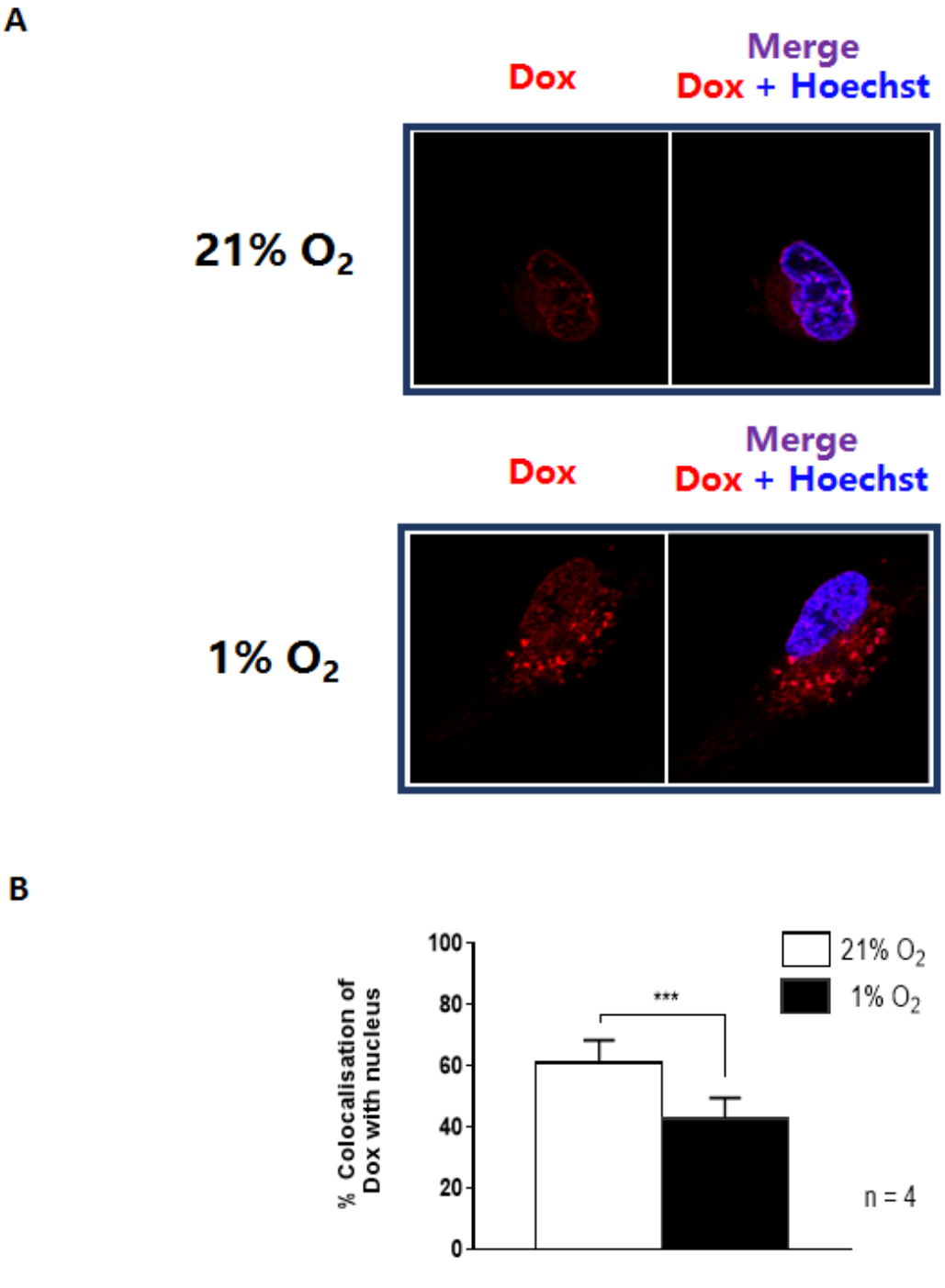

Figure 2. Subcellular localization of doxorubicin under hypoxia

A) Representative images of sub-cellular distribution of doxorubicin in live HT1080 cells under normoxia and hypoxia. The nucleus was stained by incubating cells with Hoechst 33342. Cells at 1% O_2 were kept under hypoxia for 4h. **B)** The percentage of doxorubicin present at the nucleus was quantitated by using the overlapping signal from Hoechst 33342.

1.2 Regulators of pH Equilibrium in Tumor Cells

Distinct metabolic signatures of tumor cells and increased in energy demands contribute to create a harsh tumor microenvironment characterized by highly acidic ECF. These conditions exert major selective pressures on tumor cells that force them to adapt to such adverse variations. Expression and activity of a number of proton channels and exchangers can be modulated by cancer cells in order to survive tumor acidosis. Regulators of tumor cell pH equilibrium and their known functions in the process are described below.

The MCT protein family responsible for the transport of monocarboxylate substrates such as pyruvate, lactate and ketone bodies is constituted of 14 known members, but only MCT1-4 have been confirmed to have a proton linked transporter activity (Halestrap, 2012). Although each of these transporters may contribute to either efflux or influx of protons, MCT1 was shown to be mostly located in well oxygenated regions of xenograft tumors where it is involved in proton influx (Sonveaux *et al,* 2008) whereas MCT4 is better adapted to facilitate efflux (Dimmer *et al*, 2000). The activity of these transporters is driven by the concentration gradient of the monocarboxylate substrates, such as lactate, on which proton transport is dependent (Wilson *et al*, 2009). In the case lactate and proton transport, lactic acid is transiently formed during transport across the plasma membrane to be readily dissociated in the ECF. Although MCT1 and MCT4 have by far received the most attention in cancer research, MCT2 has also been found to be expressed in brain, prostate and colon cancer (Spugnini *et al*, 2015). Evidence of import and export duality of the MCT transporters in tumor goes a long way to support the theory of metabolic symbiosis in tumors. Interestingly, in-vivo inhibition of MCT1 was shown to limit tumor growth (Sonveaux *et al,* 2008). This finding may be a result of lactate metabolism being replaced by glycolysis in MCT1 expressing cells which would limit the pool of fuel sources the tumor as a whole can use. Several MCT inhibitors are currently being developed or undergoing clinical trial; one example would be the 7ACC2 compound which acts as a specific inhibitor of lactate import by MCT1 and MCT4 transporters (Draoui *et al*, 2014). Another family of proteins that is critical for inter and intracellular pH regulation is that of carbonic anhydrases (CAs); a family of 14 known zinc metalloenzymes that catalyze the reaction from one molecule of carbon dioxide and of water, two oxidative phosphorylation by-products, to a bicarbonate anion and

a proton (Supuran, 2008). The majority of CAs is needed for important physiological functions with the notable exceptions of CAIX and CAXII (Neri & Supuran, 2011). Both CAIX and CAXII are primarily expressed within tumors and are known to be determinant factors in establishing the pH gradient reversal often observed in tumors (Vullo *et al*, 2003). Expression of CAIX or CAXII in tumors is sometimes correlated with increased expression and activity of chloride couple bicarbonate transporters ($Cl^-/HCO3^-$) that allow recapture of $HCO3^-$ that further exacerbates the pH gradient across tumor cell membranes by raising pH_i (Morgan *et al,* 2007). CAIX and CAXII differ where the tumor localization of the former is highly concentrated in hypoxic regions or necrotic tumor core, and the later is more evenly distributed across the tumor (Tafreshi *et al*, 2012). Of all the tumor associated pH regulators presented in the section, CAIX and CAXII may well be the proteins associated with most advanced stage of cancer as described in the EMDR model. In fact, these two CA enzymes are associated with poor clinical outcomes and have been identified as having important roles for most stages of tumor progression; namely tumor growth, tumor cell survival, acidification of the ECF, invasion, initial stages of the metastatic cascade and resistance to chemotherapy (Benej *et al*, 2014). Attempts to inhibit CA activity to prevent cancer progression have generally been rendered more challenging by the fact that many tumor cells models respond to CAIX inhibitors by compensating with expression of CAXII (Lou *et al*, 2011). The exception is breast cancer for which CAIX is solely expressed in many models.

Chloride channels (ClC) and Cl^-/H^+ antiporters constitute a diverse set of proteins that share the characteristic of transporting chloride ions and protons and of regulating intracellular pH and cell volume (Picollo and Pusch, 2005). ClC-3 in particular, has been shown to be highly expressed in metastatic carcinomas, was associated with poor survival outcomes and was suggested to be an interesting therapeutic target (Xu *et al*, 2015). This protein superfamily has however received very little attention when compared with the other transporters mentioned.

The vacuolar ATPase (V-ATPase) is a proton pump primarily located at the surface of intracellular vesicles (Sennoune *et al*, 2004) that may also intermittently linger within the plasma membrane through recycling of endosomal/lysosomal compartments (Steffan *et al,*

2009). V-ATPase is a large complex multi-subunit protein that actively pumps hydrogen ions (Forgac, 2007) from the cytoplasm into vesicles (or into the ECF). As V-ATPase activity and expression is elevated in many tumors and endosomal turnover is accelerated by low pH_e, V-ATPase is believed to play an important role in preventing cytoplasmic acidification and thus enabling cellular adaptation to the harsh tumor microenvironment. The coupling of V-ATPase with endosomal trafficking (Martìnez-Zaguilán *et al,* 1999) results in indirect proton extrusion from vesicle recycling, an event that exacerbates the pH gradient across the plasma membrane of tumor cells by lowering pH_e and contributing to tumor hallmarks such as invasion, metastasis (Feng *et al,* 2013) and multidrug resistance (von Schwarzenberg *et al*, 2014) as previously described. Through regulation of endosomal pH, expression and activity of V-ATPase is also believed to affect the cellular functions of endocytosis and autophagy (Spugnini *et al*, 2015); and to have an impact on ion-trapping. For these reasons, and the fact that V-ATPase expression is particularly elevated in highly metastatic breast cancer cells, inhibition of V-ATPase has been seen as a promising therapeutic strategy for many years; however clinical trials of various inhibitors have either revealed high toxicity or limited efficacy to date (Perez-Sayans *et al*, 2012).

1.2.1 Plasmalemmal Sodium/Hydrogen Exchangers

The SLC9 gene family is a protein family that is expressed in organisms ranging from prokaryotes to mammals; it is composed of a total of 13 known Na^+/H^+ exchangers (NHE) of which nine closely related exchangers form the distinct SLC9A subfamily (Fuster and Alexander, 2014). Little is currently known of the remaining four members of the SLC9 family, these exchangers are outside the scope of the current discussion. Of the nine closely related SLC9A family members, five are primarily localized at the plasma membrane whereas four are usually located on intracellular membranes. Although tissue distribution (Table 3) and functional roles of plasmalemmal NHE exchangers vary significantly, all of these exchangers have a common function in regulating pH homeostasis and cell volume (Donowitz *et al*, 2013). Each NHE exchanger share a common general structure that is formed of 12 transmembrane domains forming a channel capable of binding and translocating Na^+ and H^+ ions. NHE's are often N or O-glycosylated on extracellular loops and contains a long C-terminal cytoplasmic tail that serves as a scaffold for intracellular

signaling (Counillon *et al*, 1993). Post-translational modification of NHE C-terminals can impact the transporter's activity, target the transporter to discrete areas of the membrane or influence turnover dynamics (Fuster and Alexander, 2014).

Table 3: Localization and tissue distribution of human NHE plasmalemmal proteins

NHE family member (protein/gene name)	Cellular localization	Tissue distribution
NHE1/SLC9A1	Plasma membrane Basolateral membrane of epithelial cells	Ubiquitous
NHE2/SLC9A2	Plasma membrane Apical membrane of epithelial cells	Gut, skeletal muscles, kidney, brain, uterus testis, heart and lung.
NHE3/SLC9A3	Plasma membrane Recycling endosomes of epithelial cells	Kidney, gut, heart, brain and lung.
NHE4/SLC9A4	Plasma membrane Basolateral membrane of epithelial cells	Gut, kidney, brain, uterus and skeletal muscles.
NHE5/SLC9A5	Plasma membrane Recycling endosomes and synaptic vesicles	Brain, testis, spleen and skeletal muscles.

(Adapted with permission from Fuster & Alexander, 2014, Springer License n° 4107700591546 and with permission from Zhao *et al*, 2016, Elsevier Science and Technology Journals License n° 4107711153866.)

Because of it's ubiquitous expression, NHE1 is mostly recognized for it's housekeeping functions. Its discrete localization at the plasma membrane may shift between different cell types, but its general function remains to control intracellular pH homeostasis by allowing electroneutral exchange through H^+ leakage and Na^+ influx driven by a strong electrochemical gradient. Na^+ influx is followed by Cl^- and H_2O intake which together act as an important mechanism to prevent cell shrinkage. Discrete plasma membrane localizations in polarized epithelial cells, cardiac myocytes and fibroblasts have all been associated with further functional roles in these cell types. In acinar cells of the parotid gland,

NHE1 was demonstrated to be important for fluid secretion and NaCl absorption (Park *et al*, 2001). In cardiac myocytes, the localization of NHE1 in microdomains with intercalated disks and T-tubules is believed to affect the activity of the pH sensitive ryanodine-sensitive Ca^{++} release channels by modulating Ca^{++} sensitivity of these channels (Xu *et al*, 1996). Thirdly, there is evidence that NHE1 concentrates to sites of focal adhesions in fibroblasts along the border of the lamellipodia which is believed to be important in cellular migration and chemotaxis (Denker *et al*, 2000). Most important in the context of this review is the uniquely recognized role of NHE1 in cancer progression among plasmalemmal NHE's. As for other regulators of the pH equilibrium of tumors, NHE1's function of alkalinizing intracellular pH favors prolonged survival of cancer cells, increased proliferation and is seen as a factor of malignant transformation (Reshkin *et al*, 2000). By concentrating at the leading edge, especially in the case of breast cancer, NHE1 contributes to increased proteinases degradation of the ECM and subsequently cell migration and metastasis (Denker, 2002).

As shown in table 3, NHE2-4 are each associated with a narrower tissue distribution than NHE1 and each serve for more specialized cellular functions. NHE2 is predominant in the gut where it is located in the apical membrane of epithelial cells and appears to be necessary for proper differentiation of these tissues (Schultheis, 1998). NHE3 has predominantly been studied for its role in renal physiology where it is critical for sodium reabsorption from the proximal tubule, regeneration of bicarbonate buffer in the proximal tubule and water reabsorption (Li *et al*, 2013). NHE4 also appears to play distinct role in the gut and kidneys although these are still poorly characterized. NHE5 is primarily expressed in the brain where it is important for dendritic spine growth and Trk tyrosine kinase trafficking (Diering *et al*, 2013). NHE5 and NHE3, which are closely related homologs, have the particularity of recycling between the cell surface and endosomes (Fuster and Alexander, 2014).

1.2.2 Intracellular Sodium/Hydrogen Exchangers

The four intracellular Na^+/H^+ exchangers, form an evolutionarily distinct subgroup within the larger NHE protein family. They are thus all closely related homologs that are ubiquitously expressed in human tissues and that are primarily located in organellar membranes rather than at the cell surface (Zhao *et al*, 2016). Of those exchangers, NHE6 and NHE9 are both

commonly located in distinct but overlapping endosomal compartments (Table 4) whereas NHE7 and NHE8 are usually located in the trans and medial Golgi respectively. Besides sharing a similar cellular localization, NHE6 and NHE9 are also highly expressed in the brain and neuronal cells more particularly. Inactivating mutations in either exchanger is also associated with neurological diseases (Table 4).

Table 4: Cellular location and diseases associated with human NHE intracellular proteins

NHE family member (protein/gene name)	Cellular localization	Known associated diseases
NHE6/SLC9A6	Sorting and recycling endosomes	X-linked Angelman-like condition Christianson syndrome Autism
NHE7/SLC9A7	TGN	Cancer
NHE8/SLC9A8	Medial Golgi to TGN	None
NHE9/SLC9A9	Late endosomes	Autism Epilepsy ADHD

(Adapted with permission from Fuster & Alexander, 2014, Springer License n° 4107700591546 and with permission from Zhao *et al*, 2016, Elsevier Science and Technology Journals License n° 4107711153866.)

The fact that NHE proteins are commonly expressed in the brain should not come as a surprise as many neural functions such as membrane voltage, ligand-gated ion channels, neurotransmitter systems, intracellular signal transduction and gap junction communication, are dependent on precise pH regulation (Takahashi and Copenhagen, 1996). Alkaline ECF is generally correlated with increased neural excitability, while acidic ECF has the opposite effect (Ruusuvuori and Kaila, 2014). Little is currently known of the physiological roles of NHE7 whereas NHE8 is believed to have largely redundant roles with NHE3 as it has a comparable tissue distribution in the kidneys and gut; and KO mice of the two exchangers display similar phenotypes (Xu *et al*, 2013). NHE8 however seems to play a larger role in

neo-natal individuals whereas the expression and activity of NHE3 is more important in adults (Becker *et al*, 2007).

The endosomal/lysosomal system is composed of fluid membrane endosomal compartments that gradually lean toward increasingly more acidic pH balance as it goes form early or recycling endosome (≈ pH 6.3-6.5), to late endosome (≈ pH 6.0) and lysosomes (≈ pH 5.0-5.5) (Ohgaki *et al*, 2011). The secretory pathway also forms increasingly more acidic compartments as it goes for the endoplasmic reticulum (ER, ≈ pH 7.2), to the Golgi (≈ pH 6.0-6.7) and to secretory vesicles (≈ pH 5.2-5.7). The finely tuned pH balance across these sub-cellular compartments is somewhat influenced by activity of V-ATPase but is more importantly determined by NHEs and chloride coupled proton exchangers (Steinberg *et al*, 2010). Maintenance of that pH balance is critical for endosomal pathway trafficking, dissociation ligand-receptor complexes and calibration of the enzymatic activity, such as that of lysosomal proteases (Ohgaki *et al*, 2011).

NHE6 is known to affect pH homeostasis in endosomes by pairing H^+ leakage with either Na^+ or K^+ entry. Although ion balance in endosomal compartments is likely also functionally relevant, it remains largely misunderstood to date. Inactivating mutations of NHE6 have been shown to result in over-acidification of endosomes, in a few cells models including polarized hepatoma HEPG2 cells (Ohgaki *et al*, 2010) and to disturb many of the functions dependent on proper pH regulation as described above (Ohgaki *et al*, 2010). In HeLa cells however, inhibition of NHE6 did not significantly alter endosomal pH as loss of NHE6 was compensated with expression of NHE9 (Roxrud *et al*, 2009).

Of the four intracellular NHE, there have been reported cases of NHE7 and NHE9 contributing to cancer progression. NHE7 was found to enhance cell-to-cell adhesion, invasion, anchorage-independent growth and to induce tumor formation and growth in an MDA-MB-231 cell model (Onishi *et al,* 2011). Alternatively, NHE9 was observed to contribute to cancer progression in glioblastomas by alkalinizing endosomes and preventing EGFR degradation, which caused sustained oncogenic signaling through MAPK and Akt pathways (Kondapalli *et al,* 2015).

Unlike for some of the plasmalemmal NHE's, for which many protein interactions and modifications of the C-terminal cytoplasmic tail that modulate exchanger activity and localization have been well characterized, understanding of how intracellular signaling affects intracellular NHE's is largely lacking.

1.3 The Versatile RACK1 Scaffolding Protein

The RACK1 protein, also known as guanine nucleotide-binding protein subunit beta-2-like-1 (GNB2L1), is an ubiquitous protein expressed by most eukaryotic organisms (Gibson, 2011). It was originally named RACK1 for receptor for activated C kinase 1 as it was first discovered as an interaction partner of protein kinase C (PKC). As is typical of proteins of the Tryptophan-Aspartate 40 (WD40) repeat family, RACK1 can be recognized by it's distinct 7 bladed beta-propeller structure (**Figure 3**) (Li and Xie, 2015). This particular shape is ideal for RACK1's role as a scaffolding protein as it allows it to interact with multiple partners at once as part of large protein complexes. These interacting proteins may serve a myriad of cellular functions and be present in diverse cellular localizations. In some cases, several WD40 repeat proteins can interact with each other (including RACK1 oligomers) to form even more intricate protein complex structures (Chen *et al*, 2004).

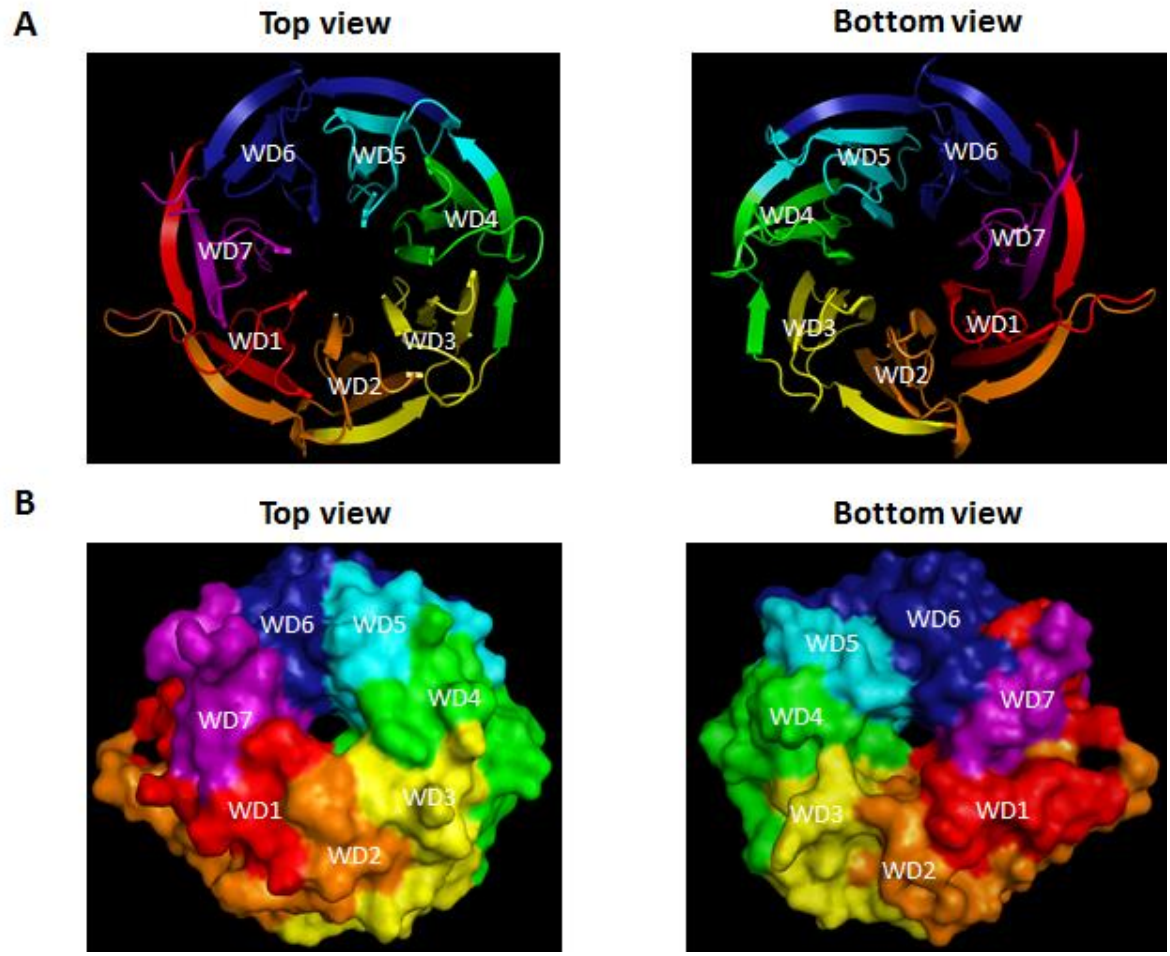

Figure 3. Three-dimensional structure of the RACK1 scaffold protein

A) Cartoon representation of the RACK1 protein and its 7 WD repeat domains each shown in a different color. **B)** Surface representation of the RACK1 protein and its 7 WD repeat domains each shown in a different color. Images captured with PyMOL Molecular Graphics System, Version 1.8 Schrödinger, LLC.

Aside from simply acting as a scaffold for protein complexes, RACK1 was proposed by Li and Xie to be capable of influencing its binding partners in four distinct ways. RACK1 is capable of "shuttling partners from one site to another, modifying the activity of the partners, changing intermolecular interaction (enhancing association/dissociation), and modulating the stability of binding proteins" (Li and Xie, 2015). An example of protein shuttling would be the matching shift in localization of RACK1 and PKC isozymes that occurs in several cell types following the activation of PKC (Ron *et al*, 1999). Binding of RACK1 and PKC, which requires PKC to be in an active conformation (Adams *et al*, 2011), has also been reported to result in increased PKC kinase activity (Ron *et al*, 1994).

Due to sheer number of direct or indirect interaction partners that have been associated with RACK1 throughout the years, the current section will need to be narrowed down to observations that have been made linking RACK1 to pH regulators and to the ambivalent role RACK1 plays in cancer. There have been multiple reports of RACK1 acting either as a pro-carcinogenic or as an anti-carcinogenic agent to date. Examples include the detailed molecular mechanisms that describe how RACK1 promotes or impairs proliferation or how it can tip anti- and pro-apoptotic signaling one way or another (Li and Xie, 2015). The current consensus in the research community is that the role RACK1 plays in relation to cancer is context dependent of the diverse signaling pathways it can interact with in different cell models.

Dr. Kanazawa and his research group, showed with a yeast-two-hybrid screening experiment that RACK1 was able of interacting with NHE6, NHE7 and NHE9 (Ohgaki *et al*, 2008). The WD40 domains 5-7 were sufficient to mediate those protein-protein interactions. The same study showed that RACK1 knockdown in Hela cells had the impact of elevating recycling endosome pH and of reducing basal cell surface levels of NHE6 in this cell model.

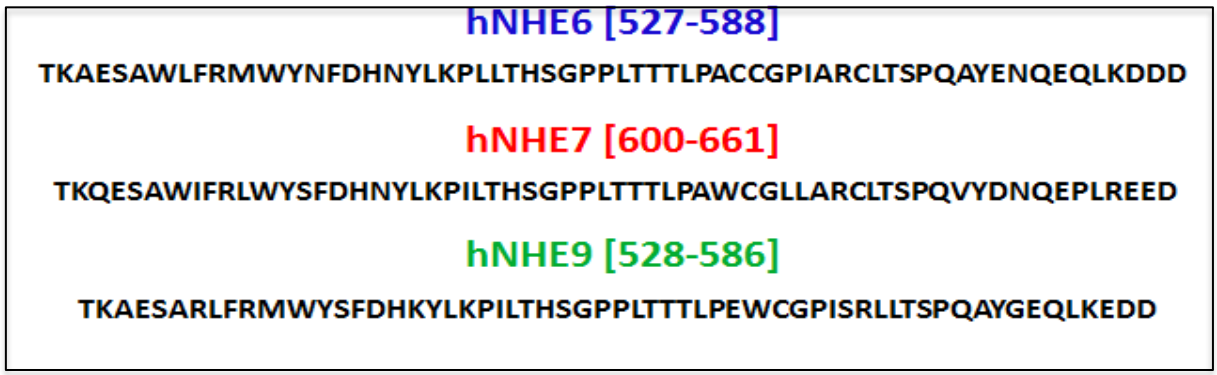

Figure 4. Sequences of interaction with RACK1 amongst human NHE proteins

Amino acid sequences of human NHE identified by Ohgaki et al (2008) to interaction with RACK1 protein.

Additionally, recombinant maltose binding protein (MBP) fusion protein pull-down experiments identified a sequence of 60 to 62 amino acids (the sequence in NHE9 is shorter by two residues) necessary for that interaction to occur (**Figure 4**) (Ohgaki *et al* 2008/2010). The team concluded that RACK1 can influence the distribution of NHE6 between endosomes and the cell surface to regulate endosomal pH.

The four influences RACK1 can have on interacting partners provide some clues to how RACK1 may help modulate NHE6 protein levels. An examination of reported examples of RACK1 involvement in anchorage of plasma protein is needed to gain a more complete understanding of how RACK1 may influence cellular pH regulation. The most detailed of such examples, is the interaction of RACK1, demonstrated in several cancer cell lines, with the cytoplasmic tail of IGF1R, which is required for the recruitment of proteins necessary for IGF1R signaling (Zhang *et al*, 2006). These proteins include Shc, insulin receptor substrate (IRS) 1/2 and activator of transcription factor 3 (Stat 3). Another prominent example of regulation of surface levels of a plasma membrane ion channel by RACK1 is that of cystic fibrosis transmembrane regulator (CFTR) in secretory epithelial cells (Smith *et al,* 2013). Although this particular study showed that RACK1 does not interact directly with CFTR, it also showed that RACK does interact directly with filamin A (FlnA), a cytoskeletal adaptor, and that this interaction is necessary to maintain cell surface levels of CFTR.

Another interesting insight into RACK1 signaling can be obtained from examining protein interactions from similar WD40 proteins. One such protein is the Gβ1 protein which is critical for G-protein coupled receptor (GPCR) signaling and which shares 57% homology with RACK1 in humans and is also composed of seven WD40 repeat domains (Chen *et al*, 2004). The Gβ1 protein interacts with Gα in a strong transient interaction in GPCR and, as is typical of strong transient interactions, is triggered to dissociate upon activation of the receptor. It is conceivable that RACK1 undergoes similar binding patterns with its many interaction partners.

With regard to metastasis and chemoresistance, RACK1 does seem to play a somewhat clearer role. RACK1 is necessary for stabilization of intermediate filament protein vimentin and focal adhesion kinase (FAK) that play an important role for endothelial cell invasion in the early stages of the metastatic cascade (Dave *et al*, 2013). RACK1 was also shown to colocalize with NHE5 at points of focal adhesions, which further hints at a role in cell migration (Ichiro *et al*, 2006). Unlike for the interaction between RACK1 and intercellular NHE exchangers, the binding domain for NHE5 was found to be contained in WD40 domains 1-3. Although, the NHE5 sequence interacting with RACK1 was not specifically identified, it would not correspond to the same sequence identified in intracellular NHE exchangers since that portion of the cytoplasmic tail is missing from NHE5. Finally, RACK1 was reported to control cell surface level of ABCG2 receptor in HeLa although the exact molecular mechanism was not elucidated (Ikebuchi *et al*, 2013). This same study showed that RACK1 overexpression induced resistance to mitoxantrone which was reversed upon treatment with the fumitremorgin C selective ABCG2 inhibitor.

Hypothesis

Following the initial observations described previously, we formulated the hypothesis that the localization of NHE6 plays an important role in both the endosomal/lysosomal acidification and loss of nuclear doxorubicin triggered by hypoxia. Additionally, we hypothesize that a direct protein-protein interaction with the scaffold protein RACK1 is critical for the development of a pH-dependent chemoresistance phenotype.

Our study was divided into two successive steps each associated with a main objective and a set of sub-objectives.

Objective #1: To evaluate the effect of hypoxia on the interaction of NHE6 with RACK1 in cancer cells, and to assess the impact of that interaction on pH-dependent chemoresistance.

- To assess the interaction between NHE6 and RACK 1 under hypoxia.
- To construct a peptide that can compete with the interaction of NHE6 with RACK1 and thus serve as a specific tool to evaluate the biological impacts of that interaction.
- To assess the effect of the NHE6-RACK1 competing peptide on pH-dependent chemoresistance.
- To investigate the upstream mechanism leading to NHE6/RACK1 interaction under hypoxia.

Objective #2: To identify key amino acid residues responsible for NHE6-RACK1 interaction.

- To determine the degree of conservation of residues within the RACK1 binding domain of human NHE6.
- To perform an *in-silico* analysis of the bio-chemical properties of the RACK1 binding domain.
- To locate the site of NHE interface at the surface of RACK1.
- To perform a protein-peptide docking protocol to approximate interface affinity between RACK1 binding sites and NHE6-derived peptides.

2. MATERIAL AND METHODS

2.1 Antibodies and Reagents

All antibodies used for co-immunoprecipitation (IP) or immunofluorescence (IF) were acquired from commercial suppliers. The rabbit monoclonal antibody against NHE6 was obtained from Abcam (Cambridge, UK). The anti-human influenza hemagglutinin (HA) epitope tag mouse monoclonal antibody was purchased from Covance (Princeton, NJ). Mouse and rabbit antibodies directed against RACK1 were respectively obtained from BD Biosciences (Franklin Lakes, NJ) and Cell Signaling Technologies (Danvers, MA). A mouse antibody for α-Tubulin was acquired from Sigma Aldrich (St. Louis, MO). Nigericin used for pH calibration solutions was also obtained from Sigma Aldrich. Mouse anti-EEA1 and anti-Rab5 were both purchased from Santa Cruz Biotechnology (Dallas, TX). All Alexa Fluor secondary antibodies, 4',6'-diamidino-2-phenylindole (DAPI), Hoechst 33342, lysotracker, pyranine (HPTS), EZ-Link^{TM} Sulfo-NHS-SS-Biotin, Streptavidin Texas Red conjugate, CellROX Green Reagent and Alexa-conjugated Transferrin were obtained from Thermo Fisher Scientific (Waltham, MA). Doxorubicin was obtained from the CHUS Fleurimont hospital pharmacy (Sherbrooke, Qc).

2.2 Cell Culture and Hypoxic Incubation

Adherent HT1080 fibrosarcoma cells (ATCC) were cultured in 15 cm petri dishes with Eagle's minimum essential medium (EMEM) while adherent MDA-MB-231 breast cancer cells were cultured with Dulbecco's Modified Essential Medium. Culture media were supplemented with 10% heat-inactivated fetal bovine serum (FBS) and 40μg/ml gentamycin. For cell subculture, a 0.25% Trypsin and 0.53mM EDTA phosphate-buffered saline (PBS) solution was used to detach the cells. A sub-culture ratio ranging from 1:4 to 1:10 was used for HT1080 cells and from 1:2 to 1:4 for MDA-MB-231 cells. Depending on the degree of confluence, the culture medium was, every 2-3 days, either replaced for fresh culture medium or the cells were passaged into new petri dishes. For the cell freezing procedure, freeze medium was made from fresh culture medium further supplemented with 10% FBS (for a total of 20% FBS) and with 10% dimethyl sulfoxide (DMSO). Cells (1-2 x10^6 depending on

the cell type) were aliquoted into CryoTubes and frozen at -80°C. Cell aliquots were subsequently transferred into liquid nitrogen for long term storage. Cell culture under normoxic environment was carried into a 37°C humidified atmosphere of 21% O_2 and 5% CO_2. Cell culture under hypoxic environment was carried into an In Vivo^2 400 hypoxia workstation (Ruskinn) with identical conditions except for 1% O_2 (depleted oxygen was replaced with nitrogen). Whenever it is mentioned in a protocol that cells are placed under hypoxia, corresponding cells are treated in the same manner under normoxia. Live cells were visualized using an Olympus FV1000 (Olympus, Tokyo, Japan) scanning confocal microscope and placed in a humidified chamber with controlled temperature (37°C) and CO_2 (5%).

2.3 Plasmid Constructs and Expression in Human Cell Lines

peGFP-N3-NHE6 variant 2 was a kind gift from Dr Hiroshi Kanazawa. Whenever amino acid sequence numbers are used to describe amino acids position in the current thesis, they will thus always refer to variant 2 of human NHE6. In order to construct the pcDNA3-HA/NHE6 plasmid, the segment corresponding to NHE6 coding sequence was removed from peGFP-N3-NHE6 using the BamH1 and EcoR1 restriction sites and spliced into pcDNA3-HA generously provided by Dr Jean-Luc Parent. The NHE6$^{527\text{-}588}$ segment was amplified from peGFP-N3-NHE6 using the following pair of primers:

forward 5'-ATGCGGATCCACCAAAGCAGAGAGTGCTTG-3'

reverse 5'-GCATGAATTCTTAATCATCATCTTTCAACTGTT-3'

The resulting fragment was subsequently inserted into pcDNA3-HA to yield the vector pcDNA3-HA/NHE6$^{527\text{-}588}$ which was then used for stable transfection. HT1080 cells were transfected with polyethylenimine (PEI, MirusBio, PA) whereas MDA-MB-231 cells were transfected with Lipofectamine 2000 (Sigma Aldrich). Cells were then selected using Geneticin (G418) at a concentration of 400µg/ml in the case of HT1080 cells and at a concentration of 2mg/ml in the case of MDA-MB-231 cells. peGFP-N3-NHE6 was transfected into HT1080 cells with PEI and into MDA-MB-231 cells with Lipofectamine 2000 for transient expression of eGFP-NHE6 and fluorescence microscopy visualization.

2.4 Intracellular pH Measurement

The pH sensing ratiometric dye pyranine (HPTS) was used for pH measurement of the endosomal/lysosomal compartments either alone or in conjugation with 5-(and-6)-Carboxy SNARF-1 used for pH measurements of the cytoplasm; both pH indicators were purchased from Life Technologies. Briefly, cells were cultured into 35mm petri dishes (BD Biosciences) to which was added 1mM of HPTS for a total of 16h for HT1080 cells and 40h for MDA-MB-231 cells (in which endocytosis is slower). Two hours prior to hypoxic stimulation, culture medium was replaced with serum-free medium for starvation and fresh HPTS was added. Cells were then placed at 1% O_2 or left at 21% O_2 for a total of 4h. When cytoplasmic pH measurement was performed, 5 μM SNARF-1 was added for the final 20 min of the 4h incubation. Serum-free medium that had been equilibrated for 6h into the hypoxia workstation was used to wash the excess HPTS and SNARF-1 probes from cells incubated in hypoxia. Live cells were then brought to the confocal microscope where and the petri dish containing the cells was mounted directly in the petri dish imaging chamber under a controlled environment. Pictures were rapidly taken using a 40x objective and fluorescence emission was recorded to be later converted into pH values. Further details of the technique have been described in a previous study (Lucien *et al.*, 2014).

2.5 Intracellular Localization of Doxorubicin

Adherent HT1080 cells were seeded onto 25mm diameter glass coverslips (Thermo Fisher Scientific) placed inside 35mm petri dishes and allowed to grow to a confluence of approximately 20%. EMEM culture medium was replaced with 0.5% FBS medium for an overnight starvation. The next morning, a 50ml falcon was filled with 0.5% FBS EMEM and placed into the hypoxia workstation for 6h to equilibrate the O_2 concentration. Cell culture medium was changed for fresh EMEM and cells were either kept in the incubator or placed into the hypoxia workstation for 4h. Following 1h of hypoxic incubation, doxorubicin was added to the culture medium at a concentration of 2μM. Hoechst 33342 was then added 1h30 min later at a concentration of 5 μg/ml. After cell exposition to doxorubicin for 2h, the cells were washed with fresh 0.5% FBS EMEM and incubated for 1h. Cells were washed once again immediately before visualization; the glass coverslip on which cells were cultured was transferred to a rack adapted to the microscope platform and 1ml of EMEM was added to the

chamber atop the cells. Live HT1080 cells were brought to the confocal microscope and the rack was placed into the controlled environment chamber. A 63x objective was used with immersion oil to visualize the cells; a 405nm diode laser was used to excite the Hoechst stain fluorophore and a 543nm helium neon laser to excite the doxorubicin fluorophore. Doxorubicin light emission was collected between wavelengths of 580nm and 625nm. Typically, 5 pictures were taken for each petri dish with 2-3 cells per field thus yielding 10-15 cells to be analyzed for each condition. Image analysis was performed using the Fluoview software package. For both probes, intensity thresholds were set to remove any background, these thresholds were maintained constant for the analysis of all series of pictures in the experiment. For each cell, the percentage of nuclear doxorubicin was calculated by doing a ratio of doxorubicin signal intensity co-localized with positive Hoechst pixels over the total doxorubicin intensity. Average nuclear doxorubicin was then calculated for each series (corresponding to one petri dish and one experimental condition).

2.6 Immunofluorescence

Adherent cells were cultured on 15mm diameter glass coverslips (Thermo Fisher Scientific) inside well plates. Following the appropriate treatments, cells were fixed in 1% paraformaldehyde (PFA) dissolved in PBS, for 10 min at room temperature. From this step onward, cells were kept from direct exposure to light. Afterwards, cells were permeabilized in 0.05% Saponin (Sigma Aldrich) for 20 min and blocked in 2% bovine serum albumin (BSA) for 30 min; both steps were carried at room temperature and both compounds were dissolved in PBS. Cells were incubated with the primary antibody for 1h30 min at room temperature and, following a quick wash step, were then incubated with the secondary antibody for 1h at 4°C. Specific antibodies and their dilutions in the 2% BSA solution are listed in the table below (Table 5). Nuclear staining was performed by incubating the cells for 5 min at room temperature with DAPI. Cells were mounted on a microscope slide with VECTASHIELD Antifade Mounting Medium (Vector Laboratories, Burlingame, CA) to protect fluorophores from photobleaching. Images were taken with a scanning confocal microscope using a 63x objective with immersion oil. On seldom occasions, images were alternatively taken using an Axioskop 2 phase-contrast/epifluorescence microscope (Carl Zeiss, Thornwood, NY).

Table 5: Listing of antibodies used for IF and their dilutions

Targeted against	Tag	Host	Class	Supplier	Dilution
HA epitope tag	None	Mouse	Monoclonal	Covance	1:500
EEA1	None	Mouse	Polyclonal	Santa Cruz	1:100
Rab5	None	Mouse	Polyclonal	Santa Cruz	1:100
Mouse	Alexa Fluor 488	Goat	Polyclonal	Thermo Fisher	1:200
Mouse	Alexa Fluor 543	Goat	Polyclonal	Thermo Fisher	1:200

2.7 Cell Surface Biotinylation

Adherent cells transiently expressing eGFP-NHE6 were cultured in 12-well plates and grown to approximately 70% confluence on 15mm diameter glass coverslips (Thermo Fisher Scientific). The experiment was carried in duplicates for each cell line and experimental condition. Culture medium was replaced with fresh serum free medium and cells were left undisturbed for 2h prior to the hypoxic stimulation. Both PBS C/M (1mM $CaCl^2$/0.5mM $MgCl^2$) and a quenching solution (PBS C/M + 750mg Glycine) were freshly prepared and an aliquot of each of these solutions was placed in the hypoxic chamber for a total of 6h before use in order to equilibrate the O_2 concentration. Half of the cells were placed into the hypoxic workstation for a duration of 4h. EZ-Link™ Sulfo-NHS-SS-Biotin (Thermo Fisher Scientific) was dissolved into PBS C/M at a concentration of 0.3mg/ml immediately before use. After being washed three times with PBS C/M, the cells were covered with the biotin solution and incubated for 5 min with a gentle rocking motion. The biotin solution was removed and the cells were washed twice with the quenching solution to cleave any excess Biotin reagent that may not have yet reacted. Cells were then removed from the hypoxic workstation and immediately fixed for 10 min at room temperature in 1% PFA dissolved in PBS. Afterwards, cells were washed thoroughly with PBS and blocked for 1 h in 5% BSA dissolved in PBS (pH adjusted at 8.0). Streptavidin Texas Red conjugate (Thermo Fisher Scientific) diluted to 5µg/ml in the 5% BSA solution mentioned above was used to stain biotinylated cell-surface proteins (and other biomolecules containing primary amines) for 1h at 4°C. Coverslips were washed and mounted on microscope slides using VECTASHIELD Antifade Mounting Medium (Vector Laboratories).

The scanning confocal microscope was used with a 63X objective to take pictures of 15-20 cells per experimental condition; pictures were taken at the depth representing the widest surface area for each cell. Duplicates were used only if one coverslip was unusable or broken. The cells systematically selected for data analysis were all of normal size (outliers were excluded), had even biotin staining at the cell-surface and had similar levels of eGFP-NHE6 fluorescence intensity. The Fluoview software package was used for quantification of plasma membrane eGFP-NHE6. Intensity thresholds were set for both eGFP and Texas Red in order to remove any background or non-specific signal. These thresholds were kept constant for the analysis of all the series of pictures included in the experiment. For each cell, the percentage of cell membrane eGFP-NHE6 was calculated by performing a count of eGFP-NHE6 positive pixels co-localized with the biotin labeled cell membrane and dividing with the total number of eGFP positive pixels. For each series, the average cell membrane percentage of eGFP-NHE6 was calculated.

2.8 Complementary Confocal Microscopy Protocols

Alexa-Fluor 546-conjugated transferrin (Thermo Fisher Scientific) was added to adherent cells at a concentration of 25μg/ml for 30 min prior to live cell visualization in order to mark early and recycling endosomes. This protocol was used either in conjugation with the HPTS probe or in cells expressing eGFP-NHE6. Similarly, cells were stained with lysotracker deep red (Thermo Fisher Scientific) for 30 min at 100nM to mark lysosomes. CellROX Green Reagent (Thermo Fisher Scientific) was used as an indicator of reactive oxygen species (ROS). The fluorescent probe was added to adherent cells at a concentration of 5μM for 30 min before being washed and brought to the confocal microscope for visualization. A 40mWnm diode laser was used to excite the CellROX Green Reagent probe at 488nm. The fluorescent signal was collected around the emission maximum of 520nm. Light emission intensity, reflecting the extent of oxidative stress, was quantified in arbitrary units using the Fluoview software package. The average fluorescence intensity per cell was calculated; in order to stain the nuclei and differentiate between individual cells Hoechst 33342 was used (see above procedure). This technique was also applied in conjugation with the intracellular localization of doxorubicin protocol.

2.9 Western Blotting and co-Immunoprecipitation

Cells were grown in 10 or 15cm petri dishes to a confluence of approximately 70%, serum starved for 2 h and lysed on ice with NP-40 lysis buffer (50 mM Tris-HCL pH 8.0, 150 mM NaCl, 1% NP-40, 5mM EDTA, phosphatase and protease inhibitors) after indicated stimulations (see Figure legends). Time-courses of hypoxic stimulations were performed using intermittent start times to allow simultaneous harvesting of the cells from all experimental conditions. Cell lysates were collected and mildly agitated for 30 min before being centrifuged at 13,000 RPM (30 min, 4°C) in order to recover sample supernatant. Protein concentration in each sample was determined using the colorimetric BCA reagent (Thermo Fisher Scientific) in accordance with manufacturer's instructions.

Samples prepared for co-IP were adjusted to equal protein concentrations in 500µl lysis buffer (ranging from 350 to 500µg depending on the experiment). Remaining total protein lysates were kept at 4°C to serve as inputs. Samples were pre-cleared for 45 min using protein G-agarose beads (Sigma Aldrich) and supernatants were collected. Protein lysates were conjugated with the corresponding antibody by incubating overnight at 4°C with mild agitation. Protein G-agarose beads were added to the lysates the following morning and allowed to bind antibodies for 3h at 4° with mild agitation. Following thorough washing with NP-40 buffer, the beads were suspended into 30µl of 4X Laemmli loading buffer (250mM Tris-HCl pH 6.8, 4% sodium dodecyl sulfate [SDS], 40% Glycerol, 0.05% bromophenol blue). Similarly, Laemmli loading buffer was added to inputs (20µg of proteins) in a 1:3 ratio to obtain a 1X concentration. β-mercaptoethanol was added separately to either sample at a concentration of 5%. Samples were incubated for 30 min at room temperature in Laemmli buffer; this variation of protein denaturation is done alternatively to boiling to avoid creating transmembrane protein aggregates. Separating gels of 10% acrylamide (40% Acrylamide: Bis-Acrylamide 35.5:1, Thermo Fisher Scientific) and stacking gels of 4% Acrylamide were freshly prepared. SDS polyacrylamide gel electrophoresis (PAGE) was used to separate proteins by migrating in a running buffer (0.1% SDS, 25mM Tris-Base and 192mM Glycine) for approximately 90 min at 110V. Proteins were subsequently transferred from the gel onto a polyvinylidene fluoride membrane (PVDF, Sigma Aldrich) using a wet transfer apparatus filled with transfer buffer (20% methanol, 25mM Tris-Base and 192mM glycine). PVDF membranes were washed for 20 min in Tris-buffered saline (TBS) and placed in a Blotto-

Tween 20 blocking solution (5% non-fat carnation dry milk, 0.05% Tween 20 in a TBS solution) for 1h on a rotary plate. Membranes were then immunoblotted with the primary antibody overnight at 4°C on a rotary plate; antibody concentrations were optimized with manufacturer's instructions. Membranes were then submitted to appropriate wash steps and incubated for 3 h with horseradish peroxidase (HRP) conjugated secondary mouse or rabbit antibodies (Abcam) at a concentration of 1:10000. HRP chemiluminescence detection was performed using the Luminata Crescendo HRP substrate (EMD Millipore, Billerica, MA) as well as autoradiography hyperfilms.

2.10 Multiple Sequence Alignment and Conservation Analysis

Human Na^+/H^+ exchanger protein family was constructed from the 9 coding sequences from UniProt.org database corresponding to the longest isoform of each protein. The evolutionary relationship between these proteins was captured in a Newick tree format which was then used as input in phytools to visualize and customize the phylogenetic tree.

Included in the multiple sequence alignment were the three human paralog sequences for NHE6, NHE7 and NHE9. Corresponding orthologs for two other mammalian species, the mouse and the giant panda, with highly homologous sequences, were also included in the bank of protein sequences. Additionally, seven more distantly related species (under 80% homology between NHE6 and homolog) were selected for the bank of protein sequences; considering the low number of sequenced NHE orthologs outside the clade of mammals, these species were selected on basis of availability on the UniProt.org database. Only orthologs including a cytoplasmic segment in their sequence were conserved for multiple sequence alignment (MSA). The number of identified paralogs eligible for analysis per species ranged from one to three; the entire dataset yielded twenty-five protein sequences. MSA was performed by entering UniProt identifiers into the Uniprot.org sequence alignment tool. The Jalview software was used to visualize the MSA output and to calculate amino acid residue conservation scores. Conservation index calculation is based on the Analysis of Multiply Aligned Sequences (AMAS) method of MSA (Livingstone, 1993) and measures the conservation of physico-chemical properties of amino acid residues.

2.11 Protein Disorder Propensity Analysis

We explored four possible prediction methods for protein disorder propensity. The first of these is Meta-Disorder predictor (MD_raw) which is a neural-network based predictor that uses multiple independent sources of information to make predictions. The second predictor explored was the NORSnet method which is also based on neural network and focuses on distinguishing between long segments with non-regular secondary structures and well-folded proteins. The next prediction tool examined was the Ucon method which combines protein internal contacts with pairwise energy potentials to predict long unstructured regions. Lastly, we also looked at the PROFbval method which predicts the flexibility or rigidity of residues based on protein sequence. For our application, in which we aimed to reveal disorder differences on a micro level, we found that the MD_raw and Ucon methods provided the most sensitivity. These two methods also correlated closely with one another and were thus the two methods of choice used for our study. The standardized disorder scores were calculated by converting the lowest score for any individual residue within the protein to 0, the highest score to 1 and by grading any other scores obtained along that scale. This approach allowed comparing directly the scores obtained through either method.

2.12 3D Molecular Visualization

The PDB file named 4AOW for human RACK1 was obtained on the Research Collaboratory for Structural Bioinformatics (RCSB) protein data bank (PDB) website. The reported protein structure (Ruiz Carrillo, 2012) corresponds to crystals of three molecules and is available at a resolution of 2.45Å. PDB files were viewed using PyMOL 3D molecular visualization system.

2.13 3D Peptide Folding and Molecular Docking Refinement Protocol

PEP-FOLD 2.0 (Shen *et al*, 2014), a tool for *de novo* peptide structure prediction, was used to generate likely 3D peptide structures from original 10 aa FASTA sequences corresponding to NHE6 regions of interest. From the 10 peptides generated with each sequence, only the first model was used as an initial conformation for the subsequent molecular docking refinement protocol.

Input models for molecular docking protocols were prepared using PyMol viewer. Previously generated peptides were manually placed in the vicinity of predicted sites at the surface of RACK1. Those positions were saved into PDB files containing coordinates of the two molecules and submitted to the FlexPepDock protocol (Raveh *et al*, 2010), designed for high resolution modeling of peptide-protein interactions. The FlexPepDock protocol yielded 200 possible structures (combinations of positions and conformations) obtained by trial and error for each peptide. This protocol obeys the Rosetta method and uses a Monte Carlo algorithm for conformational energy minimization. With each structure was calculated an interface energy score (I_sc), which is an indication of the stability of the complex formed. I_sc is expressed in Rosetta energy units. For each peptide, the structure with the lowest I_sc, which represents the most energetically favourable interaction, was selected and conserved for data analysis.

2.14 Statistical Analysis

Two-tailed paired or unpaired Student's t-test were used to determine statistical differences between groups of data. The confidence level for statistical difference was set at 95% with *: $p \leq 0.05$, **: $p \leq 0.01$, ***: $p \leq 0.001$. Linear correlation of data was performed to determine the Pearson r coefficient; the confidence interval was set at 95%.

3. RESULTS

Adherent HT1080 fibrosarcoma cells were used as the primary model in studying the interaction between NHE6 and RACK1 proteins. This cell line offered the handling advantages of dividing fairly rapidly and they can be easily transfected. This hypoxia responsive cell line was thus a convenient model to establish proof-of-concept and to investigate a novel mechanism involved in pH-dependent chemoresistance. Additionally, MDA-MB-231 mammary gland adenocarcinoma cells were used to confirm results from some of the key experiments. MDA-MB-231 were a more challenging cell line to handle due to slower division and to being a less-efficient transfection host; however, this cell line serves as a model for breast adenocarcinoma for which anthracyclines are commonly used as first line treatment in the clinic.

The results falling under objective #1 and its sub-objectives are covered in sub-sections 3.1 to 3.5 whereas the results falling under objective #2 are covered in sub-sections 3.6 to 3.9.

3.1 Exposition to Hypoxia Induces Formation of a Complex Between Transiently Expressed NHE6 and RACK1.

Co-immunoprecipitation assays were used to determine whether hypoxia affects the formation of a complex between transiently expressed NHE6 and the native RACK1 protein. HT1080 cells were transiently transfected with pcDNA3-HA or pcDNA3-HA/NHE6 and either kept in normoxia or placed under hypoxic condition for the indicated amount of time. NHE6-HA was immunoprecipatated with an anti-HA mouse monoclonal antibody. Levels of α-tubulin and of RACK1 in total lysates were fairly consistent among samples (Figure 5A). Expression of NHE6-HA was also consistent and immunoprecipitation of the protein was even across the four samples. The intensity of the RACK1 band in NHE6 immunoprecipitates was barely detectable for cell samples incubated at 21% O_2, but increased with longer incubation times at 1% O_2 (Figure 5A). Immunoprecipitated RACK1 bands were quantified and shown to increase by 16 folds for cells kept 4h in hypoxia compared to cells kept in normoxia (Figure 5B). A separate but similar experiment was performed where a 30 min incubation time at 1% O_2 was included (Figure 5C).

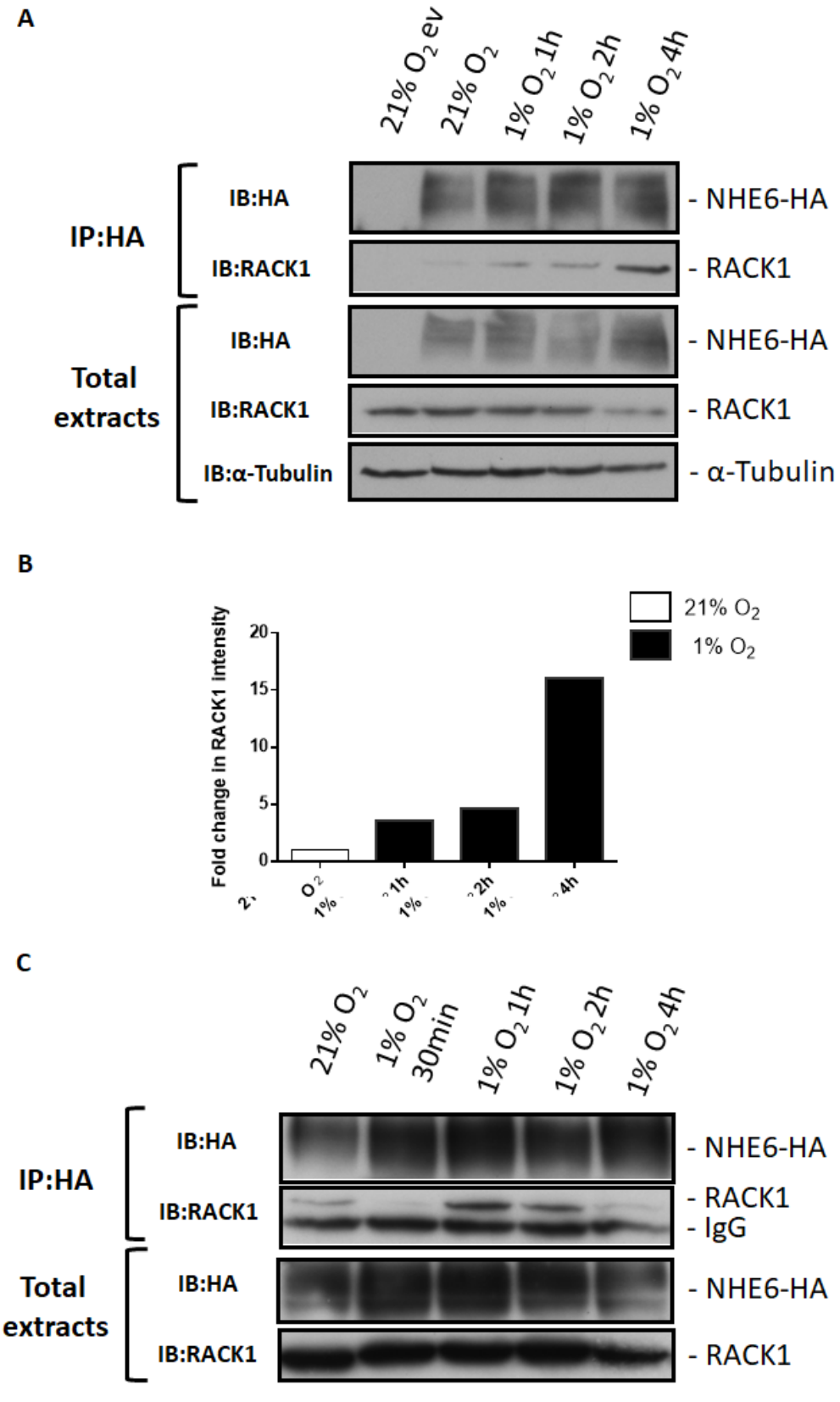
A
21% O2 ev
21% O2
1% O2 1h
1% O2 2h
1% O2 4h
IP:HA
IB:HA
- NHE6-HA
IB:RACK1
- RACK1
Total extracts
IB:HA
- NHE6-HA
IB:RACK1
- RACK1
IB:α-Tubulin
- α-Tubulin
B
21% O2
1% O2
Fold change in RACK1 intensity
20
15
10
5
0
C
21% O2
1% O2 30min
1% O2 1h
1% O2 2h
1% O2 4h
IP:HA
IB:HA
- NHE6-HA
IB:RACK1
- RACK1
- IgG
Total extracts
IB:HA
- NHE6-HA
IB:RACK1
- RACK1

Figure 5. Co-Immunoprecipitation of RACK1 with Transiently Expressed NHE6-HA in Cells Subjected to Hypoxia

A) HT1080 cells were incubated at 21% O_2 or 1% O_2 for the indicated period of time. Total cell extracts were collected following cell lysis whereas the remaining cell lysates were incubated with mouse anti-HA monoclonal antibodies and protein G-agarose beads. An anti-RACK1 rabbit monoclonal antibody was used to reveal RACK1. The first lane corresponds to experimental control samples where ev describes HT1080 cells transfected with pcDNA3-HA empty vector. The remaining lanes represent HT1080 cells transiently expressing NHE6-HA. Transient transfections were performed 24h ahead of the first incubation times. B) Quantification of RACK1, shown in A, that co-precipitate with NHE6. The slight band for the cells incubated at 21% O2 was set to a default value of 1. The bands corresponding to cells incubated at 1% O2 were expressed in fold change. C) Same general procedure as in A with the exception that an anti-RACK1 mouse monoclonal antibody was used.

Endogenous RACK1 levels as well as expression of NHE6-HA in total cell extracts were relatively constant across all experimental conditions. NHE6-HA was fairly well immunoprecipitated in all samples, but the presence of co-immunoprecipitated RACK1 was clearly more elevated in cells incubated in hypoxia for 1h and 2h. In this particular experiment, the amount of RACK1 in complex with NHE6 clearly diminished at the longer incubation time of 4h. Two additional experiments (not shown) also displayed an increase in co-immunoprecipitated RACK1 in cells exposed to hypoxia with peak amounts of RACK1 observed during the 1 to 4h incubation period. The kinetics of co-precipitated RACK1 were too variable to gain any additional insight from combining the results in a single densitometry.

3.2 Cellular Expression of a Peptide Derived from the SLC9A6 Gene.

The portion of the SLC9A6 gene corresponding to $NHE6^{527-588}$ was isolated and amplified from peGFP-N3-NHE6 and then inserted upstream from the HA-tag coding sequence of the pcDNA3-HA vector. A positive clone obtained through sub-cloning was sequenced at the Génome Québec Innovation Centre (McGill University) to insure accuracy of the cloning and identity of the cloned sequence. Expression of the HA-tagged peptide was initially validated in HT1080 cells (**Figure 6**) and MDA-MB-231 cells (results not shown) by immunofluorescence using an anti-HA mouse monoclonal antibody. Negative controls were performed using cells transfected with pcDNA3 and no fluorescent signal was detected in

those samples (data not shown). A strong speckled pattern of fluorescence was revealed in cells overexpressing the NHE6$^{527-588}$ peptide (**Figure 6**). We failed to detect the NHE6$^{527-588}$ peptide by immunoblotting presumably due to its small size (predicted to be 7KDa).

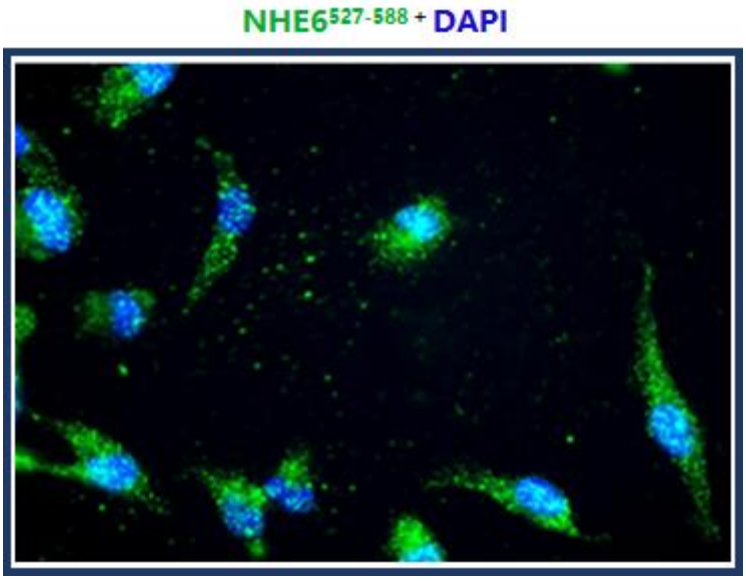

Figure 6. Immunofluorescence image of the NHE6$^{527-588}$ peptide

The HA-tagged NHE6$^{527-588}$ peptide was transiently expressed in HT1080 cells. Anti-HA mouse monoclonal antibody was used to detect the peptide in fixed cells. Cells were then stained with anti-mouse Alexa-fluor 488 antibody and observed under a Zeiss Axioskop 2 phase-contrast/epifluorescence microscope.

3.3 Assessment of the Functional Effects from Expression of the NHE6$^{527-588}$ Peptide.

3.3.1 Expression of the NHE6$^{527-588}$ Peptide Prevents Formation of an Hypoxia-Inducible Complex between Transiently Expressed NHE6 and Endogenous RACK1.

Co-immunoprecipitation experiments were performed in order to determine whether the expression of the NHE6$^{527-588}$ peptide affects hypoxia-induced formation of a complex between NHE6 and RACK1. The peGFP-N3-NHE6 vector was transiently transfected into either parental MDA-MB-231 cells or MDA-MB-231 cells stably expressing the NHE6$^{527-588}$ peptide. No control lacking transfected peGFP-N3-NHE6 vector was included in this particular experiment. For the parental cell line, either pcDNA3-HA or pcDNA3-HA/NHE6$^{527-588}$ was transiently transfected alongside peGFP-N3-NHE6. NHE6-GFP was immunoprecipitated with an anti-GFP rabbit polyclonal antibody. Total protein extracts

yielded similar levels of RACK1 and NHE6-GFP across all 4 samples (**Figure 7**). Despite seemingly less effective NHE6 immunoprecipitation, the sample from control cells (ev) exposed to hypoxia for 4h, clearly yielded the highest amounts of RACK1 proteins in the NHE6 immunoprecipitate. In comparison, a smaller amount of RACK1 (-0.65 fold change) was detected in the NHE6 immunoprecipitate from cells transiently expressing the $NHE6^{527-588}$ peptide whereas the sample stably expressing $NHE6^{527-588}$ peptide yielded no visible RACK1. Similar results were obtained with HT1080 cells overexpressing the $NHE6^{527-588}$ peptide (data not shown). We concluded that the $NHE6^{527-588}$ peptide indeed acted as an inhibitor of NHE6/RACK1 complex formation and that stable expression of this peptide was more effective than its transient expression. Subsequent experiments were thus performed using the stably expressing $NHE6^{527-588}$ MDA-MB-231 cell line.

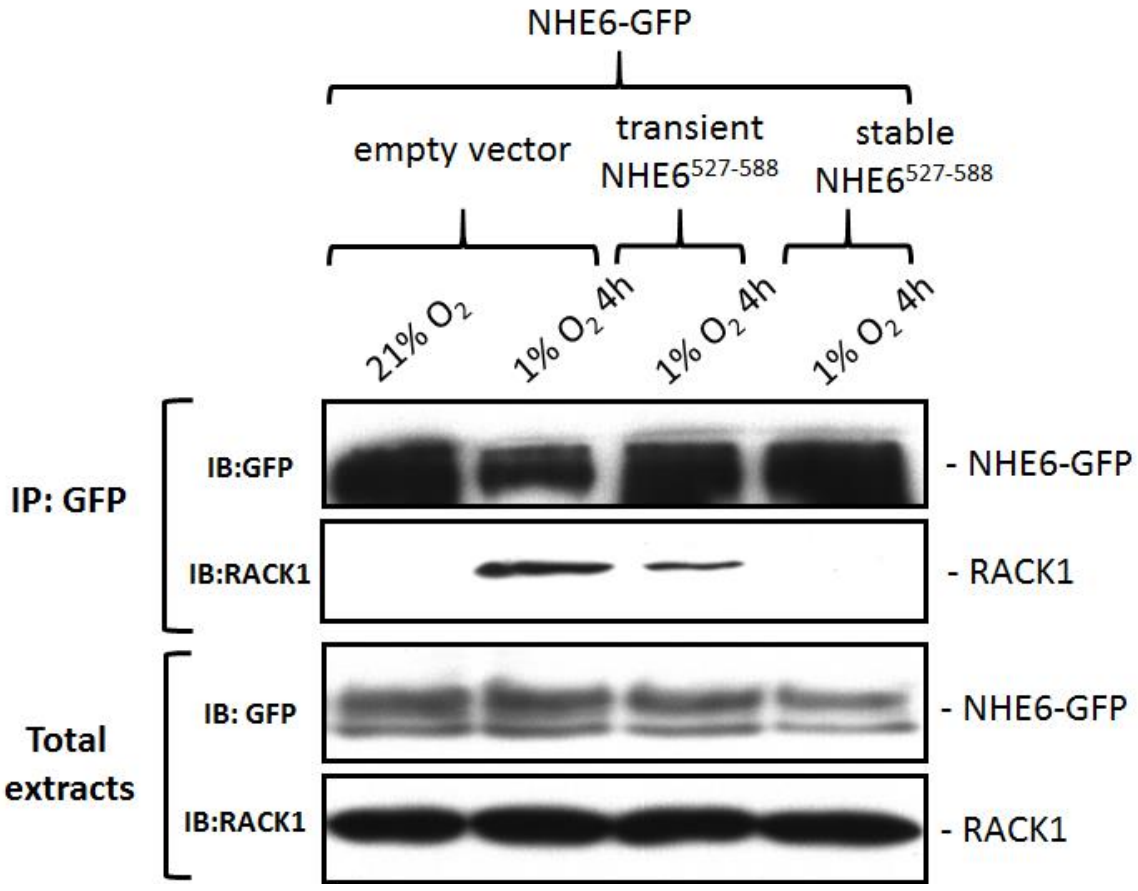

Figure 7. Co-Immunoprecipitation of RACK1 and NHE6-GFP in MDA-MB-231 cells overexpressing the NHE6$^{527-588}$ peptide.

Parental MDA-MB-231 (control cells) or MDA-MB-231 cells stably expressing pcDNA3-HA with encoded NHE6$^{527-588}$ peptide were transiently transfected with peGFP-N3-NHE6. Additionally, control cells were co-transected with pcDNA3-HA or pcDNA3-HA/NHE6$^{527-588}$. Transient transfections were performed 48h prior to incubation at 21% O_2 or 1% O_2 for 4h as previously described. Cell lysates were incubated with rabbit anti-GFP polyclonal antibodies and protein A-agarose beads. An anti-RACK1 mouse monoclonal antibody was used to reveal RACK1.

3.3.2 Hypoxia Favors NHE6 Plasmalemmal Localization in Human Cancer Cell Lines; this Trend is Countered by Expression of the NHE6$^{527-588}$ Peptide.

A cell-surface biotinylation protocol was adapted to allow simultaneous visualization of eGFP-NHE6 and its quantification at the plasma membrane. For this purpose, sulfo-NHS-SS-Biotin with Streptavidin Texas Red conjugate were used to stain cell-surface proteins. HT1080 cells incubated under hypoxia for 4h showed a distinct change in the pattern of eGFP-NHE6 distribution with an increased overlap between the eGFP-NHE6 and the cell-surface biotin signals (**Figure 8A**). The proportion of eGFP-NHE6 overlapping with the plasma membrane was shown to be significantly higher in cells incubated in hypoxia (HT1080, p=0.0063; MDA-MB-231, p=0.0019) (**Figure 8B**). Similar results were observed in HT1080 cells although plasmalemmal levels were comparatively higher in these cells. Stable expression of the NHE6$^{527-588}$ peptide prevented the increased plasmalemmal localization of eGFP-NHE6 in HT1080 cells incubated for 4h in hypoxia (NHE6$^{527-588)}$, p=0.6637) (**Figure 8C**).

A

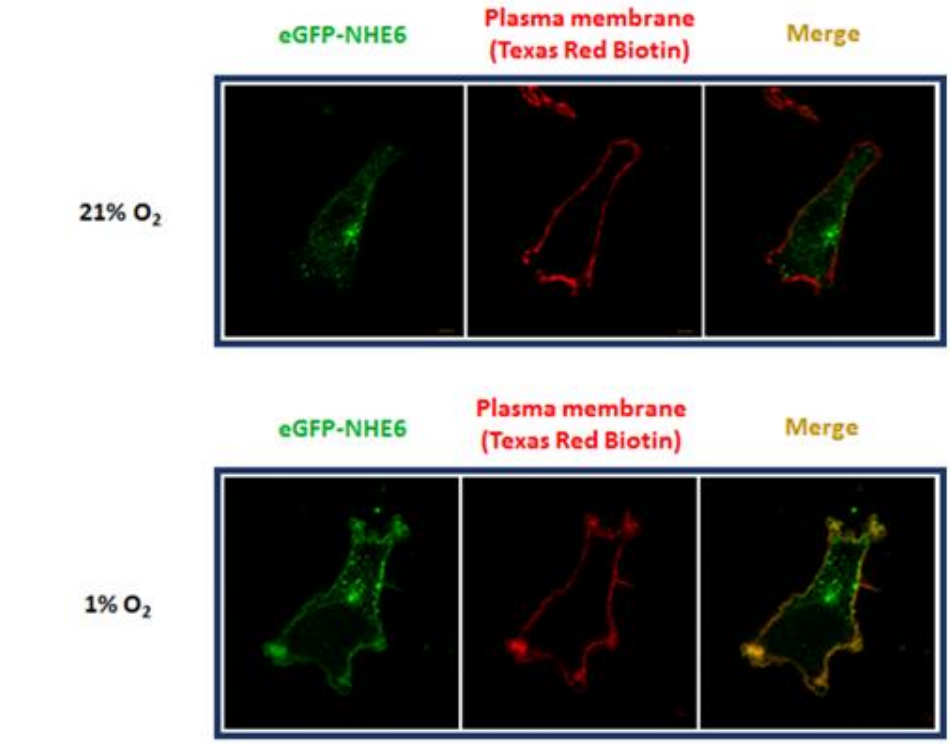
eGFP-NHE6
Plasma membrane
(Texas Red Biotin)
Merge
21% O2
eGFP-NHE6
Plasma membrane
(Texas Red Biotin)
Merge
1% O2

B

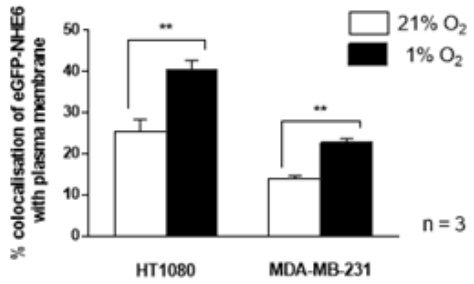
% colocalisation of eGFP-NHE6 with plasma membrane
50
40
30
20
10
0
**
**
21% O2
1% O2
n = 3
HT1080
MDA-MB-231

C

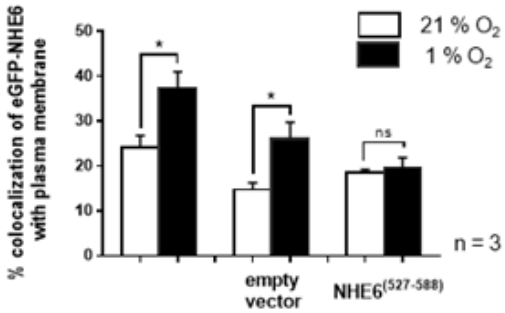
% colocalization of eGFP-NHE6 with plasma membrane
50
40
30
20
10
0
*
*
ns
21 % O2
1 % O2
n = 3
empty vector
NHE6(527-588)

Figure 8. Subcellular localization of NHE6 in hypoxia.

A) Representative images of transiently expressed eGFP-NHE6 in HT1080 cells incubated under normoxic and hypoxic conditions. Sulfo-NHS-SS-Biotin in conjugation with Streptavidin Texas Red conjugate were used to stain cell-surface proteins (including glyco-proteins) thus acting as a proxy for the cell membrane. Cells were kept in hypoxia (1% O_2) for 4h. **B)** The percentage of eGFP-NHE6 present at the plasma membrane was quantitated in both HT1080 and MDA-MB-231 cells by using the overlapping signal from Biotin. **C)** The percentage of eGFP-NHE6 at the plasma membrane was similarly quantitated in stably expressing $NHE6^{(527-588)}$ HT1080 cells (or empty vector expressing cells). The asterisks used to indicate statistical differences correspond to: * $p<0.05$, ** $p<0.01$ and *** $p<0.001$.

3.3.3 The Acidification of the Endosomal/Lysosomal pH in Cells Exposed to Hypoxic Conditions is Attenuated by Expression of the $NHE6^{527-588}$ Peptide.

As previously reported (Lucien *et al.*, 2014), incubation of live cells with HPTS has the result of incorporating the probe into endosomes and lysosomes, which allows subsequent ratiometric measurements of the pH in these cell compartments. The adequate localization of the probe was validated for both HT1080 and MDA-MB0231 cells by co-incubating the cells with transferrin and lysotracker, respectively used to label endosomes and lysosomes, respectively. HPTS was shown to localize in similar proportions in endosomes and lysosomes in HT1080 cells (**Figure 9A**) whereas it primarily localized in endosomes in MDA-MB-231 cells. In both cases, HPTS was predominantly localized in either endosomes or lysosomes with only 8.7% and 8.0% of the probe respectively excluded from either compartment. Different incubation times in hypoxia were performed and revealed that both the endosomal and lysosomal compartments were effectively acidified in HT1080 cells at the 3h and 4h time points (3h, p=0.0111; 4h, p=0.0015) (**Figure 9B**). The sharpest decrease in pH was observed in cells incubated 4h in hypoxia, with values ranging from 6.6 in normoxia to 5.8; longer incubation times in hypoxia yielded similar results to the 4h time point (not shown). Endosomal/lysosomal acidification in hypoxia was also observed in MDA-MB-231 cells at the 4h time point (**Figure 9C**). Expression of the $NHE6^{527-588}$ peptide in cells prevented or attenuated acidification of the endosomal/lysosomal compartments in both HT1080 and MDA-MB-231 cell lines (HT1080 $NHE6^{527-588)}$, p=0.5286; MDA-MB-231 $NHE6^{527-588)}$; p=0.5693).

A

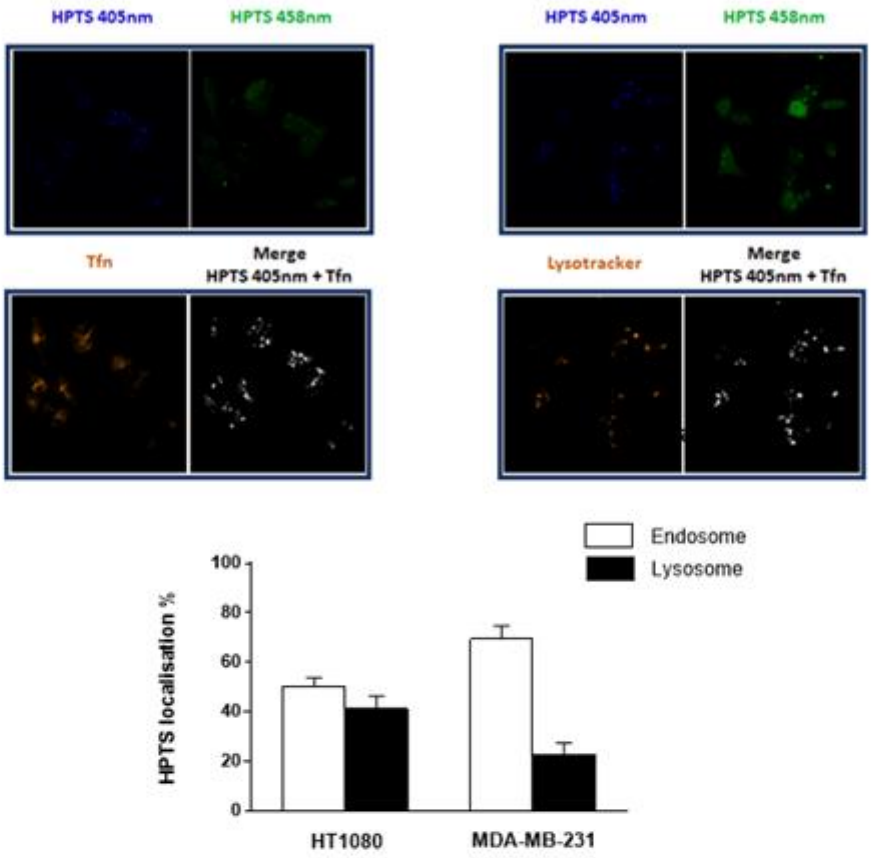
HPTS 405nm
HPTS 458nm
HPTS 405nm
HPTS 458nm
Tfn
Merge
HPTS 405nm + Tfn
Lysotracker
Merge
HPTS 405nm + Tfn
Endosome
Lysosome
HPTS localisation %
100
80
60
40
20
0
HT1080
MDA-MB-231

B

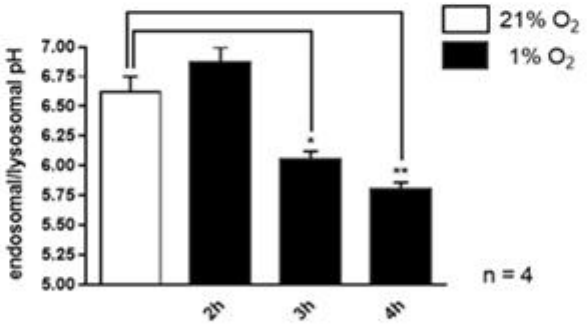
21% O2
1% O2
endosomal/lysosomal pH
7.00
6.75
6.50
6.25
6.00
5.75
5.50
5.25
5.00
*
**
n = 4
2h
3h
4h

C

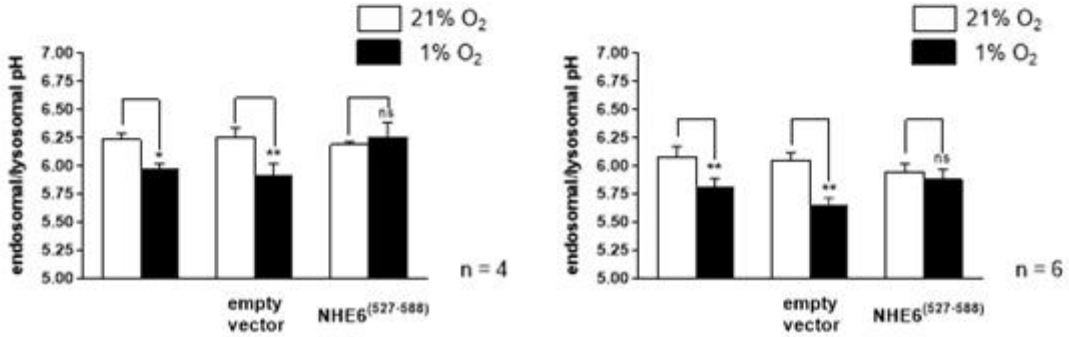
21% O2
1% O2
endosomal/lysosomal pH
7.00
6.75
6.50
6.25
6.00
5.75
5.50
5.25
5.00
*
**
ns
n = 4
empty vector
NHE6(527-588)
21% O2
1% O2
endosomal/lysosomal pH
**
**
ns
n = 6
empty vector
NHE6(527-588)

Figure 9. Measurement of endosomal/lysosomal pH in living cells.

A) Visualization of HPTS incorporated in live HT1080 cells at both fluorescence excitation maxima (405nm and 458nm). Cells were simultaneously incubated with transferrin and lysotracker in order to label endosomes and lysosomes, respectively. The signals used for identifying sub-cellular compartments were merged with images collected from excitation at 405nm (which produced the sharper signal). Merged images were used to calculate the percentage of HPTS present in each sub-cellular compartment. The same procedure was followed for MDA-MB-231 cells. B) HT1080 cells pre-incubated with HPTS were incubated under normoxia or hypoxia (1% O_2) for the indicated times. Live cells were excited at 458nm and 405 nm and HPTS fluorescence intensity was collected. The resulting 458/405nm ratios were converted to pH values using pre-made pH calibration curves. **C)** pH measurements were performed in stably expressing $NHE6^{(527-588)}$ HT1080 and MDA-MB-231 cells (or equivalent empty vector cells) as indicated in B. Cells were incubated in hypoxia for 4h. The asterisks used to indicate statistical differences correspond to:
* $p<0.05$, ** $p<0.01$ and *** $p<0.001$.

3.3.4 Localization of Doxorubicin in the Nucleus is Diminished in Hypoxia; Expression of $NHE6^{527-588}$ Peptide Restores the Nuclear Levels of Doxorubicin.

The experimental design showing subcellular distribution of doxorubicin in HT1080 cells presented in the preliminary findings was replicated using cells stably expressing $NHE6^{527-588}$. Although spots of extra nuclear doxorubicin in hypoxia were not as clearly defined in empty vector expressing cells (**Figure10A**) as in our earlier experiments, the trend showed less nuclear doxorubicin in cells incubated in hypoxia (empty vector, p=0.0047) (**Figure10B**). Conversely, the cellular distribution of doxorubicin was not visibly altered by hypoxia (**Figure10A**), an observation that was confirmed by the quantification of nuclear doxorubicin ($NHE6^{527-588}$, p=0.6088) (**Figure10B**).

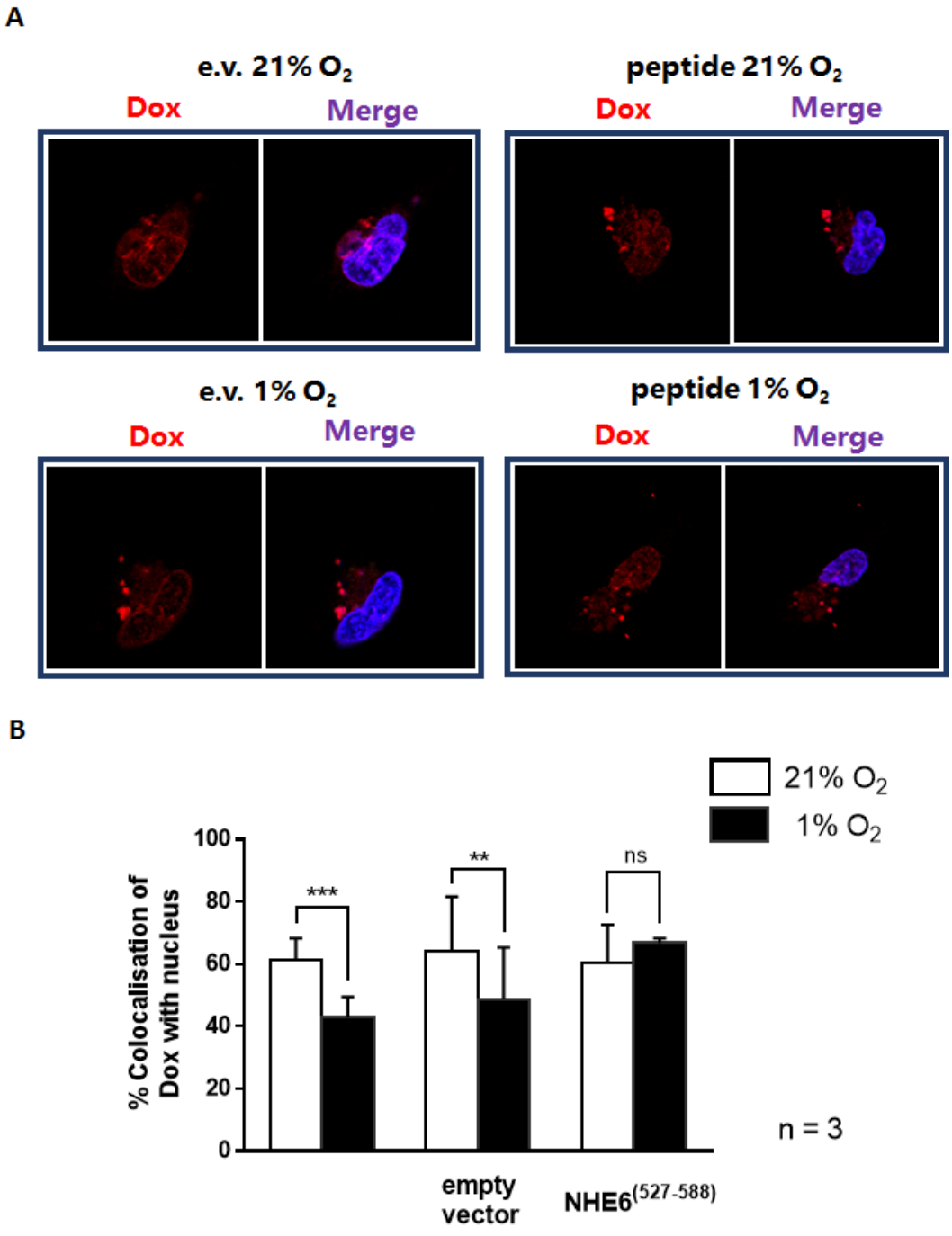

Figure 10. Subcellular distribution of doxorubicin in stably expressing NHE6 (527-588) HT1080 cells.

A) Representative images of sub-cellular distribution of doxorubicin in live HT1080 cells, stably expressing the NHE6$^{(527\text{-}588)}$ peptide or the control empty vector and incubated under normoxic or hypoxic conditions for 4 h. The nucleus was stained by incubating cells with Hoechst 33342. **B)** The percentage of doxorubicin present at the nucleus was quantitated using the overlapping signal from Hoechst 33342. The asterisks used to indicate statistical differences correspond to: * p<0.05, ** p<0.01 and *** p<0.001.

3.4 Activation of PKC Produces Effects Similar to Hypoxia on NHE6 Localization, Endosomal/Lysosomal pH Modulation and Doxorubicin Distribution.

Phorbol 12,13-dibutyrate (PDBU), an activator of classical and novel PKC isozymes, was used to assess the implication of PKC signaling in pH-associated chemoresistance. HT1080 cells transiently expressing eGFP-NHE6 and treated for 2h with 100nM PDBU revealed a clear change in the distribution of NHE6 (**Figure 11A**). EGFP-NHE6 in PDBU-treated cells appeared more abundantly located at the plasma membrane in both experiments. The proportion of eGFP-NHE6 at the plasma membrane was however not quantitated. Parallel pH measurements indicated a much lower endosomal/lysosomal pH of 4.82 in cells subjected to 100nM PDBU as opposed to a pH of 6.00 in untreated cells (**Figure 11B**). This experiment was only performed once and could not be validated for statistical significance. Visualization of live HT1080 cells pre-incubated for 2h with 100nM PDBU before addition of doxorubicin revealed an increase in extra-nuclear spots of the drug (**Figure 11C**). A tendency towards less nuclear doxorubicin for HT1080 cells treated with PDBU was revealed (PDBU 100nM compared to untreated, p=0.0493) (**Figure 11D**). Another sample of HT1080 cells was treated in parallel with 200nM of GF109203X for 30 min prior to being incubated in hypoxia for 4h and incubated with doxorubicin as mentioned above. GF109203X at concentrations under 1μM is used as a selective inhibitor of PKC isozymes activation (Toullec *et al*, 1991). Pre-treatment with GF109203X (GF) seems to have prevented the endosomal/lysosomal acidification as observed in untreated hypoxic cells; statistical significance could not, however, be attained within three duplicates of the experiment (GF 200nM, p=0.1234) (**Figure 11D**).

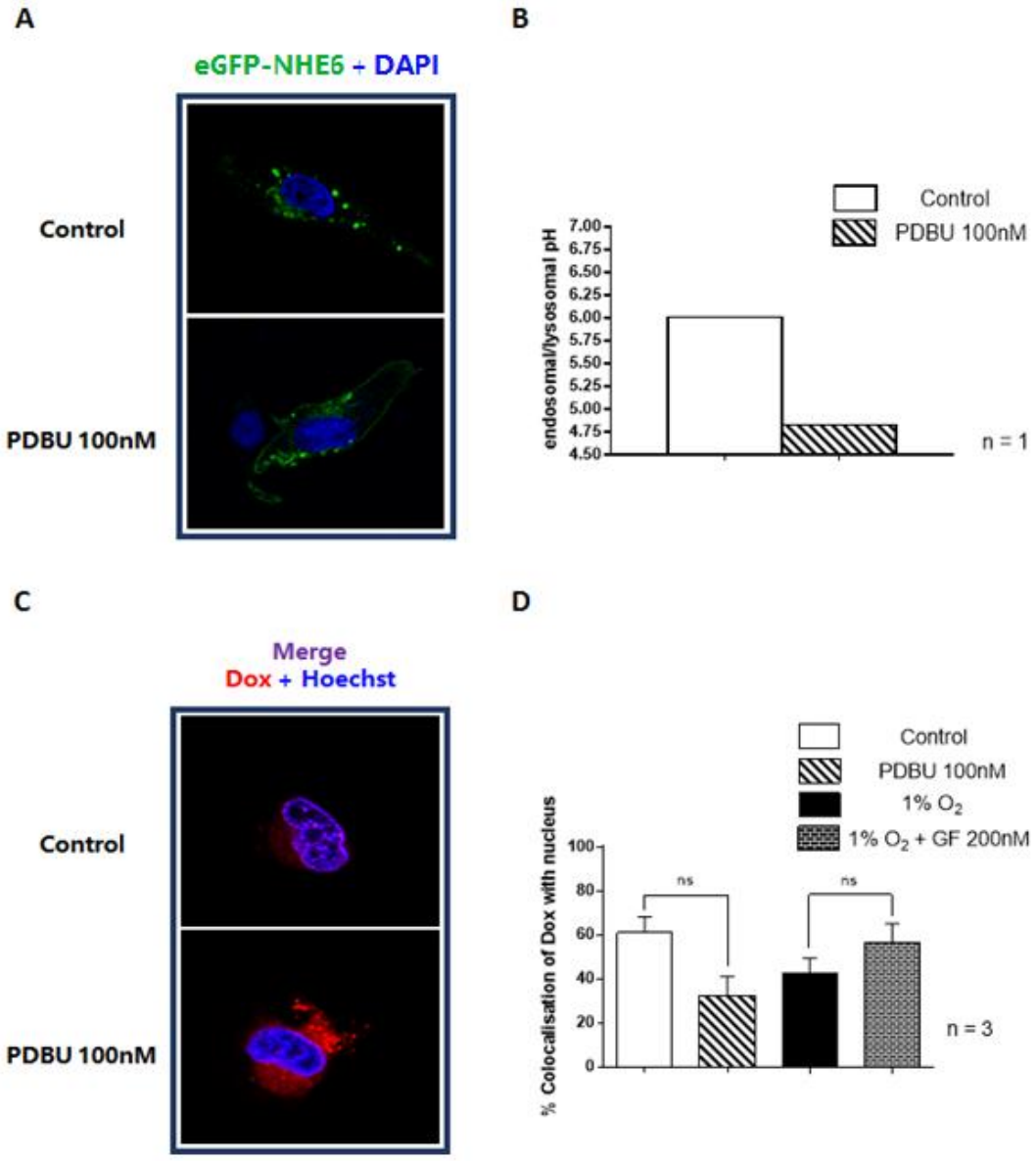

Figure 11. Effect of PKC activity modulation on NHE6 localisation, endosomal/lysosomal pH and doxorubicin distribution.

A) Representative images of transiently expressed eGFP-NHE6 in untreated HT1080 cells or cells treated with 100nM PDBU for 2h. The nuclei were stained by incubating cells with DAPI. **B)** Endosomal/lysosomal pH measurements were performed in live HT1080 cells and MDA-MB-231 cells as indicated in Figure 10B. HT1080 cells were treated with 100nM PDBU for 2h prior to visualization. **C)** Representative images of sub-cellular distribution of doxorubicin in live HT1080 cells incubated for 2h with PDBU or control cells. Nuclei were stained with Hoechst 33342. **D)** The percentage of doxorubicin present at the nucleus was quantitated by using the overlapping signal from Hoechst 33342.

3.5 Reactive Oxygen Species Produced in Hypoxia Correlate Positively with Extra-Nuclear Distribution of Doxorubicin.

Hypoxia is known as a common stimulus for the generation of mitochondrial reactive oxygen species (ROS) and for ROS produced through NADPH oxidases (Klimova and Chandel, 2008). ROS are also among the molecules known to trigger the switch between the inactive and the active conformations of PKC isozymes. We first validated the capacity of hypoxia to stimulation of ROS production in our HT1080 experimental cell model. For this, total ROS were stained using CellROX Green indicator. Results showed an increase in ROS production (4.8 fold, p=0.0328) in hypoxic over normoxic cells (**Figure 12A**). In order to investigate whether there is a link between total ROS and pH-dependent chemoresistance, the simultaneous staining of ROS and nuclei were performed on live HT1080 cells following incubation with doxorubicin. The results revealed that the amounts or ROS are variable from cell to cell within each culture (**Figure 12B**). Notably, cells exhibiting higher levels of ROS have more extra-nuclear spots of doxorubicin (left circle) than cells with lower levels of ROS (right circle). CellROX Green signal intensity levels were quantitated and correlated for each individual cell with the proportion of nuclear doxorubicin (**Figure 12C**). For each of the three experiments carried out, a statistically significant negative correlation was found between the percentage of nuclear doxorubicin and the amount of total ROS in cells or surrounding the cells. Further statistical details describing the linear correlation relationships are provided in **Figure 12C**.

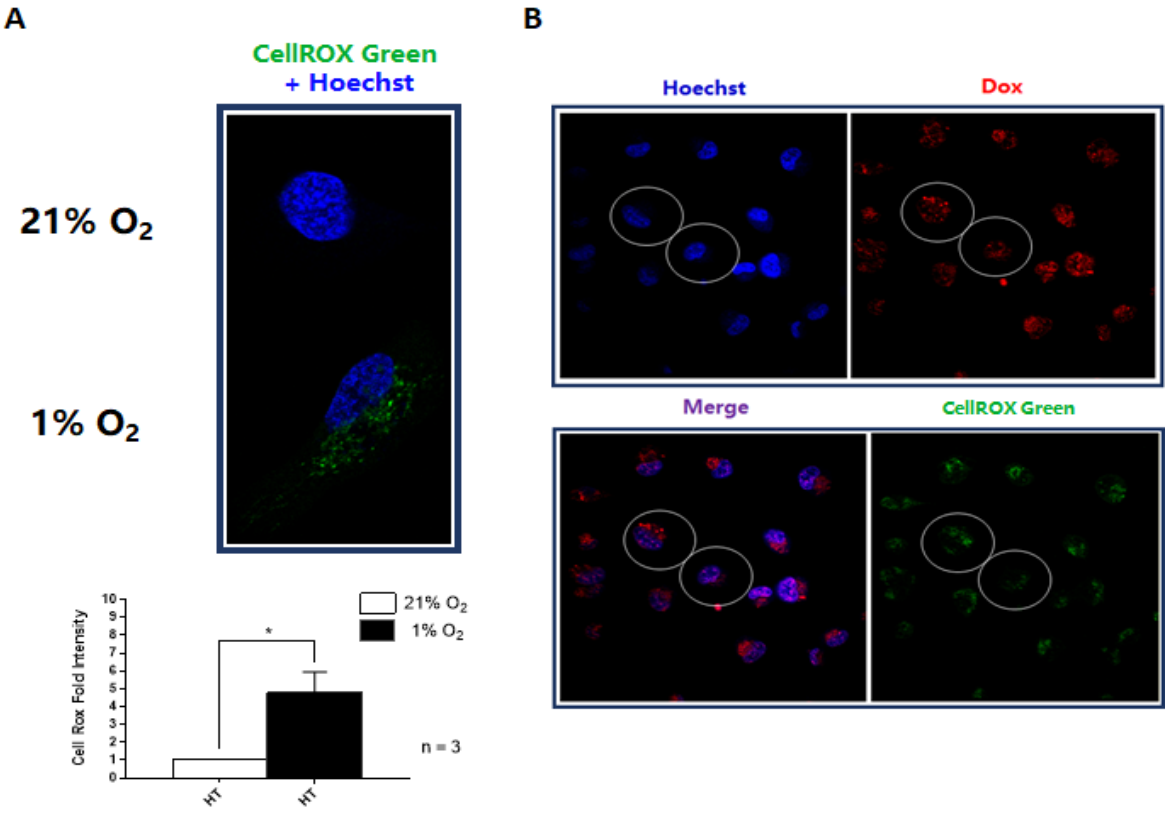

C

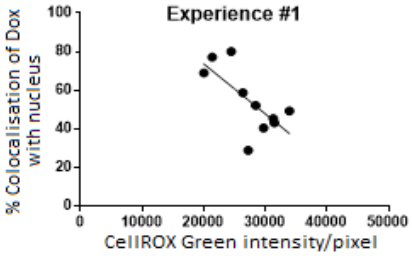

Pearson r = -0.698
P value = 0.013
R squared = 0.487

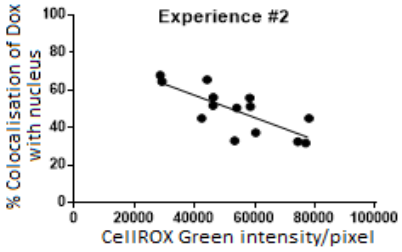

Pearson r = -0.758
P value = 0.001
R squared = 0.575

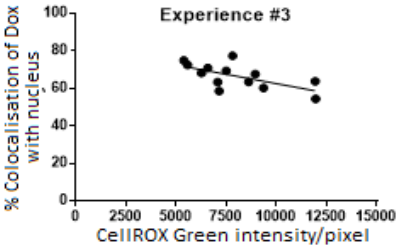

Pearson r = -0.635
P value = 0.010
R squared = 0.403

Figure 12. ROS production in hypoxia and correlation with doxorubicin distribution in live HT1080 cells.
A) Representative images of CellROX Green indicator of reactive oxygen species in live HT1080 cells incubated under normoxia or hypoxia for 4h. The nuclei were stained by incubating cells with Hoechst 33342. CellROX green signal was collected around the emission maxima of 520nm. Signal intensity is expressed in fold based on a value of 1 for cells kept under normoxia. **B)** Field of live HT1080 cells placed 4h under hypoxia and incubated during that time in succession with doxorubicin for 2h and with CellROX Green reagent for 30 min. Cells contained in the field display varying doxorubicin distribution and varying degrees of ROS. The cell shown in the left circle has a low percentage of nuclear doxorubicin and high level of ROS. The cell shown in the right circle has a high percentage of nuclear doxorubicin and low levels of ROS. **C)** Experimental conditions described in B were repeated on three occasions. Nuclear doxorubicin and CellROX Green were calculated for individual cells and data were used to determine the Pearson r correlation coefficient and the coefficient of determination. The asterisks used to indicate statistical differences correspond to: * $p<0.05$, ** $p<0.01$ and *** $p<0.001$.

3.6 Multiple Sequence Alignment of Human NHE6, 7 & 9 with Orthologs from Other Species Reveal a Strongly Conserved Sequence within the RACK1 Binding Domain.

The DNA coding sequences of the nine human Na^+/H^+ exchangers were aligned to construct a phylogenetic tree of the NHE protein family and to reveal similarities and differences between members of the family (**Figure 13**). As expected, the plasma membrane exchangers formed a sub-family of five closely related proteins members. Within that sub-family NHE1, 2 and 4 were all within a short evolutionary distance; these three exchangers are the only members of the family to contain a calmodulin binding domain. The four remaining members of the protein family are all intracellular exchangers and three of those, NHE6, 7 and 9, form a closely related subset. A RACK1 binding domain has been identified for these three members of the NHE family whereas human NHE8 does not contain such domain.

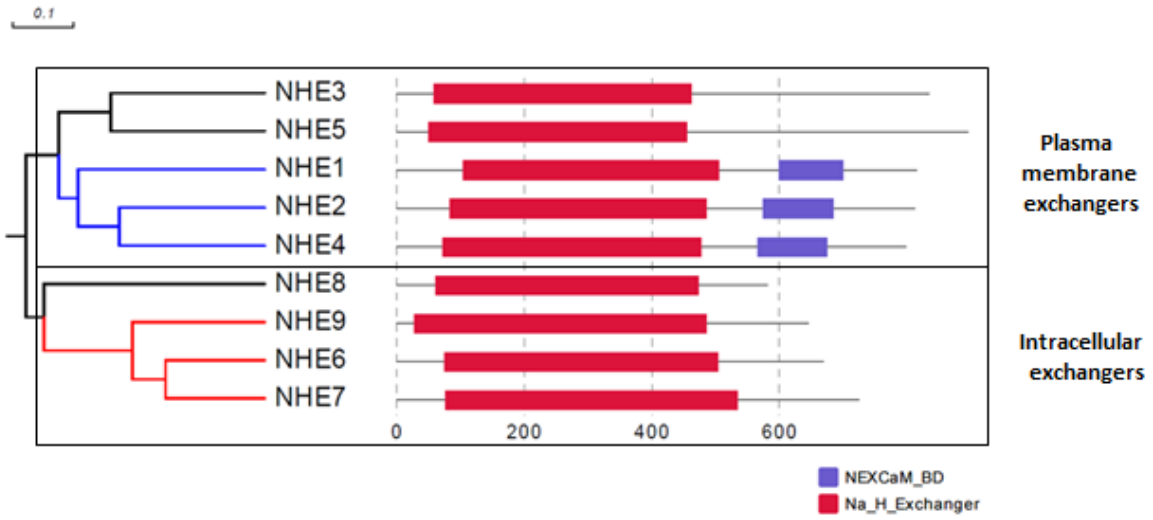

Figure 13. Phylogenetic tree of human NHE proteins divided into subfamilies

Phylogenetic tree constructed using the sequences of the nine human NHE paralogs (longest isoforms). Evolutionary distance shown on the x axis is expressed accordingly to the proportion of nucleotide substitution. The first five exchangers shown at the top constitute a subfamily defined by their plasmalemmal subcellular localization. This subfamily can be further divided into proteins containing calmodulin binding domains (blue branches) and those that do not contain such domains. The last four exchangers shown at the bottom constitute a subfamily defined by their intracellular localization. This subfamily can equally be further divided into proteins containing a RACK1 binding domain (red branches) and those that do not contain such domain.

A total of twenty-five protein sequences arising from NHE6, NHE7, NHE9 and corresponding orthologs from 9 species other than human were selected for multiple sequence alignment. The twenty-five genes selected as well as the corresponding species are listed in table 6. Also indicated is the % homology between human NHE6 and its orthologous gene found in different species.

MSA of the twenty-five proteins reveals regions of residue conservation for the entire set of sequences. The 12 known transmembrane domains as well as the RACK1 binding domain of human NHE6 were aligned underneath the map of residue conservation to better delineate areas of high conservation and areas of low conservation (**Figure 14A**). The twelve transmembrane domains have a tendency to situate themselves within the boundaries of either regions of high conservation (deep blue) or of medium conservation (light blue), they seldom crossover areas of low conservation (white). A close-up of the map corresponding to

the cytoplasmic tail reveals that the region of interaction with RACK1 is contained within the largest and most conserved portion of cytoplasmic component of this NHE protein subset (**Figure 14B**). Further zooming on the RACK1 region of interaction shows the conservation index for each individual residue (**Figure 14C**). Within this well-conserved region, it is possible to further isolate a portion of the most well-conserved 28 amino acids within the cytoplasmic tail. For human NHE6 variant B this sequence would start at F-536 and end at P-563.

Table 6: Intracellular NHE sequences included in the dataset used for MSA.

Species (common name, uniprot taxon identifier and binomial nomenclature)	Paralogs (human equivalent)	Uniprot Identifiers	% homology (NHE6 homolog with human NHE6)
Human, 9606, Homo sapiens	NHE6, 7 & 9	Q92581, Q96T83, Q8IVB4,	100
Mouse, 10090, Mus musculus,	NHE6, 7 & 9	A1L3P4, Q8BLV3, Q8BZ00	96
Panda géant, 9646, Ailuropoda melanoleuca	NHE6, 7 & 9	G1L8J1, D2HXE1, G1M2B1	92
Green anole (lizard), 28377, Anolis Carolinensis	NHE6 & 9	H9GJ49, G1KJ91	79
Chicken, 9031, Gallus gallus	NHE6, 7 & 9	F1NCB2, F1NEV4, F1NYM1	79
Zebra finch, 59729, Taeniopygia guttata	NHE6, 7 & 9	H0YXF3, H0ZK15, H0ZEK3	78
Frog, 8364, Xenopus silunanra tropicalis	NHE6 & 7	F6PUK5, F7BFD2	77
Turtle, 13735, Pelodiscus sinensis	NHE6, 7 & 9	K7FR39, K7FV38, K7GDV6	75
Spotted gar (fish), 7918, Lepisosteus oculatus	NHE6 & 7	W5ND83, W5MNB8	72
Blind cave fish, 7994, Astyanax mexicanus	NHE6	W5KM86	57

A

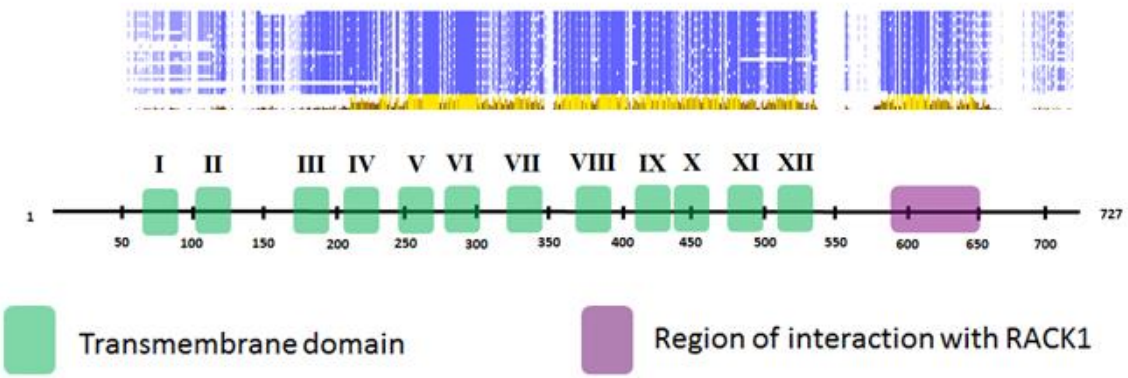
I
II
III
IV
V
VI
VII
VIII
IX
X
XI
XII
1
727
50
100
150
200
250
300
350
400
450
500
550
600
650
700
Transmembrane domain
Region of interaction with RACK1

B

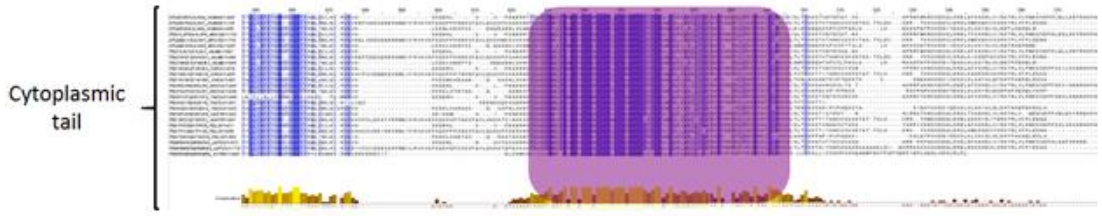
Cytoplasmic tail

C

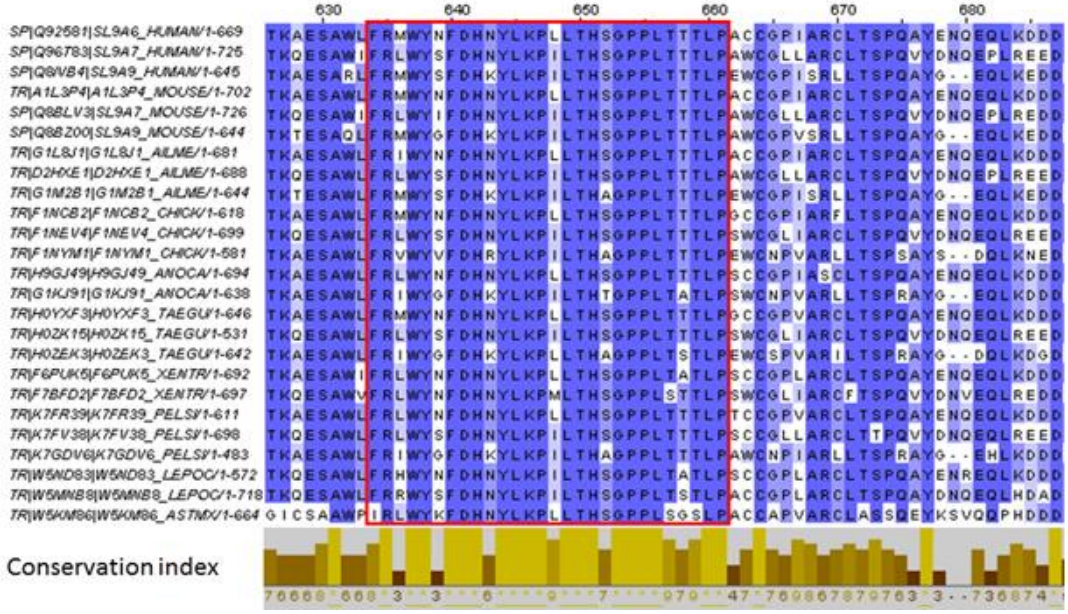
630
640
650
660
670
680
SP|Q92581|SL9A6_HUMAN/1-669
SP|Q96T83|SL9A7_HUMAN/1-725
SP|Q6VB4|SL9A9_HUMAN/1-645
TR|A1L3P4|A1L3P4_MOUSE/1-702
SP|Q8BLV3|SL9A7_MOUSE/1-726
SP|Q8BZ00|SL9A9_MOUSE/1-644
TR|G1L8J1|G1L8J1_AILME/1-681
TR|D2HXE1|D2HXE1_AILME/1-688
TR|G1M2B1|G1M2B1_AILME/1-644
TR|F1NCB2|F1NCB2_CHICK/1-618
TR|F1NEV4|F1NEV4_CHICK/1-699
TR|F1NYM1|F1NYM1_CHICK/1-581
TR|H9GJ49|H9GJ49_ANOCA/1-694
TR|G1KJ91|G1KJ91_ANOCA/1-638
TR|H0YXF3|H0YXF3_TAEGU/1-646
TR|H0ZK15|H0ZK15_TAEGU/1-531
TR|H0ZEK3|H0ZEK3_TAEGU/1-642
TR|F6PUK5|F6PUK5_XENTR/1-692
TR|F7BFD2|F7BFD2_XENTR/1-697
TR|K7FR39|K7FR39_PELSI/1-611
TR|K7FV38|K7FV38_PELSI/1-698
TR|K7GDV6|K7GDV6_PELSI/1-483
TR|W5ND83|W5ND83_LEPOC/1-572
TR|W5MNB8|W5MNB8_LEPOC/1-718
TR|W5KM86|W5KM86_ASTMX/1-664
Conservation index

Figure 14. MSA analysis of a subfamily of intracellular Na^+/H^+ exchangers.

A) MSA of the twenty-five protein dataset listed in table 6 aligned with the principal domains of the human NHE6 protein. Deep blue areas indicate regions of high conservation, light blue areas indicate regions of medium conservation and white areas indicate regions of low conservation. Tall yellow bars shown beneath also indicate regions of high conservation and are based on the conservation index calculated with the AMAS method. Although no protein has a total length of 727 amino acids, the 1st residue is aligned with the protein with the longest N-terminal segment and the 727th residue is aligned with the protein with the longest C-terminal segment. **B)** Close-up of the cytoplasmic tail containing the region of interaction with RACK1 is highlighted in purple. **C)** Close-up of the region of interaction with RACK1. The conservation index shown at the bottom is calculated on a scale of 1 to 10, with score of 10 indicated by *. A red box is used to highlight a sequence of 28aa that is the most conserved within this region.

3.7 Analysis of NHE6 RACK1 Binding Domain as a Segment Involved in Inducible Transient Protein-Protein Interactions.

Results obtained thus far through co-immunoprecipitation and protein-protein interaction behaviour of similar WD40 repeat proteins (Chen *et al*, 2004) lead us to believe that the NHE6 RACK1 interaction fits the description of a strong inducible transient protein-protein interaction. This section will seek to analyze the biochemical properties of NHE6 residues at or near the interaction interface and compare those findings to common characteristics for transient interactions.

3.7.1 A Segment of the Human NHE6 RACK1 Binding Domain is Enriched in Neutral Polar Residues.

Transient interfaces tend to be quite compact and smaller in size than permanent interfaces (Perkins, 2010). These interfaces are also enriched in neutral polar residues; this observation is somewhat intuitive considering that these protein segments need to be soluble to allow interacting proteins to dissociate as is the nature of transient protein-protein interactions. Six of the twenty standard amino acids fall under the category of neutral polar residues (**Figure 15A**), these include Serine (S), Threonine (T), Cysteine (C), Tyrosine (Y), Asparagine (N) and Glutamine (Q). A segment of thirty-three amino acids enriched in neutral polar residues could be identified within the RACK1 binding domain of NHE6 (**Figure 16B**). This segment is composed at 45.5% of neutral polar residues whereas the entire cytoplasmic tail of human

NHE6 is only composed at 27.5% of neutral polar residues. The thirty-three amino acid segment stretches from T-551 to Q-583.

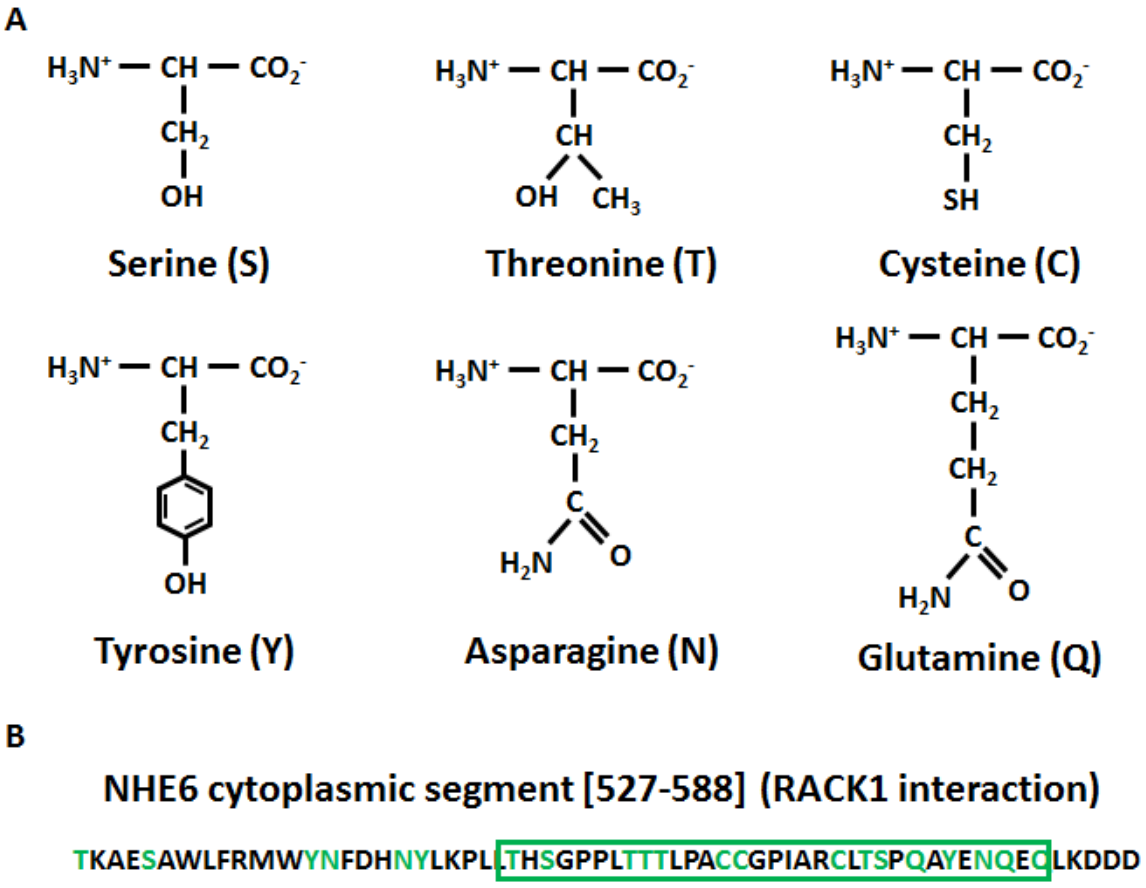

Figure 15. Neutral polar residue enrichment in transient interfaces.

A) Representation of the six standard amino acids sharing the characteristic of neutral polar residues. **B)** Annotated sequence of the NHE6 [527-588] RACK1 interaction region showing neutral polar residues in green. The green box indicates the segment most enriched in neutral polar amino acids.

3.7.2 The Human NHE6 RACK1 Binding Domain has Characteristics of an Intrinsically Disordered C-terminal Region and Contains Several Possible Anchoring Residues.

Another feature of transient protein interactions is that they tend to occur within intrinsically disordered (ID) proteins (Perkins *et al*, 2010). ID can best be described as proteins or protein segments, that lack a specific structure; or in other words that can adopt a wide range of conformations. The distal part of the NHE1 C-terminal tail has previously been shown to be ID and was proposed to contain molecular recognition features (MORFs) necessary for

proper NHE1 trafficking to the plasma membrane (Nørholm *et al*, 2011) Protein disorder propensity analysis based on the UCON and MD_Raw methods were applied to the cytoplasmic C-terminal segment of NHE6. The scores obtained through the two methods were well correlated with each other and showed that the cytoplasmic C-terminal segment of NHE6 is generally disordered (**Figure 16A**). As the characteristics of transitory protein-protein interactions remain poorly defined in the literature, we examined the molecular details of the p53 interactions with MDM2 and Taz2 proteins (Huang and Liu, 2011) as a comparison model for the NHE6 and RACK1 interaction. These interactions are some of the few transient interactions for which precise molecular regulation has been described and involve anchorage residues necessary to create the protein interface. The same methods were thus also applied to the first 40 amino acids of human P53 (**Figure 16B**), which are contained in the P53 transactivation domain. Similarly, this segment of P53 was generally disordered. In both cases protein residue disorder was examined in more details where it was observed that a segment of 33 amino acids, ranging from A-529 to L-561, was below the threshold for disordered nucleotide residues (**Figure 16C**). Likewise, the P53 segment contained 6 amino acids, all within F-19 and L-26, which were also below the threshold for disordered nucleotide residues. Three of these residues, F-19, W-23 and L-26, correspond to the three residues that have been identified as anchorage residues involved in the transient interaction with MDM2 (Huang and Liu, 2011) (**Figure 16D**). Highlighted in purple within the NHE6 sequence are the Arginine (R), Tyrosine (Y), Phenylalanine (F) and Tryptophan (W) amino acids which are known to often serve the function of anchorage residues. It must be noted that theses residues are concentrated in the region ranging from W-533 to Y-545 which corresponds to the most intrinsically disordered region of the NHE6 cytoplasmic C-terminal segment.

A

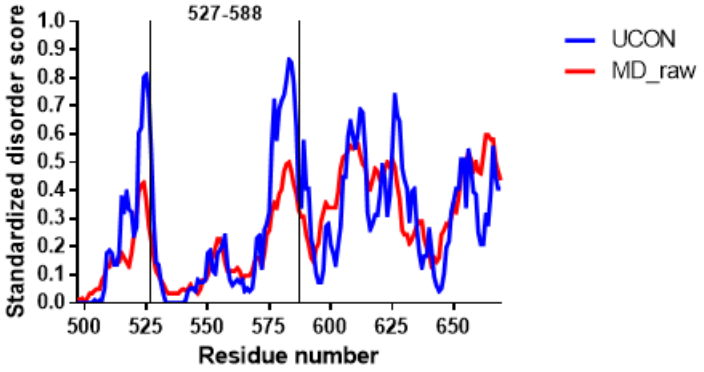

B

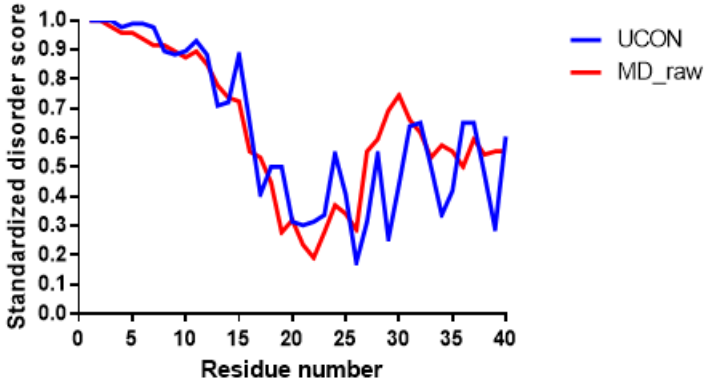

C

NHE6 cytoplasmic segment [527-588] (RACK1 interaction)

TKAESAWLFRMWYNFDHNYLKPLLTHSGPPLTTTLPACCGPIARCLTSPQAYENQEQLKDDD

P53 N-terminal segment [1-40] (transactivation domain)

MEEPQSDPVSEPPLSQETFSDLWKLLPENNVLSPLPSQAM

Ordered **Intermediate** **Disordered**

D

NHE6 cytoplasmic segment [527-588] (RACK1 interaction)

TKAESAWLFRMWYNFDHNYLKPLLTHSGPPLTTTLPACCGPIARCLTSPQAYENQEQLKDDD

P53 N-terminal segment [1-40] (transactivation domain)

MEEPQSDPVSEPPLSQETFSDLWKLLPENNVLSPLPSQAM

Figure 16. Protein segment disorder propensity predicted using two alternative methods.

A) Standardized UCON and MD_raw disorder scores of the NHE6 cytoplasmic segment, the RACK1 interaction sequence [527-588] is shown within brackets. **B)** Standardized UCON and MD_raw disorder scores of the P53 N terminal segment. **C)** Annotated sequences from A (only RACK1 interaction sequence) and B. Ordered residues shown in black correspond to UCON scores of $x < 0.1$, intermediate sequences shown in blue correspond to UCON scores of $0.1 \leq x < 0.25$ and disordered sequences correspond to UCON scores of $x \geq 0.25$. D) Annotated sequences showing residues of the NHE6 cytoplasmic segment suspected of acting as anchorage residues (purple) binding to a RACK1 surface cavity and the previously confirmed anchor residues on the P53 N-terminal segment which are involved in the interaction of p53 to a surface cavity of MDM2.

3.8 Overlapping Residues Forming a Cavity at the Surface of RACK1 and Possibly Involved in the Interaction with NHE6 were Identified Through Two Alternative Methods.

Since the human NHE6-RACK1 binding domain contains several well-conserved proline residues within its core, we investigated the possibility that NHE6 binds RACK1 in a similar type of protein-protein interaction as described for proline-rich motifs (PRMs). PRM recognition has been shown to involve clusters of exposed aromatic residues called “aromatic cradles” (Ball *et al*, 2005). Systematic inspection of the crystal structure of human RACK1 (PDB file: 4AOW), revealed two clusters of exposed aromatic residues at the surface of RACK1. One of these sites was found within the WD2 domain on the top face (arbitrarily determined) of RACK1; as shown in **Figure 17A**, it involves a histidine residue (H), a phenylalanine residue (F) and a tryptophan residue (W). The second site was found located between the WD4 and WD5 and involves two tryptophan residues (W) and one tyrosine residue (Y). A third site that involves four residues of the WD6 domain was also found on the bottom face of RACK1 (**Figure 17B**); this site involves two tyrosine (Y) residues, one phenylalanine residue (F) and one tryptophan (W) residue. Alternatively, the IsoCleft Finder tool (Kurbatova, 2013) was used to detect cavities at the surface of RACK1 that were projected to be involved in molecular interactions based on similarities found in an existing database of proteins with known molecular interactions. Only one site was identified through this method in domains WD5-7 that can correspond to the typical small size of transient protein-protein interactions (**Figure 17C**). This cavity is formed by a total of 12 residues

found on the WD5 and WD6 domains of the bottom face of the human RACK1 protein. The two sites identified on the bottom face of RACK1 partially overlapped with the two tyrosine residues found on both sites; the remaining residues were adjacent to each other. This possible binding site will simply be referred to as tentative NHE binding pocket moving forward.

A

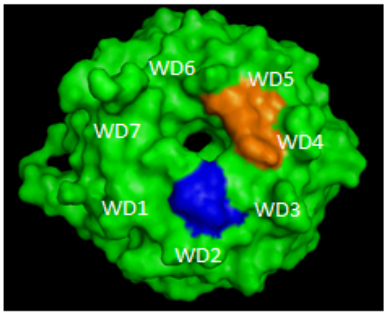

WD 1 MTEQMTLRGTLKGHNGWVTQIATTPQFPDMILSASRDKTIIMWKLTRD
WD 2 ETNYGIPQRALRGHSHFVSDVVISSDGQFALSGSWDGTLRLWDLTTG
WD 3 TTTRRFVGHTKDVLSVAFSSDNRQIVSGSRDKTIKLWNTLGVC
WD 4 KYTVQDESHSEWVSCVRFSPNSSNPIIVSCGWDKLVKVWNLANCKLK
WD 5 TNHIGHTGYLNTVTVSPDGSLCASGGKDGQAMLWDLNEG
WD 6 KHLYTLDGGDIINALCFSPNRYWLCAATGPSIKIWDLEGKIIVDEL
WD 7 KQEVISTSSKAEPPQCTSLAWSADGQTLFAGYTDNLVRVWQVTIGTR

B

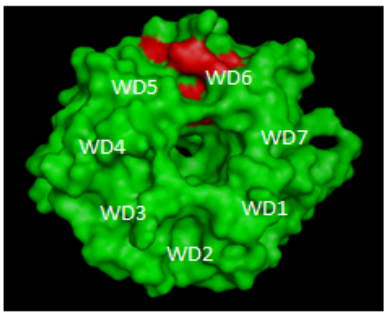

WD 1 MTEQMTLRGTLKGHNGWVTQIATTPQFPDMILSASRDKTIIMWKLTRD
WD 2 ETNYGIPQRALRGHSHFVSDVVISSDGQFALSGSWDGTLRLWDLTTG
WD 3 TTTRRFVGHTKDVLSVAFSSDNRQIVSGSRDKTIKLWNTLGVC
WD 4 KYTVQDESHSEWVSCVRFSPNSSNPIIVSCGWDKLVKVWNLANCKLK
WD 5 TNHIGHTGYLNTVTVSPDGSLCASGGKDGQAMLWDLNEG
WD 6 KHLYTLDGGDIINALCFSPNRYWLCAATGPSIKIWDLEGKIIVDEL
WD 7 KQEVISTSSKAEPPQCTSLAWSADGQTLFAGYTDNLVRVWQVTIGTR

C

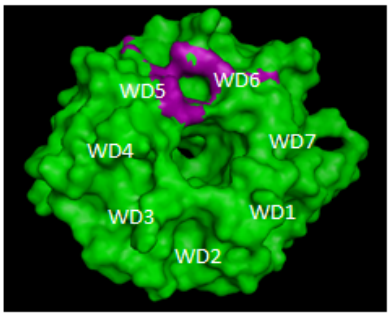

WD 1 MTEQMTLRGTLKGHNGWVTQIATTPQFPDMILSASRDKTIIMWKLTRD
WD 2 ETNYGIPQRALRGHSHFVSDVVISSDGQFALSGSWDGTLRLWDLTTG
WD 3 TTTRRFVGHTKDVLSVAFSSDNRQIVSGSRDKTIKLWNTLGVC
WD 4 KYTVQDESHSEWVSCVRFSPNSSNPIIVSCGWDKLVKVWNLANCKLK
WD 5 TNHIGHTGYLNTVTVSPDGSLCASGGKDGQAMLWDLNEG
WD 6 KHLYTLDGGDIINALCFSPNRYWLCAATGPSIKIWDLEGKIIVDEL
WD 7 KQEVISTSSKAEPPQCTSLAWSADGQTLFAGYTDNLVRVWQVTIGTR

Figure 17. Identification of potential protein binding sites at the surface of RACK1.

A) View of the top face of the RACK1 protein and amino acid sequence of the 7 WD repeat domains. The first site corresponding to the description of an aromatic cradle (blue) involves three aromatic residues (HFW) of the WD2 domain. The second site corresponding to the description of an aromatic cradle (orange) involves two tryptophan residues of WD4 domain and one tyrosine residue of the WD5 domain. **B)** View of the bottom face of the RACK1 protein. The third site corresponding to the description of an aromatic cradle (red) involves four aromatic residues (YFYW) of the WD6 domain. **C)** View of the bottom face of the RACK1 protein. The possible interaction site identified through IsoCleft Finder (violet) involves twelve residues contained in the WD5 and WD6 domains. Images captured with PyMOL Molecular Graphics System, Version 1.8 Schrödinger, LLC.

3.9 NHE6 Segment Rich in Potential Anchorage Residues around Y-539 is Predicted to be Involved in Forming an Energetically Favourable Complex with RACK1.

A peptide-protein molecular docking refinement protocol was used as a tool to help further refining key residues in the NHE6 RACK1 binding domain. To do so, the [527-588] NHE6 sequence of 62 amino acids was separated into eleven arbitrarily generated 10 amino acid overlapping peptides and each one was assigned a letter as shown in **Figure 18A**. We then generated a 3D structure with the most likely initial conformation for every peptide using the PEP-FOLD *de novo* peptide structure prediction tool. We then initiated the FlexPepDock protocol using each of these eleven peptides in close proximity to the tentative NHE binding site at the surface of RACK1. The protocol yielded 200 possible structures of which only the Rosetta score value for the most energetically favourable structure was retained and presented under **Figure 18B**. The most energetically favourable structure created yielded a result of -18.263 Rosetta energy units; it was a structure formed with Peptide C which spans from W-538 to K-547 of the NHE6 sequence. The interface energy score for this peptide was significantly lower than other peptides except for peptide B, D and J (peptide B, $p=0.0763$; peptide D, $p=0.0901$ and peptide J, $p=0.0983$). The search for key residues of the NHE6 RACK1 binding domain was further refined by creating four more 10 amino acid peptides derived from Peptide C (**Figure 18C**). The derived peptides were created by sequentially removing one amino acid from the C-terminal end and adding another to the N-terminal end. Two of these new peptides produced structures that were even more energetically favourable than Peptide C (**Figure 18D**).

A

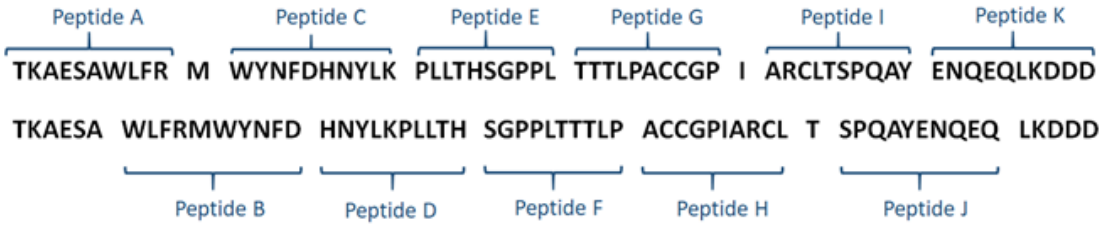

B

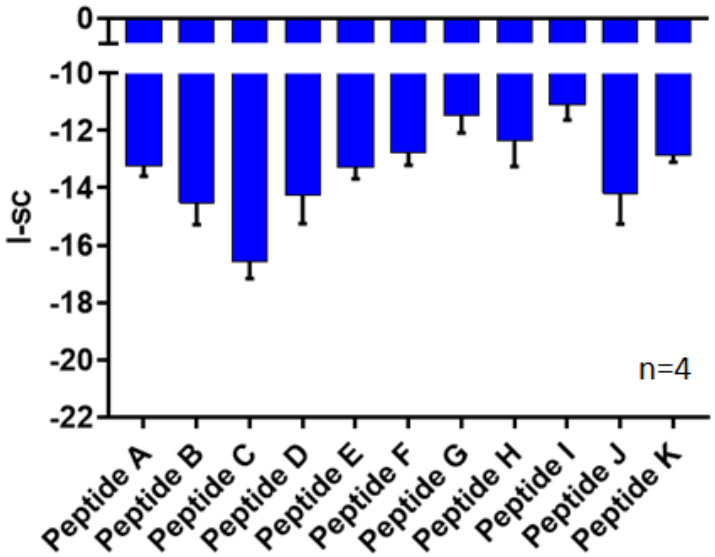

C

Peptide C-4 534 LFRMWYNFDH 543
Peptide C-3 535 FRMWYNFDHN 544
Peptide C-2 536 RMWYNFDHNY 545
Peptide C-1 537 MWYNFDHNYL 546
Peptide C 538 WYNFDHNYLK 547

D

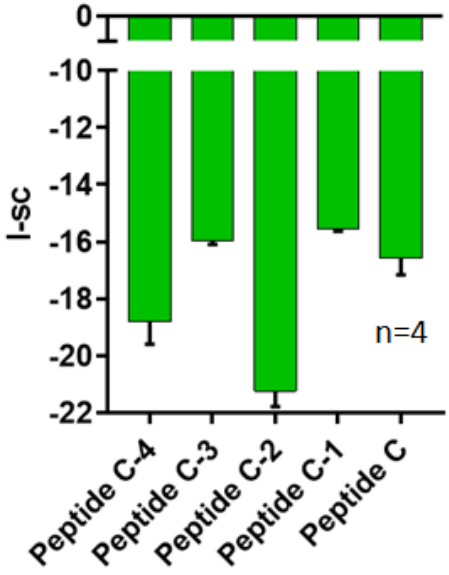

Figure 18. Simulation of peptide-protein interaction through molecular docking refinement protocol.

A) Arbitrary separation of the 62aa [527-588]-NHE6 segment into 11 overlapping 10aa peptides identified from A to K. **B)** Interface energy score of the 11 peptides submitted to Flexpepdock molecular docking refinement protocol with the tentative NHE binding pocket at the surface of RACK1. Interface energy score is expressed in Rosetta energy units. **C)** Generation of four intermediate peptides to peptides B and C. New peptides were identified from C-1 to C-4. **D)** I_sc of peptide C and four derivatives submitted to Flexpepdock molecular refinement protocol with the possible RACK1 binding site.

These energetically favourable peptides correspond to Peptide C-2 with -21.2428 Rosetta energy units and Peptide C-4 with -18.8083 Rosetta energy units. The interface energy score associated with Peptide C-4 was significantly lower than any other peptide tested through the docking protocol.

Following the molecular docking refinement protocol experiment, we inspected the 3D generated structures with the lowest interface energy score for each simulation presented in **Figure 18D** to identify which residues could act as anchorage residues at the predicted NHE binding pocket of RACK1. Shown in **Figure 19** is the putative RACK1 binding pocket and flexamples of interaction interfaces for the three peptides previously predicted to form the most energetically favourable interactions with RACK1; residues partially or completely buried in or around the predicted NHE binding pocket of RACK1 are shown in red. The buried residues were identified for each of the 20 structures examined (4 structure for each of the 5 peptides); the distribution of buried residues is shown in percentage in **Figure 19A**. From all structures examined, 5 residues were found to be partially or completely buried in at least 50% of cases. These residues in order of prevalence were, Y-539 (95%), F-535 (88%), R-536 (75%), W-538 and Y-545 (67%). Since Tyrosine 539 was found to be the most often buried in our simulations it is predicted to be central to the NHE6/RACK interaction interface. Several of the residues previously marked as possible anchorage residues were observed to form favourable interactions with RACK1, in this model, by becoming buried in surface cavities.

A

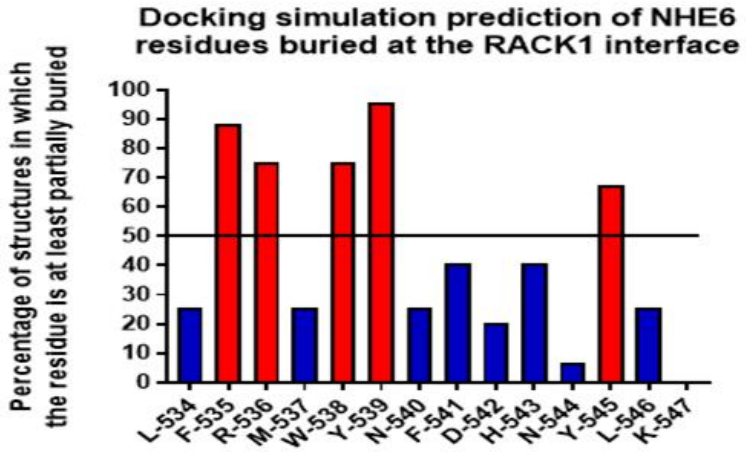
Docking simulation prediction of NHE6 residues buried at the RACK1 interface
Percentage of structures in which the residue is at least partially buried
100
90
80
70
60
50
40
30
20
10
0
L-534
F-535
R-536
M-537
W-538
Y-539
N-540
F-541
D-542
H-543
N-544
Y-545
L-546
K-547

B

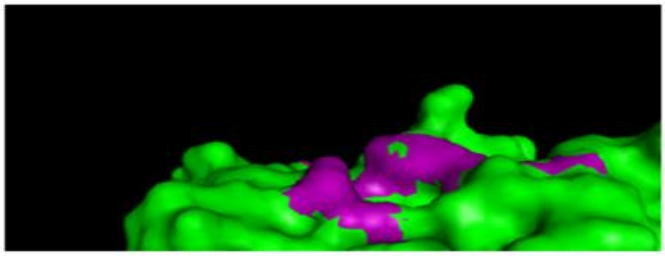

C

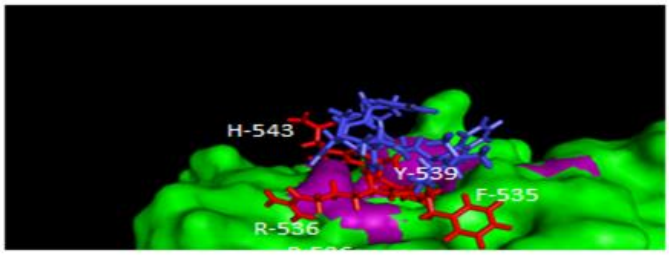
H-543
Y-539
F-535
R-536

D

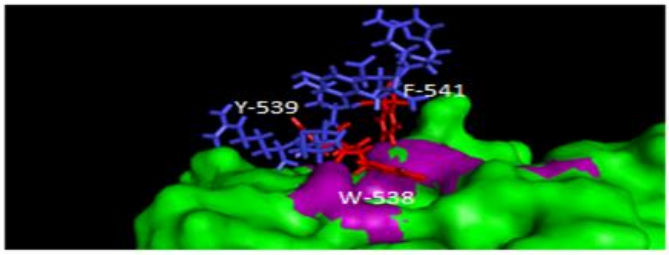
F-541
Y-539
W-538

E

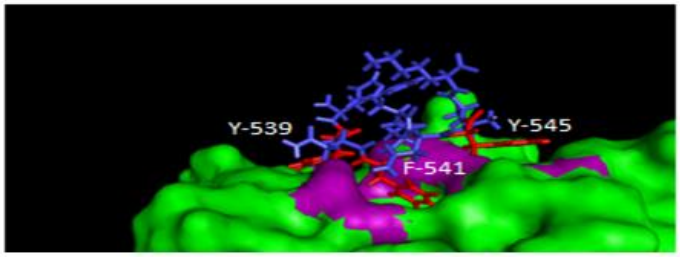
Y-539
Y-545
F-541

Figure 19. Examination of peptide-protein molecular docking results for buried residues.

A) Frequency in which each residue, from the top structures generated with docking simulations, was found to be at least partially buried in the predicted binding pocket identified at the surface of RACK1. The residues that were found to be buried in at least 50% of the structures examined are shown in red. **B)** View of the predicted NHE binding pocket of RACK1 identified using IsoCleft Finder (violet) at the surface of the bottom face of RACK1 (green). **C)** View of peptide C-4 after docking, residues that are partially or completely buried are shown in red, other residues are shown in blue. Of the four residues implicated, Y-539 occupies the innermost cavity. **D)** View of peptide C-2 after docking. Of the three residues implicated, W-538 occupies the innermost cavity. **E)** View of peptide C after docking. Of the three residues implicated, F-541 occupies the innermost cavity. Images captured with PyMOL Molecular Graphics System, Version 1.8 Schrödinger, LLC.

4. DISCUSSION

The current work shows evidence that hypoxia increases RACK1 and NHE6 complex formation in both HT1080 and MDA-MB0231 cell lines. We also provide evidence that formation of such a complex is reversible and has structural and functional properties of transient protein-protein interactions. Since direct protein interaction between RACK1 and NHE6 had previously been reported to occur (Ohgaki *et al*, 2008) and had been shown to play a part in regulating cell surface level of NHE6, this finding was the first indication that RACK1 may be linked to our previous findings on hypoxia triggered plasma membrane NHE6 increase, intra-vesicular compartments acidification, doxorubicin intracellular cluster formation and resistance to doxorubicin. To confirm the relationship between RACK1 and NHE6 interaction and the list of effects observed in hypoxia above, we constructed a mammalian expression vector for expression of a peptide corresponding to the 527-588 segment of the human NHE6 sequence known to interact with RACK1. The expressed $NHE6^{527-588}$ peptide, in our experimental cell models, was meant to interact with RACK1 and thus compete with the native interaction. Functionality of this peptide was first validated by an immunoprecipitation experimental design that showed interference with the formation of a complex between human NHE6 and RACK1 otherwise triggered by hypoxia (**Figure 7)**. Although such competing effect could be appreciated following transient or stable expression of the peptide, a seemingly more drastic result with the stably expressed peptide has brought us to favour stable expression for the following steps of the experimental design. The use of a stable empty vector cell line as experimental control in this initial experiment would have however been preferable to ensure beyond doubt that the differences between the transient and stable peptide cell lines are not due to cellular alterations following Geneticin selection.

The next phase of our study involved assessment of expressed $NHE6^{527-588}$ peptide capacity to prevent NHE6 translocation to the plasma membrane; an effect previously shown to be mediated through a process involving NHE6 and RACK1 interaction. HT1080 or MDA-MB-231 exposition to 1% O_2 hypoxia for 4h induced an increase in plasmalemmal NHE6 localization for both cells; an effect that was effectively repressed by $NHE6^{527-588}$ peptide expression (**Figure 8**). Since our working hypothesis postulated that NHE6 translocation to

the plasma membrane would contribute to acidification of endosomal/lysosomal compartments, leading to weak base therapeutic trapping and ultimately increased resistance to those therapeutics; we next proceeded to test the impact of NHE6$^{527\text{-}588}$ peptide expression on each of these presumably cascading ramifications. Consistent with the previous result, expression of NHE6$^{527\text{-}588}$ peptide in hypoxic cells was indeed found to produce a protective effect against endosomal/lysosomal acidification (**Figure 9**) and what appears to be doxorubicin trapping (**Figure 10**). In a parallel set of experiments (performed by another student of the laboratory, Fabrice Lucien) using MTT survival assays conducted with the same cell lines, it was shown that resistance to several weak base therapeutics, but not to weak acid therapeutics, was reinforced with exposition to hypoxia (Lucien *et al*, 2017) (result not shown). Once again, this effect was diminished through expression of the NHE6$^{527\text{-}588}$ peptide, giving further support to the hypothesis that the different effects observed under hypoxia in this study are interconnected as described above. It should be noted that under normoxia, stable expression of the NHE6$^{527\text{-}588}$ peptide in HT1080 cells had no visible effect on sensitivity to doxorubicin.

Additionally, preliminary results obtained regarding the correlation of cellular ROS levels and the sub-cellular distribution of doxorubicin (**Figure 12**), taken together with results indicating that PKC mimics the effect of hypoxia on NHE6 translocation (**Figure 11),** allow us to propose a model for the series of molecular events that may have led to doxorubicin trapping in our study (**Figure 20**). We propose that hypoxia induces increased mitochondrial ROS production which acts as a secondary messenger responsible for the activation of PKC isozyme(s) (Cosentino-Gomes *et al*, 2012). Once in an open active conformation, PKC isozymes can bind RACK1 (Adams *et al*, 2011) which in many cases triggers translocation of the protein complex towards the plasma membrane (Bourd-Boittin *et al,* 2008). It is conceivable that the formation of a complex with active PKC acts as a trigger that allows formation of the transient RACK1/NHE6 interaction leading to NHE6 translocation to the plasma membrane as a PKC/RACK1/NHE6 complex. As RACK1 and NHE6 appear to be interacting in a transitory manner, it is unlikely that RACK1 itself acts to anchor NHE6 to the plasma membrane for a sustained period of time. It is more likely that RACK1 acts to favour anchorage of NHE6 through an adaptor such as FlnA. This possibility is supported by

previous findings indicating that RACK1 interacts with FlnA to regulate plasma membrane levels of the cystic fibrosis transmembrane conductance regulator (Smith *et al,* 2013). One step of this mechanism was actually validated by the study of Lucien *et al* (2017) that showed through immunoprecipitation that PKC becomes part of a complex with RACK1 and NHE6 in HT1080 and MDA-MB-231 cells following exposition to hypoxia.

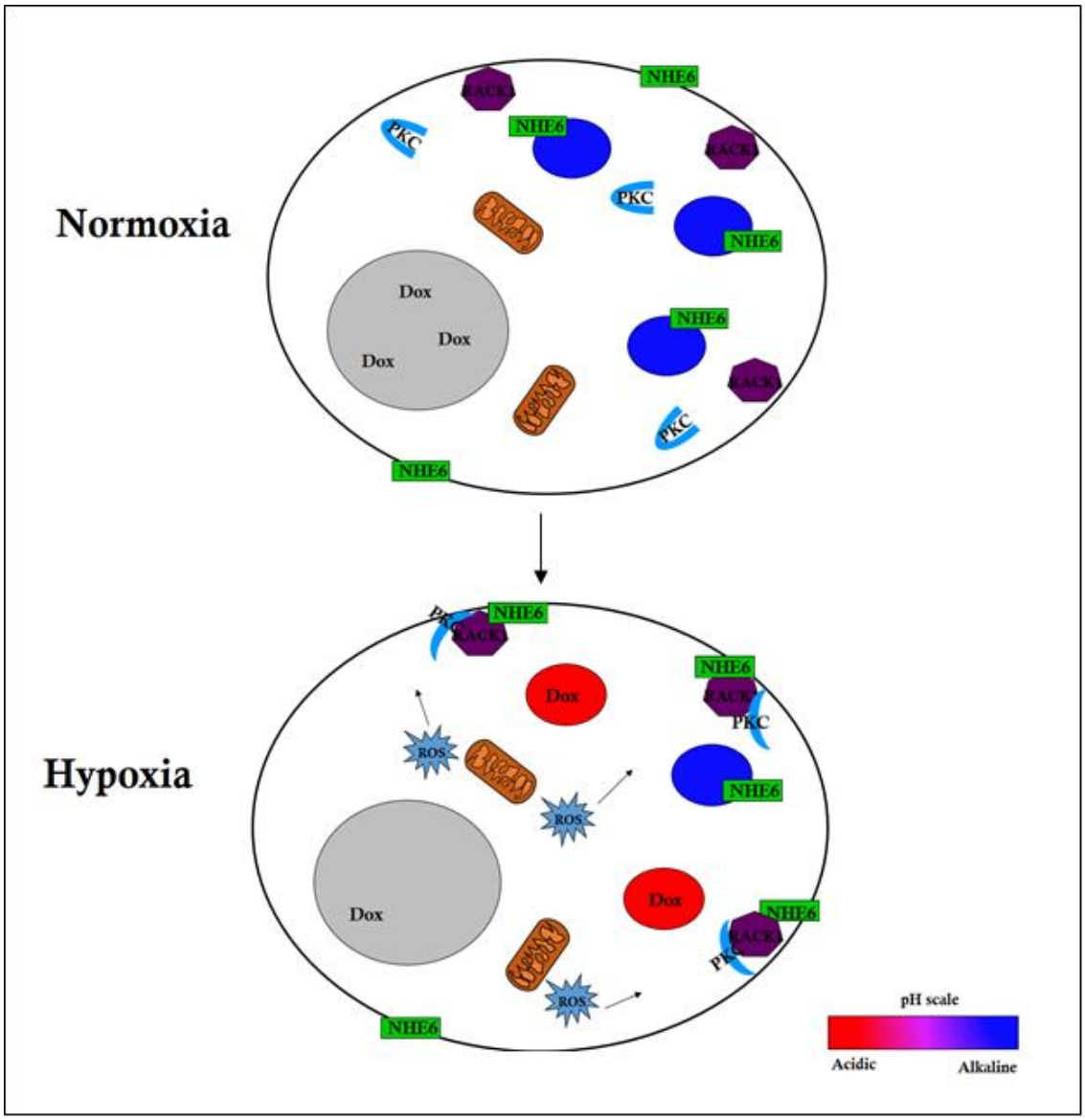

Figure 20. Proposed model of cellular events in hypoxia-induced NHE6 translocation to the plasma membrane.

Hypoxia induces increased mitochondrial ROS production that activates PKC. Once in an open active conformation, PKC binds RACK1 which triggers interaction with NHE6 and translocation of the protein complex towards the plasma membrane. RACK1 then acts to regulate cell surface levels of NHE6 by allowing the formation of a complex with an unknown adaptor protein. Reduced NHE6 levels in the endosomes results in lower pH of those compartments and increased doxorubicin ion-trapping.

The series of results illustrated above identify the interaction between NHE6 and RACK1 as a promising potential therapeutic target for the eventual development of therapeutics against chemoresistance. Although it is true that normalizing endosomal/lysosomal pH may not be enough to counter resistance to chemotherapy by itself in a microenvironment where the ECF is acidic and weak base therapeutics are partitioned out of the cell, it should be kept in mind that vesicular compartments can reach much lower pH values and that although smaller in volume, may have a larger potential to sequester weak base therapeutics. Although the activity of NHE6 when located at the plasma membrane has not been characterized to date, it is possible that similarly to NHE1, NHE6 may further contribute to ECF acidification in that location. Despite that fact, there remain several unknown variables that should ideally be uncovered before this therapeutic target can be fully exploited. Among other things, the specificity of such prospective therapeutic approach needs to be more closely examined. As the amino acid sequence from which the $NHE6^{527-588}$ peptide was derived is highly conserved in other intracellular members of the NHE protein subfamily (**Figure 14**) and human NHE7 and NHE9 have also been shown to interact with RACK1 (Ohgaki *et al*, 2008), it is highly probable that our competitive peptide also affects RACK1 interaction with these other two exchangers. Evolutionary retention of NHE6 and 9, which share a similar subcellular localization pattern, suggest that these two transporters must have a distinctive role to play; comparative studies are currently lacking to illustrate distinctions that exist between their roles. It is a definite possibility that regulation of these transporters expression, activity or localization may be impacted differently by the same stimuli. Complementary experiments from our laboratory revealed that shRNA depletion of NHE9 does not significantly alter endosomal pH and doxorubicin ion-trapping in HT1080 and MDA-MB-231 cells (Lucien *et al*, 2017). It is unclear if NHE9 is also a contributor to ion trapping of weak base therapeutics

in other cell models or if on the other hand, it serves to sensitize cancer cells to chemotherapy. If NHE9 was found to play a role counter to NHE6 regarding resistance to chemotherapy, relative expression of NHE6 and NHE9 in tumor biopsies may have to be considered in order to determine the adequate therapeutic approach. We cannot disregard that our competitive peptide may additionally prevent interactions with unexpected partners and thus have effects other than those for which it was conceived. As is the case for any experimental design, there were several limitations associated with this study that could be mitigated in the future. Namely, as mentioned throughout, further experimental controls would have occasionally been warranted to strengthen our findings. For some experiments, particularly the co-IP experiments, we would have wished to be able to further replicate the results in order to confirm our findings beyond doubt. We were ultimately unable to do so because of the timeliness, technicality and costliness associated with such experiments. Although, the confocal microscopy experiments offer much flexibility in experimental designs and permit the capture of striking images, they are not very scalable and generally restrain results to a relatively small number of cells. Other experiments such as plasma membrane protein biotinylation coupled to western blotting could prove more effective alternatives (Caldeira *et al*, 2016). Regardless of these considerations, the mechanism of chemoresistance observed in our cellular models is likely to be observed in many clinical cases and to present an interesting therapeutic target for many types of cancers.

The second portion of our study first involved detailed examination of the [527-588]-NHE6 segment in search of key amino acid residues in the NHE6/RACK1 interaction. Multiple methods of analysis that included MSA of a NHE intracellular subfamily, calculation of residue conservation index, protein disorder propensity predictions and scanning of the sequence for other characteristics of transient interactions allowed us to isolate the segment contained in [527-588]-NHE6 critical for the RACK1 interaction. The portion of the sequence in question is a 28 amino acid segment that stretches from F-536 to P-563 and that is particularly well-conserved (**Figure 14**).

The L-534 to P-563 sequence can be further subdivided into two distinct but interconnected segments. First, the proximal segment ranges from L-534 to K-547 and contains as many as

six putative anchor residues. A molecular docking simulation indicates that this region is indeed the most likely one to form an energetically favourable interaction (**Figure 18**) with the RACK1 binding site identified in figure 17. Of the six potential anchor residues previously identified, five were predicted to become buried in the RACK1 interface in at least 50% of the complex structures generated through a molecular docking protocol (**Figure 19**). Of these five residues, Y-539 was most often predicted to become buried in the complex structure (95%, **Figure 19A**). This finding is particularly interesting as phosphorylation of the cytoplasmic tail of members of the NHE protein family is one of the mechanisms that has been identified to modulate the activity and localization of these ion channels (Baumgartner *et al*, 2004). Next, the distal segment ranges from P-548 to P-563. It is a segment that is highly enriched in neutral polar residues (**Figure 15**), that contains four proline residues and that was predicted to be ID (**Figure 16**). Whereas the proximal segment of the F-536 to P-563 sequence might bind the cavity identified with Isocleft Finder through anchor residues, the distal segment might interact with the "aromatic cradle" identified in figure 17 as is typical for transient interactions. This proposed two step interaction would be logical as the structure of the proximal segment would allow for the initial point of contact to form the protein interface and the distal segment would then strengthen the interaction by wrapping itself around the "aromatic cradle". This proposed mechanism would be in line with the disorder-to-order transition that is often observed in the formation of a transient interaction between proteins (Janin *et al*, 2008). In this context, one can propose as a therapeutic strategy, the design of a peptide mimetic (London *et al*, 2008) containing the anchor residues, identified here in the proximal segment, as such a drug should prevent the initial step in the formation of the interaction interface between RACK1 and NHE6. This peptidomimetic would have to encompass some or all of the L-534 to K-547 sequence. A peptide formed of this fourteen amino acid sequence would be estimated to have a mass of 1.95 kDa[1].

Many intracellular protein-protein interactions were considered to be undruggable until the mid 2000's, but there have since been many advancements made in chemical modifications to peptide therapeutics that now make these realistic targets (Tsomaia, 2015). New peptide

[1]Genscript's peptide molecular weight calculator accessed at: https://www.genscript.com/account/customerpeptide.html

modifications have served to reduce proteolytic degradation, improve peptide conformation stability and allow greater cell permeability (Cromm *et al,* 2005). The adequate approach for chemical modifications depends on the shape of the interface; the creation of either stapled peptides or macrocycle peptides could prove to be effective in targeting the RACK1/NHE6 interaction interface (Dougherty *et al*, 2017). The approach of stapled peptides is used to stabilize structured epitopes in peptides of up to 60 amino acids (Cromm *et al,* 2005). Since α-helices are abundantly found in protein-protein interactions their stabilization can be particularly useful in the design of inhibitors. One prominent example was the design of a stapled peptide for the inhibition of the P53-MDM2 interaction mentioned within; this peptide which is named ALRN-6924 (Aileron Therapeutics) and is currently undergoing phase 1 clinical trial (Dougherty *et al*, 2017). Macrocycle peptides involve cyclization of a linear peptide by joining ends with a heteroaromatic linker (Saito & Bode, 2016). Similarly to grafted peptides, macrocycles also stabilize peptide secondary structures and can improve passive diffusion across the cell membrane. They are particularly well suited for large and relatively flat binding site surface areas where they can display antibody-like binding affinities through multiple points of contacts (Dougherty *et al*, 2017). Macrocyclic peptides typically have a molecular mass between 0.5 and 2.0 kDa (Dougherty *et al*, 2017) which places the [534-547]-NHE6 segment in the appropriate size range.

This study provided the foundation on which to establish the design of a potential peptide mimetic to be used as a therapy to prevent the occurrence of pH-mediated resistance to chemotherapy. Much effort would still be required to evaluate the safety of using such a compound as it is currently unknown if the NHE6/RACK1 interaction plays physiological roles aside from its roles described in cancer. As an example, it would be important to evaluate whether this interaction serves an important role in the brain, where NHE6 is highly expressed. NHE1 excessive activation in response to acidosis has been shown to exacerbate brain injury in perinatal hypoxia-ischemia (Uria-Avellanal & Robertson, 2014). This outcome is believed to result from intracellular Na^+ overload leading to ion flow reversal through the Na^+/Ca^{2+} exchanger and subsequently cell death. It is currently unknown if intracellular Na^+/H^+ exchangers have a similar effect or on the contrary act to attenuate ischemic brain injuries such as in the case of a stroke.

In addition to identifying the molecular determinants for future design of a peptide inhibitor, this study has made headways describing pathways involved in hypoxia induced chemoresistance. Mechanisms proposed here could eventually lead to the identification of other therapeutic targets as molecular events behind pH-mediated chemoresistance become better understood.

REFERENCES

Acuner Ozbabacan, S. E., Engin, H. B., Gursoy, A., & Keskin, O. (2011). Transient protein-protein interactions. *Protein Engineering Design and Selection*, *24*(9), 635–648.

Adams, D. R., Ron, D., & Kiely, P. A. (2011). RACK1, A multifaceted scaffolding protein: Structure and function. *Cell Communication and Signaling, 9*(1), 22.

Alfarouk, K. O., Verduzco, D., Rauch, C., Muddathir, A. K., Adil, H. H. B., Elhassan, G. O., Muntaser, E. I., Orozco, J. D. P., Cardone, R. A., Reskin, S. J. & Harguindey, S. (2014). Glycolysis, tumor metabolism, cancer growth and dissemination. A new pH-based etiopathogenic perspective and therapeutic approach to an old cancer question. *Oncoscience*, *1*(12), 777–802.

Ali, A. Y., Farrand, L., Kim, J. Y., Byun, S., Suh, J. Y., Lee, H. J., & Tsang, B. K. (2012). Molecular determinants of ovarian cancer chemoresistance: New insights into an old conundrum. *Annals of the New York Academy of Sciences*, *1271*(1), 58–67.

Amith, S. R., Wilkinson, J. M., & Fliegel, L. (2016). Na + /H + exchanger NHE1 regulation modulates metastatic potential and epithelial-mesenchymal transition of triple-negative breast cancer cells. *Oncotarget*, *5*(16).

Arnason, T., & Harkness, T. (2015). Development, Maintenance, and Reversal of Multiple Drug Resistance: At the Crossroads of TFPI1, ABC Transporters, and HIF1. *Cancers*, *7*(4), 2063–2082.

Avnet, S., Lemma, S., Cortini, M., Pellegrini, P., Perut, F., Zini, N., … Baldini, N. (2016). Altered pH gradient at the plasma membrane of osteosarcoma cells is a key mechanism of drug resistance. *Oncotarget*, *7*(39), (63408-63423).

Azam, M., Seeliger, M. a, Gray, N. S., Kuriyan, J., & Daley, G. Q. (2008). Activation of tyrosine kinases by mutation of the gatekeeper threonine. *Nature Structural & Molecular Biology*, *15*(10), 1109–18.

Ball, L. J., Kühne, R., Schneider-Mergener, J., & Oschkinat, H. (2005). Recognition of proline-rich motifs by protein-protein-interaction domains. *Angewandte Chemie (International Ed. in English)*, *44*(19), 2852–2869.

Barar, J., & Omidi, Y. (2013). Dysregulated pH in tumor microenvironment checkmates cancer therapy. *BioImpacts*, *3*(4), 149–162.

Bardenheuer, W., Lehmberg, K., Rattmann, I., Brueckner, a, Schneider, a, Sorg, U. R., … Flasshove, M. (2005). Resistance to cytarabine and gemcitabine and in vitro selection of

transduced cells after retroviral expression of cytidine deaminase in human hematopoietic progenitor cells. *Leukemia*, *19*(12), 2281–8.

Baumgartner, M., Patel, H., & Barber, D. L. (2004). Na(+)/H(+) exchanger NHE1 as plasma membrane scaffold in the assembly of signaling complexes. *American Journal of Physiology. Cell Physiology, 287*(4), C844–C850.

Becker, A.M., Zhang, J., Goyal, S., Dwarakanath, V., Aronson, P.S., Moe, O.W., Baum, M. (2007). Ontogeny ofNHE8 in the rat proximal tubule. *American Journal of Physiology: Renal Physiology 293*(1), F255–261.

Benej, M., Pastorekova, S., & Pastorek, J. (2014). Carbonic anhydrase IX: regulation and role in cancer. *Sub-cellular biochemistry. 75*, 199-219.

Bennewith, K. L., & Dedhar, S. (2011). Targeting hypoxic tumour cells to overcome metastasis. *BMC Cancer*, *11*(1), 504.

Berggård, T., Linse, S., & James, P. (2007). Methods for the detection and analysis of protein–protein interactions. *Proteomics*, *7*(16), 2833–2842.

Bos, R., Van Diest, P. J., De Jong, J. S., Van Der Groep, P., Van Der Valk, P., & Van Der Wall, E. (2005). Hypoxia-inducible factor-1α is associated with angiogenesis, and expression of bFGF, PDGF-BB, and EGFR in invasive breast cancer. *Histopathology*, *46*(1), 31–36.

Bourd-Boittin, K., Le Pabic, H., Bonnier, D., L'Helgoualc'h, A., & Theret, N. (2008). RACK1, a new ADAM12 interacting protein. Contribution to liver fibrogenesis. *The Journal of Biological Chemistry, 283*(38), 26000-26009.

Brahimi-Horn, M. C., Chiche, J., & Pouysségur, J. (2007). Hypoxia and cancer. *Journal of Molecular Medicine*, *85*(12), 1301–1307.

Bristow, R. G., & Hill, R. P. (2008). Hypoxia and metabolism. Hypoxia, DNA repair and genetic instability. Nature Reviews. Cancer, 8(3), 180–192.

Caldeira, M., Ferreira, J. S., Luísa Carvalho, A., Duarte, C. B. (2016). Biotinylation and Purification of Plasma Membrane-associated Proteins from Rodent Cultured Neurons. *Bio-protocol, 6*(10).

Catalano, V., Turdo, A., Di Franco, S., Dieli, F., Todaro, M., & Stassi, G. (2013). Tumor and its microenvironment: A synergistic interplay. *Seminars in Cancer Biology*, *23*(6), 522–532.

Caulin, A. F., & Maley, C. C. (2011). Peto's Paradox: Evolution's Prescription for Cancer Prevention Aleah. *Trends in Ecology & Evolution*, *26*(4), 175–182.

Chan, D. A., & Giaccia, A. J. (2007). Hypoxia, gene expression, and metastasis. *Cancer and Metastasis Reviews*, *26*(2), 333–339.

Chang, A. (2011). Chemotherapy, chemoresistance and the changing treatment landscape for NSCLC. *Lung Cancer*, *71*(1), 3–10.

Chapuy, B., Koch, R., Radunski, U., Corsham, S., Cheong, N., Inagaki, N., Ban, N., Wenzel, D., Reinhardt, D., Zapf, A., Schweyer, S., Kosari, F., Klapper, W., Truemper, L., & Wulf, G. G. (2008). Intracellular ABC transporter A3 confers multidrug resistance in leukemia cells by lysosomal drug sequestration. *Leukemia*, 22(8), 1576–1586.

Chen, E. I., Hewel, J., Krueger, J. S., Tiraby, C., Weber, M. R., Kralli, A., Becker, K., Yeates III, J. R., & Felding-Habermann, B. (2007). Adaptation of energy metabolism in breast cancer brain metastases. *Cancer Research*, *67*(4), 1472–1486.

Chen, J.-L., Lin, H. H., Kim, K.-J., Lin, A., Ou, J.-H. J., & Ann, D. K. (2009). PKCδ Signaling: A Dual Role in Regulating Hypoxic Stress-induced Autophagy and Apoptosis. *Autophagy*, *5*(2), 244–246.

Chen, J. L.-Y., Lucas, J. E., Schroeder, T., Mori, S., Wu, J., Nevins, J., Dewhirst, M., West, M., & Chi, J.-T. (2008). The genomic analysis of lactic acidosis and acidosis response in human cancers. *PLoS Genetics*, *4*(12), e1000293.

Chen, J., Wen, J., Zheng, Y., Yang, H., Luo, K., Liu, Q., Hu, R., Tan, Z., Huang, Q., & Fu, J. (2015). Prognostic significance of SLC9A9 in patients with resectable esophageal squamous cell carcinoma. *Tumour Biology: The Journal of the International Society for Oncodevelopmental Biology and Medecine*, *36*(9), 6797–6803.

Chen, S., Spiegelberg, B. D., Lin, F., Dell, E. J., & Hamm, H. E. (2004). Interaction of Gβγ with RACK1 and other WD40 repeat proteins. *Journal of Molecular and Cellular Cardiology*, *37*(2), 399–406.

Chen, Y., Schindler, M., & Simon, S. M. (1999). A mechanism for tamoxifen-mediated inhibition of acidification. *The Journal of Biological Chemistry*, *274*(26), 18364–73.

Chen, Z., Krmar, R. T., Dada, L., Efendiev, R., Leibiger, I. B., Pedemonte, C. H., Katz, A. I., Snazjder, J. I., & Bertorello, A. M. (2006). Phosphorylation of adaptor protein-2 mu2 is essential for Na+,K+-ATPase endocytosis in response to either G protein-coupled receptor or reactive oxygen species. *American Journal of Respiratory Cell and Molecular Biology*, *35*(1), 127–32.

Chiche, J., Brahimi-Horn, M. C., & Pouysségur, J. (2010). Tumour hypoxia induces a metabolic shift causing acidosis: A common feature in cancer. *Journal of Cellular and Molecular Medicine*, *14*(4), 771–794.

Chou, Y.-C., Chou, C.-C., Chen, Y.-K., Tsai, S., Hsieh, F. M. J., Liu, H. J., & Hseu, T.-H. (1999). Structure and genomic organization of porcine RACK1 gene. *Biochimica et Biophysica Acta*, *1489*, 315-322.

Chun, Y. S., Adusumilli, P. S., & Fong, Y. (2006). Employing Tumor Hypoxia for Oncolytic Therapy in Breast Cancer, (2005), 311–318.

Cloud-Heflin, B. A., Mcmasters, R. A., Osborn, M. T. & Chambers, T. C. (1996), Expression, Subcellular Distribution and Response to Phorbol Esters of Protein Kinase C (PKC) Isozymes in Drug-Sensitive and Multidrug-Resistant KB Cells Evidence for Altered Regulation of PKC-α. *European Journal of Biochemistry, 239*: 796–804.

Coldman, A. J., & Goldie, J. H. (1983) A model for the resistance of tumor cells to cancer chemotherapeutic agents. *Mathematical Biosciences*, *(65)*2: 291–307.

Condon, K. H., Ho, J., Robinson, C. G., Hanus, C., & Ehlers, M. D. (2013). The Angelman Syndrome Protein Ube3a/E6AP Is Required for Golgi Acidification and Surface Protein Sialylation. *Journal of Neuroscience*, *33*(9), 3799–3814.

Counillon, L., Pouyssegur, J., Reithmeier, R.A. (1994) The Na+/H + exchanger NHE-1 possessesN- and O-linked glycosylation restricted to the first N-terminal extracellular domain. Biochemistry 33(34): 10463–10469.

Cosentino-Gomes, D., Rocco-Machado, N., & Meyer-Fernandes, J. R. (2012). Cell signaling through protein kinase C oxidation and activation. *International Journal of Molecular Sciences*, *13*(9), 10697–10721.

Croker, A. K., & Allan, A. L. (2012). Inhibition of aldehyde dehydrogenase (ALDH) activity reduces chemotherapy and radiation resistance of stem-like ALDHhiCD44+ human breast cancer cells. *Breast Cancer Research and Treatment*, *133*(1), 75–87.

Cromm, M. C., Spiegel, J., & Grossmann, T. N. (2015). Hydrocarbon Stapled Peptides as Modulators of Biological Function. *American Chemical Society, 10,* 1362-1375.

Crowder, S. W., Balikov, D. A., Hwang, Y. S., & Sung, H. J. (2014). Cancer Stem Cells under Hypoxia as a Chemoresistance Factor in Breast and Brain. *Current Pathbiology Reports*, *2*(1), 33-40.

Curigliano, G., & Criscitiello, C. (2014). Successes and Limitations of Targeted Cancer Therapy in Breast Cancer. *Progress in Tumor Research, 41*, 15–35.

Dakubo, G. (2010). Mitochondrial reactive oxygen species and cancer. *Handbook of Free Radicals: Formation, Types and Effects*, 99–116.

Dave, J. M., Kang, H., Abbey, C. A., Maxwell, S. A., & Bayless, K. J. (2013). Proteomic Profiling of Endothelial Invasion Revealed Receptor for Activated C Kinase 1 (RACK1)

Complexed with Vimentin to Regulate Focal Adhesion Kinase (FAK) *, *The Journal of Biochemical Chemistry 288*(42), 30720–30733.

Davies, G. F., Berg, A., Postnikoff, S. D. L., Wilson, H. L., Arnason, T. G., Kusalik, A., & Harkness, T. A. A. (2014). TFPI1 mediates resistance to doxorubicin in breast cancer cells by inducing a hypoxic-like response. *PLoS ONE*, *9*(1).

De Juan, D., Pazos, F., & Valencia, A. (2013). Emerging methods in protein co-evolution. *Nature Reviews Genetics*, *14*(4), 249–261.

Denker, S.P., Huang, D.C., Orlowski, J., Furthmayr, H., Barber, D.L. (2000) Direct binding of the Na–H exchanger NHE1 to ERM proteins regulates the cortical cytoskeleton and cell shape independently of H(+) translocation. *Mol Cell 6*(6):1425–1436.

Denker, S. P. (2002). Cell migration requires both ion translocation and cytoskeletal anchoring by the Na-H exchanger NHE1. *The Journal of Cell Biology*, *159*(6), 1087–1096.

Dent, R., Trudeau, M., Pritchard, K. I., Hanna, W. M., Kahn, H. K., Sawka, C. A., Lickley, L. A., Rawlinson, E., Sun, P., & Narod, S. A. (2007). Triple-negative breast cancer: Clinical features and patterns of recurrence. *Clinical Cancer Research*, *13*(15), 4429–4434.

DeVita, V. T., & Chu, E. (2008). A history of cancer chemotherapy. *Cancer Research*, *68*(21), 8643–8653.

DeVita, V. T., & Rosenberg, S. A. (2012). Two Hundred Years of Cancer Research. *New England Journal of Medicine*, *366*, 2207–2214.

Diering, G.H., Numata, Y., Fan, S., Church, J., Numata, M. (2013). Endosomal acidification by Na+/H+ exchanger NHE5 regulates TrkA cell-surface targeting and NGF-induced PI3K signaling. *Molecular Biology of the Cell 24*, 3435–3448.

Di Marco, A., Cassinelli, G. & Arcamone, F. (1981). The discovery of Daunorubicin. *Cancer Treatment Reports, 65*(4), 3–8.

Dimmer, K. S., Friedrich, B., Lang, F., Deitmer, J. W., & Bröer, S. (2000). The low-affinity monocarboxylate transporter MCT4 is adapted to the export of lactate in highly glycolytic cells. The Biochemical Journal, 350 Pt 1, 219–27.

Doktorova, H., Hrabeta, J., Khalil, M. A., & Eckschlager, T. (2015). Hypoxia-induced chemoresistance in cancer cells: The role of not only HIF-1, *159*(2), 166–177.

Donowitz, M., Tse, M. C., & Fuster, D. (2013). SLC9/NHE gene family, a plasma membrane and organellar family of Na+/H+ exchangers *. *Mol Aspects Med*, *34*, 236–251.

Dougherty, P. G., Qian, Z., & Pei, D. (2017). Macrocycles as protein-protein interaction inhibitors. *Biochemical Journal, 474*(7), 1109-1125.

Draoui, N., & Feron, O. (2011). Lactate shuttles at a glance: from physiological paradigms to anti-cancer treatments. *Disease Models & Mechanisms*, *4*(6), 727–732.

Draoui, N., Schicke, O., Seront, E., Bouzin, C., Sonveaux, P., Riant, O., & Feron, O. (2014). Antitumor activity of 7-aminocarboxycoumarin derivatives, a new class of potent inhibitors of lactate influx but not efflux. Molecular Cancer Therapeutics, 13(6), 1410–8.

Egeblad, M., Nakasone, E. S., & Werb, Z. (2010). Tumors as organs: Complex tissues that interface with the entire organism. *Developmental Cell*, *18*(6), 884–901.

Erler, J. T., Bennewith, K. L., Nicolau, M., Dornhöfer, N., Kong, C., Le, Q.-T., … Giaccia, A. J. (2006). Lysyl oxidase is essential for hypoxia-induced metastasis. *Nature*, *440*(7088), 1222–1226.

Feng, S., Zhu, G., McConnell, M., Deng, L., Zhao, Q., Wu, M., Zhou, Q., Wang, J., Qi, J., Li, Y-P., & Chen, W. (2013). Silencing of atp6v1c1 prevents breast cancer growth and bone metastasis. International Journal of Biological Sciences, 9(8), 853–862.

Ferlay, J., Soerjomataram, I., Dikshit, R., Eser, S., Mathers, C., Rebelo, M., Parkin, D. M., Froman, D., & Bray, F. (2015). Cancer incidence and mortality worldwide: Sources, methods and major patterns in GLOBOCAN 2012. *International Journal of Cancer*, *136*(5), E359–E386.

Fisher, R., Pusztai, L., & Swanton, C. (2013). Cancer heterogeneity: implications for targeted therapeutics. *British Journal of Cancer*, *108*(3), 479–485.

Forgac, M. (2007). Vacuolar ATPases: rotary proton pumps in physiology and pathophysiology. Nature Reviews. Molecular Cell Biology, 8(11), 917–929.

Fraser, H. B., Hirsh, A. E., Wall, D. P., & Eisen, M. B. (2004). Coevolution of gene expression among interacting proteins. *Proceedings of the National Academy of Sciences of the United States of America*, *101*(24), 9033–8.

Fu, D. (2013). Where is it and How Does it Get There - Intracellular Localization and Traffic of P-glycoprotein. *Frontiers in Oncology*, *3*(December), 321.

Fukura, N., Ohgaki, R., Matsushita, M., Nakamura, N., Mitsui, K., & Kanazawa, H. (2010). A membrane-proximal region in the C-terminal tail of NHE7 is required for its distribution in the trans-golgi network, distinct from NHE6 localization at endosomes. *Journal of Membrane Biology*, *234*, 149–158.

Fung-Kee-Fung, M., Oliver, T., Elit, L., Oza, A., Hirte, H. W., & Bryson, P. (2007). Optimal chemotherapy treatment for women with recurrent ovarian cancer. *Current Oncology, 14*(5), 195–208.

Fuster, D. G., & Alexander, R. T. (2014). Traditional and emerging roles for the SLC9 Na+/H+ exchangers. *Pflugers Archiv European Journal of Physiology*, *466*, 61–76.

Gatenby, R. A., Smallbone, K., Maini, P. K., Rose, F., Averill, J., Nagle, R. B., Worrall, L., & Gillies, R. J. (2007). Cellular adaptations to hypoxia and acidosis during somatic evolution of breast cancer. *British Journal of Cancer*, *97*(5), 646–53.

Gerweck, L. E. (2006). Tumor pH controls the in vivo efficacy of weak acid and base chemotherapeutics. *Molecular Cancer Therapeutics*, *5*(5), 1275–1279.

Gibson, T. J. (2012). RACK1 research - Ships passing in the night? *FEBS Letters*, *586*(17), 2787–2789.

Gilkes, D. M., & Wirtz, D. (2014). Hypoxia and extracelluar matrix:drivers of tumor metastasis. *Nature Review Cancer*, *14*(6), 430–439.

Glavinas, H., Krajcsi, P., Cserepes, J., Sarkadi, B. (2004). The role of abc transporters in drug resistance, metabolism and toxicity. *Curr. Drug Deliv,14*(8), 27–42.

Gottesman, M. M., Fojo, T., & Bates, S. E. (2002). Multidrug Resistance in Cancer: Role of Atp-Dependent Transporters. Nature Reviews Cancer, 2(1), 48–58.

Greaves, M. (2007). Darwinian medicine: a case for cancer. *Nature Reviews Cancer*, *7*, 213–221.

Greaves, M. (2016). Leukaemia “firsts” in cancer research and treatment. *Nature Reviews Cancer*, *16*(3), 163–172.

Gusarova, G. A., Dada, L. A., Kelly, A. M., Brodie, C., Witters, L. A., Chandel, N. S., & Sznajder, J. I. (2009). α1-AMP-activated protein kinase regulates hypoxia-induced Na,K-ATPase endocytosis via direct phosphorylation of protein kinase C ζ. *Mol Cell Biol*, *29*(13), 3455–3464.

Halestrap, A. P. (2012). The monocarboxylate transporter family-Structure and functional characterization. IUBMB Life, 64(1), 1–9.

Hallett, R. M. (2015). Treatment-induced cell cycle kinetics dictate tumor response to chemotherapy. *Oncotarget*, *6*(9), 7040–7052.

Hall, M. D., Handley, M. D., & Gottesman, M. M. (2009). Is resistance useless? Multidrug resistance and collateral sensitivity. *Trends in Pharmacological Sciences*, *30*(10), 546–556.

Hanahan, D., & Weinberg, R. A. (2011). Review Hallmarks of Cancer : The Next Generation. *Cell*, *144*(5), 646–674.

Homolya, L., Váradi, A., & Sarkadi, B. (2003). Multidrug resistance-associated proteins: Export pumps for conjugates with glutathione, glucuronate or sulfate. *BioFactors (Oxford, England)*, *17*(1–4), 103–114.

Hosogi, S., Kusuzaki, K., & Inui, T. (2014). Cytosolic chloride ion is a key factor in lysosomal acidification and function of autophagy in human gastric cancer cell, *18*(6), 1124–1133.

Huang, Y., & Liu, Z. (2011). Anchoring intrinsically disordered proteins to multiple targets: Lessons from N-terminus of the p53 protein. *International Journal of Molecular Sciences*, *12*(2), 1410–1430.

Hu, C. T., Wu, J. R., & Wu, W. S. (2013). The role of endosomal signaling triggered by metastatic growth factors in tumor progression. *Cellular Signalling*, *25*(7), 1539–1545.

Ikebuchi, Y., Ito, K., Takada, T., Anzai, N., & Kanai, Y. (2010). Receptor for Activated C-Kinase 1 Regulates the Cell Surface Expression and Function of ATP Binding Cassette G2. *Drug Metabolism and Disposition, 38*(12), 2320–2328.

Ilie, A., Weinstein, E., Boucher, A., McKinney, R. A., & Orlowski, J. (2014). Impaired posttranslational processing and trafficking of an endosomal Na+/H+ exchanger NHE6 mutant (Δ 370WST372) associated with X-linked intellectual disability and autism. *Neurochemistry International*, *73*(1), 192–203.

Imai, T., Horiuchi, A., Wang, C., Oka, K., Ohira, S., Nikaido, T., & Konishi, I. (2003). Hypoxia attenuates the expression of E-cadherin via up-regulation of SNAIL in ovarian carcinoma cells. *The American Journal of Pathology*, *163*(4), 1437–1447.

Isoyama, S., Dan, S., Nishimura, Y., Nakamura, N., Kajiwara, G., Seki, M., Irimura, T., & Yamori, T. (2012). Establishment of phosphatidylinositol 3-kinase inhibitor-resistant cancer cell lines and therapeutic strategies for overcoming the resistance. *Cancer Science*, *103*(11), 1955–1960.

Itamochi, H., Kigawa, J., & Terakawa, N. (2008). Mechanisms of chemoresistance and poor prognosis in ovarian clear cell carcinoma. *Cancer Science*, *99*(4), 653–658.

Janin, J., Bahadur, R.P., and Chakrabarti, P. (2008). Protein-protein interaction and quaternary structure. *Q. Rev. Biophys. 41*, 133–180.

Jia, D., Duan, F., Peng, P., Sun, L., Liu, X., Wang, L., Wu, W., Ruan, Y., & Gu, J. (2013). Up-regulation of RACK1 by TGF-β1 promotes hepatic fibrosis in mice. *PloS One*, *8*(3), e60115.

Jiao M & Nan K. (2012). Activation of PI3 kinase/Akt/HIF-1α pathway contributes to hypoxia-induced epithelial-mesenchymal transition and chemoresistance in hepatocellular carcinoma. *International Journal of Oncology*, *40*(2), 461–468.

Kalinina, O. V., Gelfand, M. S., & Russell, R. B. (2009). Combining specificity determining and conserved residues improves functional site prediction. *BMC Bioinformatics*, *10*, 174.

Keith, B., Johnson, R. S., & Simon, M. C. (2012). HIF1α and HIF2α: sibling rivalry in hypoxic tumour growth and progression. *Nature Reviews. Cancer*, *12*(1), 9–22.

Khan, W., Duffy, F., Pollastri, G., Shields, D. C., & Mooney, C. (2013). Predicting binding within disordered protein regions to structurally characterised peptide-binding domains. *PloS One*, *8*(9), e72838.

Kiely, P. A, Leahy, M., O'Gorman, D., & O'Connor, R. (2005). RACK1-mediated integration of adhesion and insulin-like growth factor I (IGF-I) signaling and cell migration are defective in cells expressing an IGF-I receptor mutated at tyrosines 1250 and 1251. *The Journal of Biological Chemistry*, *280*(9), 7624–33.

Kirkwood, J. M., Tarhini, A., Sparano, J. A., Patel, P., Schiller, J. H., Vergo, M. T., Benson III, A. B., & Tawbi, H. (2013). Comparative clinical benefits of systemic adjuvant therapy for paradigm solid tumors. *Cancer Treatment Reviews*, *39*(1), 27–43.

Klimova, T., & Chandel, N. S. (2008). Mitochondrial complex III regulates hypoxic activation of HIF. *Cell Death and Differentiation, 15*(4), 660–666.

Kondapalli, K. C., Llongueras, J. P., Capilla-González, V., Prasad, H., Hack, A., Smith, C., Guerrero-Cázares, H., Quiñones-Hinojosa, A., & Rao, R. (2015). A Leak Pathway for Luminal Protons in Endosomes Drives Oncogenic Signaling in Glioblastoma. *Nature communications. 6*: 6289.

Kroemer, G., & Pouyssegur, J. (2008). Tumor Cell Metabolism: Cancer's Achilles' Heel. *Cancer Cell*, *13*(6), 472–482.

Kwee, J. K. (2014). A paradoxical chemoresistance and tumor suppressive role of antioxidant in solid cancer cells: A strange case of Dr. Jekyll and Mr. Hyde. *BioMed Research International*, *2014*, 209845.

Kurbatova, N., Chartier, M., Zylber, M. I., & Najmanovich, R. (2013) IsoCleft Finder – a web-based tool for the detection and analysis of protein binding-site geometric and chemical similarities [version 2; referees: 2 approved, 1 approved with reservations]. *F1000Research* , *2*, 117.

Lamonte, G., Tang, X., Chen, J. L.-Y., Wu, J., Ding, C.-K. C., Keenan, M. M., … Chi, J.-T. (2013). Acidosis induces reprogramming of cellular metabolism to mitigate oxidative stress. *Cancer & Metabolism*, *1*(1), 23.

Lamouille, S., Xu, J., & Derynck, R. (2014). Molecular mechanisms of epithelial-mesenchymal transition. *National Review Molecular Cell Biology*, *15*(3), 178–196.

Lavi, A., Ngan, C. H., Movshovitz-Attias, D., Bohnuud, T., Yueh, C., Beglov, D., … Kozakov, D. (2013). Detection of peptide-binding sites on protein surfaces: The first step toward the modeling and targeting of peptide-mediated interactions. *Proteins: Structure, Function and Bioinformatics*, *81*(12), 2096–2105.

Lee, C. M., & Tannock, I. F. (2006). Inhibition of endosomal sequestration of basic anticancer drugs: influence on cytotoxicity and tissue penetration. *British Journal of Cancer, 94*(6), 863–869.

Lee, S.-Y., Shi, L.-S., Chu, H., Li, M.-H., Ho, C.-W., Lai, F.-Y., … Chang, T.-C. (2013). Rhodiola crenulata and Its Bioactive Components, Salidroside and Tyrosol, Reverse the Hypoxia-Induced Reduction of Plasma-Membrane-Associated Na,K-ATPase Expression via Inhibition of ROS-AMPK-PKC ξ Pathway. *Evidence-Based Complementary and Alternative Medicine: eCAM*, *2013*, 284150.

Lee, S. a, Eyeson, R., Cheever, M. L., Geng, J., Verkhusha, V. V, Burd, C., … Kutateladze, T. G. (2005). Targeting of the FYVE domain to endosomal membranes is regulated by a histidine switch. *Proceedings of the National Academy of Sciences of the United States of America*, *102*(37), 13052–13057.

Li, H.C.,Du, Z., Barone, S., Rubera, I., McDonough, A.A., Tauc, M, Zahedi, K,,Wang, T., Soleimani, M. (2013) Proximal tubule specific knockout of the Na(+)/H(+) exchanger NHE3: effects on bicarbonate absorption and ammonium excretion. *Journal of Molecular Medecine 91*(8):951–963.

Li, J., & Xie, D. (2015). RACK1, a versatile hub in cancer, *Oncogene, 34,* 1890–1898.

Lippert, T. H., Ruoff, H.-J., & Volm, M. (2011). Current status of methods to assess cancer drug resistance. *International Journal of Medical Sciences*, *8*(3), 245–253.

Lin, H. H., Li, X., Chen, J.-L., Sun, X., Cooper, F. N., Chen, Y.-R., Zhang, W., Chung, Y., Li, A., Cheng, C.-T., Yang, L., Deng, X., Liu, X., Yen, Y., Johnson, D. L., Shih, H.-M., Yang, A., & Ann, D. K. (2012). Identification of an AAA ATPase VPS4B-Dependent Pathway That Modulates Epidermal Growth Factor Receptor Abundance and Signaling during Hypoxia. *Molecular and Cellular Biology*, *32*, 1124–1138.

Lin, P. J. C., Williams, W. P., Kobiljski, J., & Numata, M. (2007). Caveolins bind to (Na+, K+)/H+ exchanger NHE7 by a novel binding module. *Cellular Signalling*, *19*(5), 978–88.

Liu, W., Shen, S. M., Zhao, X. Y., & Chen Dr., G. Q. (2012). Targeted genes and interacting proteins of hypoxia inducible factor-1. *International Journal of Biochemistry and Molecular Biology*, *3*(2), 165–178.

Livingstone, C. D. and Barton, G. J. (1993), Protein Sequence Alignments: A Strategy for the Hierarchical Analysis of Residue Conservation. *CABIOS*, 9(6), 745-756.

London, N., Raveh, B., Movshovitz-Attias, D., & Schueler-Furman, O. (2010). Can Self-Inhibitory Peptides be Derived from the Interfaces of Globular Protein-Protein Interactions? *Proteins*, *78*(15), 3140–3149.

Lou, Y., McDonald, P. C., Oloumi, A., Chia, S., Ostlund, C., Ahmadi, A., Kyle, A., auf dem Keller, U., Leung, S., Huntsman, D., Clarke, B., Sutherland, B. W., Waterhouse, D., Bally, M., Roskelley, C., Overall, C. M., Minchinton, A., Pacchiano, F., Carta, F., Scozzafava, A., Touisni, N., Winum, J-Y., Supuran, C. T. & Dedhar, S. (2011). Targeting tumor hypoxia: Suppression of breast tumor growth and metastasis by novel carbonic anhydrase IX inhibitors. Cancer Research, 71(9), 3364–3376.

Lucien, F., Brochu-Gaudreau, K., Arsenault, D., Harper, K., & Dubois, C. M. (2011). Hypoxia-induced invadopodia formation involves activation of NHE-1 by the p90 ribosomal S6 kinase (p90RSK). *PloS One*, *6*(12), e28851.

Lucien, F., Harper, K., Pelletier, P. P., Volkov, L. & Dubois, C. M. (2014). Simultaneous pH Measurement in Endocytic and Cytosolic Compartments in Living Cells using Confocal Microscopy. *J. Vis. Exp.* (86), e51395.

Lucien, F., Pelletier, P. P., Lacroix, J. M., Roy, S., Parent, J. L., Arsenault, D., Harper, K., and Dubois, C. M. (2017). Hypoxia-induced mobilization of NHE6 to the plasma membrane triggers endosome hyperacidification and chemoresistance. *Nature Communications,* accepted for publication on May 10th 2017.

Lu, M; Kotelchuck, M; Hogan, V; Jones, L; Wright, K., & Halfon, N. (2010). HHS Public Access. *Ethnicity & Disease*, *20*(1 Supplement), 1–26.

Maes, H., Kuchnio, A., Peric, A., Moens, S., Nys, K., DeBock, K., Quaegebeur, A., Schoors, S., Georgiadou, M., Wouters, J., Vinckier, S., Vankelecom, H., Garmyn, M., Vion, A.-C., Radtke, F., Boulanger, C., Gerhadt, H., Dejana, E., Dewerchin, M., Ghesquière, B., Annaert, W., Agostinis, P., & Carmeliet, P. (2014). Tumor vessel normalization by chloroquine independent of autophagy. *Cancer Cell*, *26*(2), 190–206.

Calderon-Montano, J. M., Burgos-Moron, E., Perez-Guerrero, C., Salvador, J., Robles, A., Lopez-Lazaro, M. (2011). Role of the Intracellular pH in the Metabolic Switch between Oxidative Phosphorylation and Aerobic Glycolysis - Relevance to Cancer Role of the Intracellular pH in the Metabolic Switch between Oxidative Phosphorylation and Aerobic Glycolysis - Relevance to Cancer. *WebmedCentral CANCER, 2*(3), 1-10.

Marin-Hernandez, A., Gallardo-Perez, J. C., Ralph, S. J., Rodriguez-Enriquez, S., & Moreno-Sanchez, R. (2009) HIF-1alpha modulates energy metabolism in cancer cells by inducing over-expression of specific glycolytic isoforms. *Mini Rev Med Chem, 9*(9): 1084–1101.

Martínez-Zaguilán, R., Raghunand, N., Lynch, R. M., Bellamy, W., Martinez, G. M., Rojas, B., … Gillies, R. J. (1999). pH and drug resistance. I. Functional expression of

plasmalemmal V-type H+-ATPase in drug-resistant human breast carcinoma cell lines. Biochemical Pharmacology, 57(9), 1037–1046.

Maugeri-Saccà, M., Vigneri, P., & De Maria, R. (2011). Cancer stem cells and chemosensitivity. *Clinical Cancer Research*, *17*(15), 4942–4947.

Mayorca-Guiliani, A., & Erler, J. T. (2013). The potential for targeting extracellular LOX proteins in human malignancy. *OncoTargets and Therapy*, *6*, 1729–1735.

McCahill, A., Warwicker, J., Bolger, G. B., Houslay, M. D., & Yarwood, S. J. (2002). The RACK1 Scaffold Protein: a Dynamic Cog in Cell Response Mechanisms. *Molecular Pharmacology*, *62*(6), 1261–1273.

Meads, M. B., Gatenby, R. A., & Dalton, W. S. (2009). Environment-mediated drug resistance: a major contributor to minimal residual disease. *Nature Reviews. Cancer*, *9*(9), 665–74.

Milosavljevic, N., Monet, M., Léna, I., Brau, F., Lacas-Gervais, S., Feliciangeli, S., Counillon, L., & Poët, M. (2014). The Intracellular Na+/H+ Exchanger NHE7 Effects a Na+-Coupled, but Not K+-Coupled Proton-Loading Mechanism in Endocytosis. *Cell Reports*, *7*(3), 689–696.

Mochly-Rosen, D., Das, K., & Grimes, K. (2013). Protein kinase C, an elusive therapeutic target? *Nature Reviews Drug Discovery*, *11*(12), 937–957.

Mooney, C., Haslam, N. J., Holton, T. a, Pollastri, G., & Shields, D. C. (2013). PeptideLocator: prediction of bioactive peptides in protein sequences. *Bioinformatics (Oxford, England)*, *29*(9), 1120–6.

Morgan, P. E., Pastoreková, S., Stuart-Tilley, A. K., Alper, S. L., & Casey, J. R. (2007). Interactions of transmembrane carbonic anhydrase, CAIX, with bicarbonate transporters. *American Journal of Physiology. Cell Physiology*, *293*(2), C738-48.

Moudi M., Go R., Yien C. Y. S. & Nazre M. (2013). Vinca alkaloids. *International Journal of Preventive Medecine, 4*(11), 1231–1235.

Mullard, A. (2012). NEWS & ANALYSIS Protein – protein interaction inhibitors, *11*(March), 173–175.

Muro, S., Mateescu, M., Gajewski, C., Robinson, M., Muzykantov, V. R., & Koval, M. (2006). Control of intracellular trafficking of ICAM-1-targeted nanocarriers by endothelial Na+/H+ exchanger proteins. *American Journal of Physiology. Lung Cellular and Molecular Physiology*, *290*(5), L809–L817.

Murthy, A., Gonzalez-Agosti, C., Cordero, E., Pinney, D., Candia, C., Solomon, F., … Ramesh, V. (1998). NHE-RF, a regulatory cofactor for Na+ -H+ exchange, is a common

interactor for merlin and ERM (MERM) proteins. *Journal of Biological Chemistry*, *273*(3), 1273–1276.

Nakanishi, T., & Ross, D. D. (2012). Breast cancer resistance protein (BCRP/ABCG2): Its role in multidrug resistance and regulation of its gene expression. Chinese Journal of Cancer, 31(2), 73–99.

Nakayama, K. (2009). Cellular signal transduction of the hypoxia response. *Journal of Biochemistry*, *146*(6), 757–765.

Neri, D., & Supuran, C. T. (2011). Interfering with pH regulation in tumours as a therapeutic strategy. Nature Reviews. Drug Discovery, 10(10), 767–77.

Nguyen, L. V., Vanner, R., Dirks, P., & Eaves, C. J. (2012). Cancer stem cells: an evolving concept. *Nature Reviews Cancer*, *12*, 133–143.

Nørholm, A. B., Hendus-Altenburger, R., Bjerre, G., Kjaergaard, M., Pedersen, S. F., & Kragelund, B. B. (2011). The intracellular distal tail of the Na+/H+ exchanger NHE1 is intrinsically disordered: Implications for NHE1 trafficking. *Biochemistry*, *50*(17), 3469–3480.

Numata, M. (2011). Organellar (Na+, K+)/H+ exchanger NHE7 regulates cell adhesion, invasion and anchorage-independent growth of breast cancer MDA-MB-231 cells. *Oncology Reports*, 311–317.

Ohgaki, R., Fukura, N., Matsushita, M., Mitsui, K., & Kanazawa, H. (2008). Cell surface levels of organellar Na+/H+ exchanger isoform 6 are regulated by interaction with RACK1. *Journal of Biological Chemistry*, *283*(7), 4417–4429.

Ohgaki, R., Matsushita, M., Kanazawa, H., Ogihara, S., Hoekstra, D., & Ijzendoorn, S. C. D. Van. (2010). The Na+/H+ Exchanger NHE6 in the Endosomal Recycling System Is Involved in the Development of Apical Bile Canalicular Surface Domains in HepG2 Cells. *Molecular Biology of the Cell, 21*, 1293–1304.

Ohgaki, R., Van Ijzendoorn, S. C. D., Matsushita, M., Hoekstra, D., & Kanazawa, H. (2011). Organellar Na+/H+ exchangers: Novel players in organelle pH regulation and their emerging functions. *Biochemistry*, *50*, 443–450.

Ohtsubo, T., Igawa, H., Saito, T., Matsumoto, H., Park, H. J., Song, C. W., Kano, E., & Saito, H. (2001). Acidic environment modifies heat- or radiation-induced apoptosis in human maxillary cancer cells. *International Journal of Radiation Oncology Biology Physics*, *49*(5), 1391–1398.

Olive, K. P., Jacobetz, M. a, Davidson, C. J., Mcintyre, D., Honess, D., Madhu, B., … Iacobuzio-donahue, C. (2009). Chemotherapy in a Mouse Model of Pancreatic Cancer. *Cancer Research*, *324*(5933), 1457–1461.

Onishi, I., Lin, P. J. C., Diering, G. H., Williams, W. P., & Numata, M. (2006). RACK1 associates with NHE5 in focal adhesions and positively regulates the transporter activity. *Cellular Signaling*, *19*, 194-203.

O'Reilly, E. A., Gubbins, L., Sharma, S., Tully, R., Guang, M. H. Z., Weiner-Gorzel, K., McCaffrey, J., Harrison, M., Furlong, F., Kell, M., & McCann, A. (2015). The fate of chemoresistance in triple negative breast cancer (TNBC). *BBA Clinical*, *3*, 257–275.

Orlowski, J., & Grinstein, S. (2007). Emerging roles of alkali cation/proton exchangers in organellar homeostasis. *Current Opinion in Cell Biology*, *19*(4), 483–492.

Pajonk, F., Vlashi, E., & McBride, W. H. (2010). Radiation Resistance of Cancer Stem Cell: The 4 R's of Radiobiology Revisited. *Stem Cells*, *28*(4), 639–648.

Park, K., Evans, R. L., Watson, G. E., Nehrke, K., Richardson, L., Bell, S. M., Schultheis, P. J., Hand, A. R. Shull, G. E. & Melvin, J. E. (2001). Defective Fluid Secretion and NaCl Absorption in the Parotid Glands of Na^+/ H^+ Exchanger-deficient Mice *, Journal of Biological Chemistry, *276*(29), 27042–27050.

Perez-Sayans, M., Garcia-Garcia, A., Scozzafava, A., Supuran, C. T. (2012). Inhibition of V-ATPase and Carbonic Anhydrases as Interference Strategy with Tumor Acidification Processes. *Current Pharmaceutical Design*, *18*(10): 1407-1413.

Perkins, J. R., Diboun, I., Dessailly, B. H., Lees, J. G., & Orengo, C. (2010). Transient Protein-Protein Interactions: Structural, Functional, and Network Properties. *Structure*, *18*(10), 1233–1243.

Persidis, A. (1999). Cancer multidrug resistance. *Nature Biotechnology*, *17*, 94–95.

Petriz, J.; Gottesman, M. M.; Aran, J. M. (2004). An MDR-EGFP gene fusion allows for direct cellular localization, function and stability assessment of P-glycoprotein. *Curr. Drug Delivery, 1*(1), 43–56.

Picollo, A., & Pusch, M. (2005). Chloride/proton antiporter activity of mammalian CLC proteins ClC-4 and ClC-5. Nature, 436(7049), 420–423.

Pommier, Y., Sordet, O., Antony, S., Hayward, R. L., & Kohn, K. W. (2004). Apoptosis defects and chemotherapy resistance: molecular interaction maps and networks. *Oncogene*, *23*(16), 2934–49.

Porporato, P. E., Dhup, S., Dadhich, R. K., Copetti, T., & Sonveaux, P. (2011). Anticancer targets in the glycolytic metabolism of tumors: A comprehensive review. *Frontiers in Pharmacology*, *2*(49), 1–18.

Rakha, E. A., & Chan, S. (2011). Metastatic Triple-negative Breast Cancer. *Clinical Oncology*, *23*(9), 587–600.

Rakha, E. A., Reis-Filho, J. S., & Ellis, I. O. (2008). Basal-like breast cancer: A critical review. *Journal of Clinical Oncology*, *26*(15), 2568–2581.

Raveh, B., London, N., & Schueler-Furman, O. (2010). Sub-angstrom modeling of complexes between flexible peptides and globular proteins. *Proteins: Struct., Funct., Bioinf. 78*(9), 2029-2040.

Raveh, B., London, N., Zimmerman, L., & Schueler-Furman, O. (2011). Rosetta FlexPepDock ab-initio: Simultaneous Folding, Docking and Refinement of Peptides onto Their Receptors. *PLoS ONE*, *6*(4), e18934.

Rebucci, M., & Michiels, C. (2013). Molecular aspects of cancer cell resistance to chemotherapy. *Biochemical Pharmacology*, *85*(9), 1219–1226.

Reshkin S.J., Bellizzi, A., Caldeira, S., Albarani, V., Malanchi, I., Poignee, M., Alunni-Fabbroni, M., Casavola, V., Tommasino, M. (2000). Na+/H+ exchanger-dependent intracellular alkalinization is an early event in malignant transformation and plays an essential role in the development of subsequent transformation-associated phenotypes. *Faseb Journal 14*(14):2185–2197.

Reshkin, S. J., Greco, M. R., Cardone, R. A., & Reshkin, S. J. (2014). Role of pH i , and proton transporters in oncogene-driven neoplastic transformation.

Ron, D., Chen, C., Caldwell, J., Jamiesont, L. E. E., Orrt, E., & Mochly-rosen, D. (1994). Cloning of an intracellular receptor for protein kinase C : A homolog of the f8 subunit of G proteins. *Proceedings of the National Academy of Sciences, 91*, 839–843.

Ron, D., Jiang, Z., Yao, L., Vagts, A., Diamond, I., & Gordon, A. (1999). Coordinated Movement of RACK1 with Activated βIIPKC *. *The Journal of Biomedical Chemistry, 274*(38), 27039–27046.

Roxrud, I., Railborg, C., Gilfillan, G.D., Strømme, P., & Stenmark, H. (2009). Dual degradation mechanisms ensure diposal of NHE6 mutant protein associated with neurological disease. *Experimental Cell Research, 315*(17), 3014-3027.

Ruan, Y., Sun, L., Hao, Y., Wang, L., Xu, J., Zhang, W., … Gu, J. (2012). Ribosomal RACK1 promotes chemoresistance and growth in human hepatocellular carcinoma. *Journal of Clinical Investigation*, *122*(7), 2554–2566.

Ruch, R. J., Klaunig, J. E., Kerckaert, G. A., & LeBoeuf R. A. (1990). Modification of gap junctional intercellular communication by changes in extracellular pH in Syrian hamster embryo cells. *Carcinogenesis, 11*(6), 909-913.

Ruiz Carrillo, D., Chandrasekaran R., Nilsson, M., Cornvik, T., Liew, C. W., Tan, S. M., & Lescar, J. (2012). Structure of human Rack1 protein at a resolution of 2.45Å. *Acta Crystallogr. Sect. A, 68*(8), 867-872.

Ruusuvuori, E., Kaila, K., 2014. Carbonic anhydrases and brain pH in the control of neuronal excitability. *Subcell. Biochem. 75*, 271–290.

Sahlgren, C., Gustafsson, M. V., Jin, S., Poellinger, L., & Lendahl, U. (2008). Notch signaling mediates hypoxia-induced tumor cell migration and invasion. *Proceedings of the National Academy of Sciences*, *105*(17), 6392–6397.

Saito, F., & Bode, J. W. (2016). Macrocyclic peptides: Tying up loose ends. *Nature Chemistry, 8*, 1085-1086.

Salerno, M., Avnet, S., Bonuccelli, G., Hosogi, S., Granchi, D., & Baldini, N. (2014). Impairment of Lysosomal Activity as a Therapeutic Modality Targeting Cancer Stem Cells of Embryonal Rhabdomyosarcoma Cell Line RD, *9*(10).

Sampath, D., Cortes, J., Estrov, Z., Du, M., Shi, Z., Andreeff, M., Gandhi, V., & Plunkett, W. (2006). Pharmacodynamics of cytarabine alone and in combination with 7-hydroxystaurosporine (UCN-01) in AML blasts in vitro and during a clinical trial. *Blood*, *107*(6), 2517–2524.

Schindler, M., Grabski, S., Hoff, E., & Simon, S. M. (1996). Defective pH regulation of acidic compartments in human breast cancer cells (MCF-7) is normalized in Adriamycin-resistant cells (MCF-7adr). *Biochemistry*, 35(9), 2811-7.

Schultheis, P.J., Clarke, L.L., Meneton, P., Harline, M., Boivin, G.P., Stemmermann, G., Duffy, J.J., Doetschman, T., Miller, M.L., Shull, G.E. (1998) Targeted disruption of the murine Na+/H+ exchanger iso- form2 gene causes reduced viability of gastric parietal cells and loss of net acid secretion. *J Clin Invest 101*(6):1243–1253.

Semenza, G. L. (2003). Targeting HIF-1 for cancer therapy. *Nature Reviews. Cancer*, *3*(10), 721–32.

Semenza, G. L. (2009). Regulation of cancer cell metabolism by hypoxia-inducible factor 1. *Seminars in Cancer Biology*, *19*(1), 12–16.

Sennoune, S. R., Bakunts, K., Martínez, G. M., Chua-Tuan, J. L., Kebir, Y., Attaya, M. N., & Martínez-Zaguilán, R. (2004). Vacuolar H+-ATPase in human breast cancer cells with distinct metastatic potential: distribution and functional activity. *American Journal of Physiology. Cell Physiology*, *286*(6), C1443–C1452.

Shen, Y., Maupetit, J., Derreumaux, P., & Tufféry, P. (2014) Improved PEP-FOLD approach for peptide and miniprotein structure prediction. *J. Chem. Theor. Comput. 10*, 4745-4758.

Shin, D. H., Choi, Y. J., & Park, J. W. (2014). SIRT1 and AMPK mediate hypoxia-induced resistance of non-small cell lung cancers to cisplatin and doxorubicin. *Cancer Research*, *74*(19), 298–308.

Smalley, M., Piggott, L., & Clarkson, R. (2013). Breast cancer stem cells: Obstacles to therapy. *Cancer Letters*, *338*(1), 57–62.

Smith, L., Litman, P., Kohli, E., Amick, J., Page, R. C., Misra, S., & Liedtke, C. M. (2013). RACK1 interacts with filamin-A to regulate plasma membrane levels of the cystic fibrosis transmembrane conductance regulator. *American Journal of Physiology. Cell Physiology*, *305*(1), C111–20.

Sonveaux, P., Végran, F., Schroeder, T., Wergin, M. C., Verrax, J., Rabbani, Z. N., de Saedeleer, C. J., Kennedy, K. M., Diepart, C., Jordan, B. F., Kelley, M. J., Gallez, B., Wahl, M. L., Feron, O., & Dewhirst, M. W. (2008). Targeting lactate-fueled respiration selectively kills hypoxic tumor cells in mice. Journal of Clinical Investigation, 118(12), 3930–3942.

Spugnini, E. P., Sonveaux, P., Stock, C., Perez-Sayans, M., De Milito, A., Avnet, S., Garcìa, A. G., Harguindey, S., & Fais, S. (2015). Proton channels and exchangers in cancer. *Biochimica et Biophysica Acta (BBA) - Biomembranes*, *1848*(10), 2715–2726.

Srinivasan, M., & Dunker, A. K. (2012). Proline rich motifs as drug targets in immune mediated disorders. *International Journal of Peptides*, *2012*.

Steffan, J. J., Snider, J. L., Skalli, O., Welbourne, T., & Cardelli, J. A. (2009). Na+/H+ exchangers and RhoA regulate acidic extracellular pH-induced lysosome trafficking in prostate cancer cells. *Traffic*, *10*(6), 737–753.

Steinberg, B.E., Huynh, K.K., Brodovitch, A., Jabs, S., Stauber, T., Jentsch, T.J., Grinstein, S. (2010) A cation counterflux supports lysosomal acidification. *Journal of Cell Biology 189*(7), 1171–1186.

Stylianopoulos, T. (2016). The solid mechanics of cancer and strategies for improved therapy. *Journal of Biomechanical Engineering*, (c).

Supuran, C. T. (2008). Carbonic anhydrases: novel therapeutic applications for inhibitors and activators. Nature Reviews. Drug Discovery, 7(2), 168–181.

Swaminathan, G., & Cartwright, C. A. (2012). Rack1 promotes epithelial cell–cell adhesion by regulating E-cadherin endocytosis. *Oncogene*, *31*(3), 376–389.

Tafreshi, N. K., Bui, M. M., Bishop, K., Lloyd, M. C., Enkemann, S. A., Lopez, A. S., Abrahams, D., Carter, B. W., Vagner, J., Grobmyer, S. R., Gillies, R. J., & Morse, D. L. (2012). Noninvasive detection of breast cancer lymph node metastasis using carbonic anhydrases IX and XII targeted imaging probes. Clinical Cancer Research, 18(1), 207–219.

Takahashi, K.I., Copenhagen, D.R., 1996. Modulation of neuronal function by intra-cellular pH. *Neuroscience Research*, *24*, 109-116.

Tamada, M., Nagano, O., Tateyama, S., Ohmura, M., Yae, T., Ishimoto, T., Sugihara, E., Onishi, N., Yamamoto, T., Yanagawa, H., Suematsu, M., & Saya, H. (2012). Modulation of glucose metabolism by CD44 contributes to antioxidant status and drug resistance in cancer cells. *Cancer Research*, *72*(6), 1438–1448.

Teicher, B. A. (2006). Cancer Drug Resistance. Totowa:Humana Press.

Thomas, D. A., Kantarijan, H., Smith, T. L., Koller, C., Cortes, J., O'Brien, S., Giles, F. J., Gajewski, J., Pierce, S., & Keating, M. J. Primary refractory and relapsed adult acute lymphoblastic leukemia: characteristics, treatment results, and prognosis with salvage therapy. *Cancer*, *86*(7): 1216–1230.

Tomita, H., Tanaka, K., Tanaka, T., & Hara, A. (2016). Aldehyde dehydrogenase 1A1 in stem cells and cancer. *Oncotarget*, *7*(10), 11018–32.

Toullec, D., Pianetti, P., Coste, H., Bellevergue, P., Grand-Perret, T., Ajakane, M., Baudet, V., Boissin, P., Boursier, E., Loriolle, F., Duhamel, L., Charon, D., & Kirilovsky, J. (1991). The bisindolylmaleimide GF 109203X is a potent and selective inhibitor of protein kinase C. *Journal of Biological Chemistry, 266*(24), 15771–15781.

Tsomaia, N. (2015). Peptide therapeutics: Targeting the undruggable space. *European Journal of Medicinal Chemistry, 94*, 459-470.

Tsvetkova, E., & Goss, G. D. (2012). Drug resistance and its significance for treatment decisions in non-small-cell lung cancer. *Current Oncology, 19*, 45–51.

Tubert-Brohman, I., Sherman, W., Repasky, M., & Beuming, T. (2013). Improved docking of polypeptides with glide. *Journal of Chemical Information and Modeling*, *53*(7), 1689–1699.

Ullah, M. S., Davies, A. J., & Halestrap, A. P. (2006). The plasma membrane lactate transporter MCT4, but not MCT1, is up-regulated by hypoxia through a HIF-1α-dependent mechanism. *Journal of Biological Chemistry*, *281*(14), 9030–9037.

Ullah, M. F. (2008). Cancer multidrug resistance (MDR): A major impediment to effective chemotherapy. *Asian Pacific Journal of Cancer Prevention*, *9*(1), 1–6.

Uria-Avellanal, C., & Robertson, N. J. (2014). Na+/H+ Exchangers and Intracellular pH in Perinatal Brain Injury. *Translational Stroke Research, 5*(1), 79–98.

Verdun, R. E., & Karlseder, J. (2007). Replication and protection of telomeres. Nature, 447(7147), 924–931.

Verwey, M., Joubert, A., & Visagie, M. (2016). Chemoresistance in breast cancer stem cells. *Biomedical*, *27*(1), 16–23.

Vlieghe, P., Lisowski, V., Martinez, J., & Khrestchatisky, M. (2010). Synthetic therapeutic peptides: science and market. *Drug Discovery Today*, *15*(1-2), 40–56.

von Schwarzenberg, K., Lajtos, T., Simon, L., Müller, R., Vereb, G., & Vollmar, A. M. (2014). V-ATPase inhibition overcomes trastuzumab resistance in breast cancer. Molecular Oncology, 8(1), 9–19.

Ward, C., Langdon, S. P., Mullen, P., Harris, A. L., Harrison, D. J., Supuran, C. T., & Kunkler, I. H. (2013). New strategies for targeting the hypoxic tumour microenvironment in breast cancer. *Cancer Treatment Reviews*, *39*(2), 171–179.

Weinstein, I. B., & Joe, A. K. (2006). Mechanisms of disease: Oncogene addiction--a rationale for molecular targeting in cancer therapy. *Nature Clinical Practice. Oncology*, *3*(8), 448–57.

Wild, P., Knuechel, R., Dietmaier, W., Hofstaedter, F., & Hartmann, A. (2000). Laser microdissection and microsatellite analyses of breast cancer reveal a high degree of tumor heterogeneity. *Pathobiology, 68*, 180–190.

Williams, A. C., Collard, T. J., & Paraskeva, C. (1999). An acidic environment leads to p53 dependent induction of apoptosis in human adenoma and carcinoma cell lines : implications for clonal selection during colorectal carcinogenesis, *282*, 3199–3204.

Wilson, M. C., Meredith, D., Bunnun, C., Sessions, R. B., & Halestrap, A. P. (2009). Studies on the DIDS-binding site of monocarboxylate transporter 1 suggest a homology model of the open conformation and a plausible translocation cycle. Journal of Biological Chemistry, 284(30), 20011–20021.

Wojtkowiak, J. W., Rothberg, J. M., Kumar, V., Schramm, K. J., Haller, E., Proemsey, J. B., Lloyd, M. C., Sloane, B. F., & Gillies, R. J. (2012). Chronic Autophagy Is a Cellular Adaptation to Tumor Acidic pH Microenvironments, *72*(14), 3938–3947.

Wojtkowiak, J. W., Verduzco, D., Schramm, K. J., & Gillies, R. J. (2011). Drug resistance and cellular adaptation to tumor acidic pH microenvironment. *Molecular Pharmaceutics*, *8*, 2032–2038.

Wu, K. L., Khan, S., Lakhe-Reddy, S., Jarad, G., Mukherjee, A., Obejero-Paz, C. A., Konieczkowski, M., Sedor, J. R., & Schelling, J. R. (2004). The NHE1 Na+/H+ exchanger recruits ezrin/radixin/moesin proteins to regulate Akt-dependent cell survival. *Journal of Biological Chemistry*, *279*(25), 26280–26286.

Xinhan, L., Matsushita, M., Numaza, M., Taguchi, a., Mitsui, K., & Kanazawa, H. (2011). Na+/H+ exchanger isoform 6 (NHE6/SLC9A6) is involved in clathrin-dependent endocytosis of transferrin. *AJP: Cell Physiology*, *301*(6), C1431–C1444.

Xu, B., Jin, X., Min, L., Li, Q., Deng, L., Wu, H., Lin, G., Chen, L., Zhang, H., Li, C., Wang, L., Zhu, J., Wang, W., Chu, F., Shen, J., Li, H., & Mao, J. (2015). Chloride channel-3 promotes tumor metastasis by regulating membrane ruffling and is associated with poor survival. Oncotarget, 6(4), 2434–2450.

Xu, H., Li, J., Chen, H., Wang, C., Ghishan, F.K. (2013) NHE8 plays important roles in gastric mucosal protection. *American Journal of Physiology: Gastrointestinal Liver Physiology 304(*3), G257–261.

Xu, L., Mann, G., Meissner, G. (1996) Regulation of cardiac Ca2+ release channel (ryanodine receptor) by Ca2+, H+, Mg2+, and adenine nucleotides under normal and simulated ischemic conditions. *Circ Res 79*(6):1100–1109.

Xue, J., Zhou, D., Yao, H., Gavrialov, O., McConnell, M. J., Gelb, B. D., & Haddad, G. G. (2007). Novel functional interaction between Na+/H+ exchanger 1 and tyrosine phosphatase SHP-2. *American Journal of Physiology. Regulatory, Integrative and Comparative Physiology*, *292*(6), R2406–16.

Yin, J., & Zhang, J. (2011). Multidrug resistance-associated protein 1 (MRP1/ABCC1) polymorphism: from discovery to clinical application. Zhong Nan Da Xue Xue Bao. Yi Xue Ban = Journal of Central South University. Medical Sciences, 36(10), 927–38.

Yu, K. Da, Zhu, R., Zhan, M., Rodriguez, A. A., Yang, W., Wong, S., Makris, A., Lehmann, B. D., Chen, X., Mayer, I., Pietenpol, J. A., Shao, Z.-H., Symmans, W. F., & Chang, J. C. (2013). Identification of prognosis-relevant subgroups in patients with chemoresistant triple-negative breast cancer. *Clinical Cancer Research*, *19*(10), 2723–2733.

Yu, M., Ocana, A., & Tannock, I. F. (2013). Reversal of ATP-binding cassette drug transporter activity to modulate chemoresistance: Why has it failed to provide clinical benefit? *Cancer and Metastasis Reviews*, *32*(1–2), 211–227.

Yu, M., & Tannock, I. F. (2012). Targeting Tumor Architecture to Favor Drug Penetration: A New Weapon to Combat Chemoresistance in Pancreatic Cancer? *Cancer Cell*, *21*(3), 327–329.

Yu, T., Tang, B., & Sun, X. (2017). Development of Inhibitors Targeting Hypoxia-Inducible Factor 1 and 2 for Cancer Therapy. *Yonsei Medical Journal, 58*(3), 489–496.

Zahreddine, H., & Borden, K. L. B. (2013). Mechanisms and insights into drug resistance in cancer. *Frontiers in Pharmacology*, *4*(28*)*, 1–8.

Zhang, W., Zong, C. S., Hermanto, U., Lopez-bergami, P., Ronai, Z., & Wang, L. (2006). RACK1 Recruits STAT3 Specifically to Insulin and Insulin-Like Growth Factor 1 Receptors for Activation , Which Is Important for Regulating Anchorage-Independent Growth †. *Molecular and Cellular Biology, 26*(2), 413–424.

Zhang, C., & Zhang, F. (2015). The Multifunctions of WD40 Proteins in Genome Integrity and Cell Cycle Progression. *Journal of Genomics*, *3*, 40–50.

Zhang, W., Meng, Y., Liu, N., Wen, X. F., & Yang, T. (2015). Insights into chemoresistance of prostate cancer. *International Journal of Biological Sciences*, *11*(10), 1160–1170.

Zhao, H., Carney, K. E., Falgoust, L., Pan, J. W., Sun, D., & Zhang, Z. (2016). Emerging roles of Na+/H+ exchangers in epilepsy and developmental brain disorders. *Progress in Neurobiology, 138*, 19–35.

Zhitomirsky, B., & Assaraf, Y. G. (2014). Lysosomal sequestration of hydrophobic weak base chemotherapeutics triggers lysosomal biogenesis and lysosome- dependent cancer multidrug resistance. *Oncotarget, 6*(2), 1143–1156.

Zinzi, L., Capparelli, E., Cantore, M., Contino, M., Leopoldo, M., & Colabufo, N. A. (2014). Small and Innovative Molecules as New Strategy to Revert MDR. *Frontiers in Oncology*, *4*, 2.